Aus dem Lehrstuhl für Experimentelle Ultrahochfeld Magnetresonanz
der Medizinischen Fakultät Charité – Universitätsmedizin Berlin

DISSERTATION

Entwicklung und Anwendung suszeptibilitätsgewichteter Magnetresonanztomografie für die Herzbildgebung bei ultrahohen Magnetfeldstärken

zur Erlangung des akademischen Grades
Doctor rerum medicinalium (Dr. rer. medic.)

vorgelegt der Medizinischen Fakultät
Charité – Universitätsmedizin Berlin

von

Till Hülnhagen

aus München

Datum der Promotion: 16.06.2018

Inhaltsverzeichnis

Zusammenfassung

Abstrakt

Die Charakterisierung des Herzmuskelgewebes spielt eine wichtige Rolle in der Diagnostik und Therapie kardialer Erkrankungen. Durch den hohen Weichgewebekontrast und die vielseitige Einsetzbarkeit hat sich die Magnetresonanztomografie zu einem wichtigen klinischen Werkzeug in der Diagnose und Therapieüberwachung kardialer Erkrankungen entwickelt.

Die Kartierung der effektiven transversalen Relaxationszeit T_2^* mittels suszeptibilitätsgewichteter Magnetresonanztomografie (MRT) stellt eine aufstrebende Technik zur nicht-invasiven Gewebedifferenzierung im Myokard dar. Die lineare Zunahme magnetischer Suszeptibilitätseffekte mit steigender Magnetfeldstärke macht eine Anwendung der Technik bei ultrahohen Magnetfeldstärken (UHF, $B_0 \geq 7.0$ T) besonders attraktiv. Dies unterstützt die zeitlich aufgelöste myokardiale T_2^* Kartierung und erlaubt die Untersuchung des Myokards in verschiedenen physiologischen Zuständen. Dadurch könnte eine Unterscheidung von gesundem und pathologischem Gewebe ermöglicht werden. Motiviert durch dieses Potential untersucht diese Arbeit erstmalig die Anwendung zeitlich aufgelöster T_2^* Kartierung des Myokards bei 7.0 Tesla in Patienten mit kardialen Erkrankungen im Vergleich zu gesunden Probanden und analysiert das Potential der Technik zur nicht-invasiven Gewebedifferenzierung und Untersuchung der Physiologie des Herzmuskels.

Zu diesem Zweck wurden technische und methodische Entwicklungen vorgenommen und MR-Messungen bei 7.0 T in Messphantomen sowie *in vivo* in gesunden Probanden und Patienten mit hypertropher Kardiomyopathie (HCM) vorgenommen. T_2^* im myokardialen Septum wurde zusammen mit grundlegenden Parametern der Herzmorphologie bestimmt. Der Einfluss makroskopischer Magnetfeldinhomogenitäten als mögliche Störgröße wurde mittels numerischer Simulationen und MRT-Messungen analysiert. Zudem wurde die subjektive Akzeptanz von kardialen Ultrahochfeld-MRT-Untersuchungen untersucht.

Sowohl in gesunden Probanden als auch in HCM-Patienten wurden periodische Schwankungen von T_2^* über den Herzzyklus beobachtet. Im Gegensatz zu Änderungen in der myokardialen Oxygenierung, die häufig als dominierender Faktor für T_2^* betrachtet werden, wurden als Ursache zyklische Veränderungen in der myokardialen Blutvolumenfraktion identifiziert. Dies erlaubt neue Einsichten in die myokardiale Physiologie *in vivo*. Ein wesentlicher Einfluss makroskopischer Magnetfeldinhomogenitäten konnte dagegen ausgeschlossen werden.

HCM-Patienten zeigen signifikant höhere T_2^* Werte im ventrikulären Septum als gesunde Probanden. Diese Erhöhung wurde mit einer T_2-Erhöhung in Verbindung mit Entzündungsprozessen bei der Bildung von Fibrose sowie einer verminderten Blutvolumenfraktion im Myokard erklärt. Diese Zustände werden mit einem erhöhten Risiko für einen ungünstigen Krankheitsverlauf assoziiert. T_2^* Kartierung könnte daher zur Risikoabschätzung bei HCM beitragen.

Zusammenfassend demonstriert diese Arbeit erstmalig die Anwendung von T_2^* Kartierung im Myokard bei 7.0 T in Patienten mit Herzerkrankungen im Vergleich zu gesunden Probanden. Die Ergebnisse zeigen, dass die Technik neue Einsichten in die Physiologie des Herzens erlaubt und die Unterscheidung von gesundem und krankem Gewebe vereinfachen könnte.

Abstract

Myocardial tissue characterization plays an important role in the diagnosis and treatment of cardiac diseases. Thanks to its soft tissue contrast and versatility, cardiovascular magnetic resonance imaging (CMR) has become an important clinical tool for diagnosis and for guiding therapy of cardiac diseases.

Mapping of the effective transverse relaxation time T_2^* using susceptibility weighted magnetic resonance imaging (MRI) represents an emerging technique for non-invasive myocardial tissue characterization. The linear increase of magnetic susceptibility effects with magnetic field strength renders it appealing to perform T_2^* mapping at ultrahigh magnetic fields (UHF, $B_0 \geq 7.0$ T), which also enable temporally resolved myocardial T_2^* mapping. This permits probing the myocardium at different physiological states and holds the promise to facilitate the distinction of healthy and pathologic tissue. Recognizing this potential this work demonstrates for the first time the applicability of cardiac phase resolved myocardial T_2^* mapping at 7.0 Tesla in cardiac patients compared to healthy controls and investigates its potential for tissue characterization and probing of cardiac physiology.

To achieve this goal technical and methodological developments were conducted. MR measurements were performed at 7.0 T in phantoms as well as *in vivo* in human healthy volunteers and patients suffering from hypertrophic cardiomyopathy (HCM). Ventricular septal T_2^* was analyzed together with basic parameters of cardiac morphology. The influence of macroscopic magnetic field changes as a potential confounder for myocardial T_2^* was carefully analyzed in numerical simulations and MR experiments. Additionally the subjective acceptance of UHF cardiac MRI scans was investigated.

In vivo investigations showed that ventricular septal T_2^* changes periodically across the cardiac cycle in both healthy controls and HCM patients. Cyclic changes in myocardial blood volume fraction across the cardiac cycle were identified as cause for the observed T_2^* variations as opposed to changes in myocardial oxygenation which are often considered to dominate myocardial T_2^*. This provides further insights into myocardial physiology *in vivo*. Based on macroscopic magnetic field assessments, a substantial contribution of dynamic field fluctuations on T_2^* was excluded.

Ventricular septal T_2^* was significantly elevated in HCM patients compared to healthy controls. This was associated with a T_2 increase related to edema in formation of fibrosis and a reduction in myocardial blood volume fraction in HCM. Both of these conditions are associated with a higher risk of poor outcome for HCM patients indicating that myocardial T_2^* mapping at UHF could support risk stratification in HCM.

This work demonstrates for the first time the feasibility of myocardial T_2^* mapping at 7.0 T in cardiac patients. The results indicate that this technique can provide new insights into myocardial (patho)physiology and might facilitate the distinction of healthy from pathologic tissue without need for exogenous contrast agents.

Einführung

Die Charakterisierung des Herzmuskelgewebes spielt eine wichtige Rolle in der Diagnostik und Therapie kardialer Erkrankungen. Nach wie vor stellt diese Aufgabe Ärzte vor Herausforderungen. Die Magnetresonanztomografie (MRT) ist eine nicht-invasive Bildgebungsmodalität, mit deren Hilfe, frei von ionisierender Strahlung, Bilder des Körperinneren erzeugt werden können. Gegenüber anderen Bildgebungsmethoden wie etwa Röntgen- oder Ultraschall-basierten Verfahren, zeichnet sich die MRT durch einen exzellenten Weichgewebekontrast bei gleichzeitig hoher räumlicher Auflösung und Eindringtiefe aus. Sie eignet sich daher sehr gut für die Herzbildgebung. Diese Eigenschaften haben dazu geführt, dass die MRT in zunehmendem Maße in der klinischen Praxis eingesetzt wird. Durch den Verzicht auf ionisierende Strahlung und ihren nicht-invasiven Charakter bietet sich die MRT dabei insbesondere für longitudinale Untersuchungen wie etwa zur Kontrolle von Krankheitsprogression oder Therapieerfolg an.

Im Gegensatz zu Röntgenverfahren liefert die Signalintensität in MRT-Bildern nur qualitative Aussagen. Mittels parametrischer Kartierungsverfahren von MR-Relaxationsparametern ist es jedoch möglich MRT-basiert auf nicht-invasive Weise auch quantitative Informationen über Gewebeeigenschaften zu erhalten. Dies erlaubt die Definition von Normwerten und ermöglicht den Vergleich von Ergebnissen zwischen verschiedenen Probanden oder Patienten. Unter diesen Verfahren ist insbesondere die Kartierung der effektiven transversalen Relaxationszeit T_2^* von Interesse, da T_2^* mit einer Vielzahl physiologischer Parameter wie etwa Blutoxygenierung, Blutvolumenfraktion im Gewebe, Hämatokrit oder Mikrostruktur des Gewebes zusammenhängt [2-5]. Die Technik beruht auf Unterschieden in der magnetischen Suszeptibilität und den daraus resultierenden Feldverzerrungen und wird mit Hilfe T_2^*-gewichteter (suszeptibilitätsgewichteter) MR-Techniken umgesetzt.

In der Literatur werden verschiedene Anwendungen der suszeptibilitätsgewichteten MRT des Herzen beschrieben. Studien haben unter anderem gezeigt, dass mittels T_2^*-Kartierung Perfusionsdefizite und ischämische Bereiche im Myokard identifiziert [6-8], die Funktion des Endothels untersucht [9] und Oxygenierungsänderungen in Abhängigkeit von Atemmanövern detektiert werden können [10,11]. In der klinischen Routine hat die T_2^*-Kartierung des Myokards sich als Standardmethode zur Quantifizierung von Eisenüberschuss im Herz etabliert [12].

Die lineare Zunahme magnetischer Suszeptibilitätseffekte mit der Magnetfeldstärke macht T_2^*-Kartierung besonders bei hohen Magnetfeldstärken interessant [1]. Abbildung 1 zeigt diesen Zusammenhang anhand der effektiven transversalen Relaxationsrate $R_2^* = 1/T_2^*$. Die höchste derzeit für klinische MRT verfügbare Magnetfeldstärke liegt bei 3.0 T. Durch technische Weiterentwicklungen in den letzten Jahren ist kardiale MRT für Forschungsanwendungen mittlerweile auch bei ultrahohen Magnetfeldstärken von 7.0 T möglich [13,14]. Durch die Verkürzung von T_2^* bei höheren Feldstärken und einer reduzierten Inter-Echo-Zeit, zu der Signalanteile von Fett und Wasser in Phase sind, ermöglicht die MRT bei 7.0 T erstmalig eine zeitlich aufgelöste T_2^*-Kartierung über den Herzzyklus in Aufnahmezeiten, die sich für kurze Aufnahmen unter angehaltener Atmung eignen [15]. Dagegen beschränkt sich die T_2^*-Kartierung bei klinischen Magnetfeldstärken bisher auf einzelne Herzphasen. Durch die Beobachtbarkeit von T_2^* über den gesamten Herzzyklus bei 7.0 T bietet diese Technik die einzigartige Möglichkeit, das Herz in verschiedenen physiologischen Zuständen zu untersuchen, ohne dabei externe Stimuli wie etwa pharmakologischen Stress oder Kontrastmittel verwenden zu müssen. Daher ist T_2^*-Kartierung bei ultrahohen Magnetfeldstärke insbesondere für die Untersuchung von Patienten attraktiv [16]. Durch den Signalgewinn bei 7.0 T kann zudem eine höhere räumliche Auflösung realisiert

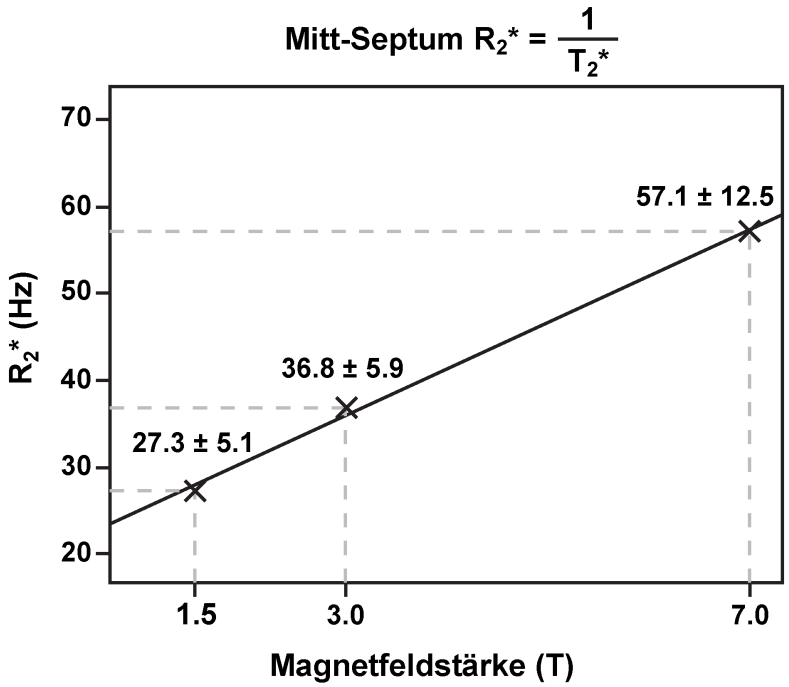

Abbildung 1: *Zusammenhang der effektiven transversalen Relaxationsrate R_2^* im ventrikulären Septum mit der magnetischen Feldstärke. Mit steigender Magnetfeldstärke nimmt R_2^* linear zu. Entsprechend verkürzt sich die effektive transversale Relaxationszeit $T_2^* = 1/ R_2^*$ mit zunehmender Feldstärke.(Adaptiert von [1])*

werden, wodurch feine strukturelle Änderungen detektiert werden können [13,14,17].

Bislang beschränkte sich der Einsatz zeitlich aufgelöster T_2^*-Kartierung des menschlichen Herzens bei 7.0 T auf eine Machbarkeitsstudie an gesunden Probanden [15]. Es bestand daher der Bedarf einer systematischen Untersuchung und Interpretation der mit Hilfe der Technik verfügbaren Informationen sowie einer Evaluierung einer möglichen klinischen Nutzbarkeit.

Hypertrophe Kardiomyopathie (HCM) ist die häufigste genetisch bedingte Erkrankung des Myokards mit einer Prävalenz von 0.2-0.5% in der Gesellschaft [18,19]. Während ein Großteil der Patienten keine Symptome zeigt, kann die Erkrankung in einem Teil der Patienten zu Herzversagen oder plötzlichem Herztod führen. Die Risikoeinschätzung spielt daher eine essentielle Rolle in der HCM-Diagnostik. Aufgrund bekannter struktureller und physiologischer Änderungen im Herzmuskel bei HCM, und der Empfindlichkeit von T_2^* auf diese Parameter, wurde die Hypothese aufgestellt, dass sich mittels hochaufgelöster T_2^*-Kartierung bei 7.0 T Unterschiede zwischen gesunden Probanden und HCM-Patienten erkennen lassen, und diese möglicherweise zusätzliche diagnostische Informationen liefern könnten.

Ziel dieser Arbeit war die Weiterentwicklung und Anwendung zeitlich aufgelöster T_2^*-Kartierung des Myokards bei 7.0 T, eine systematische Untersuchung der daraus ableitbaren Ergebnisse sowie die Evaluierung einer möglichen klinischen Anwendbarkeit im Rahmen einer ersten Vergleichsstudie zwischen gesunden Probanden und Patienten mit kardialen Erkrankungen. Dazu wurden Methodenentwicklungen und Optimierungen vorgenommen und MR Messungen bei 7.0 T in Phantomen sowie *in vivo* an gesunden Probanden und HCM-Patienten durchgeführt und ausgewertet. Zudem wurde der Einfluss makroskopischer Magnetfeldschwankungen als mögliche Störgröße für T_2^* mittels numerischer Simulationen und experimenteller Messungen untersucht.

Teilergebnisse der vorliegenden Arbeit wurden in den auf den Seiten 31 und 32 aufgeführten Publikationen veröffentlicht.

Methodik

Myokardiale T_2^*-Kartierung

T_2^* gewichtete Bildgebung und T_2^*-Kartierung wird in den meisten Fällen mit Hilfe von schnellen Gradienten-Echo MR-Bildgebungstechniken durchgeführt. Diese Techniken zeichnen sich durch einen inhärenten T_2^* Kontrast aus und eignen sich durch ihre kurzen Aufnahmedauern gut für die Herzbildgebung. Für die T_2^*-Kartierung wird für jedes Volumenelement (Voxel) des Bildes die, durch effektive transversale Relaxation bedingte, Abschwächung des MR-Signals nach einer Hochfrequenzanregung gemessen. Dazu werden Bilder in verschiedenen zeitlichen Abständen zur Anregung (Echozeit, TE) aufgenommen. Der Signalverlauf $S_m(\theta)$ wird durch

$$S_m(\theta) = S_0 sin(\theta) exp(-TE/T_2^*) \frac{[1 - exp(-TR/T_1)]}{[1 - cos(\theta) exp(-TR/T_1)]} \quad (1)$$

beschrieben. S_0 ist die Spindichte, TR die Repetitionszeit und TE die Echozeit. T_1 und T_2^* sind die spezifische longitudinale und effektive transversale Relaxationszeit. θ beschreibt den Anregungswinkel, um den die Magnetisierung durch die Hochfrequenzanregung aus der longitudinalen in die transversale ausgelenkt wird. Werden T_1 und TR konstant angenommen, lässt sich Gleichung (1) wie folgt vereinfachen:

$$S_m(\theta) \propto exp(-TE/T_2^*) \quad (2)$$

Auf Basis dieses Zusammenhangs, kann die T_2^* Zeitkonstante aus einer Serie von Bildern, die zu verschiedenen Echozeiten aufgenommen wurden, mittels einer exponentiellen Kurvenanpassung (engl. fit) bestimmt werden. Dieses Vorgehen ist beispielhaft in Abbildung 2 illustriert.

Für die T_2^*-Kartierung des Herzens wurden im Rahmen dieser Arbeit schnelle Multi-Echo Grandienten-Echo CINE-Techniken verwendet, welche eine zeitlich aufgelöste T_2^*-Kartierung des Herzens *in vivo* ermöglichen [15]. Die Einstellungen der Techniken und Messprotokolle wurden dabei speziell für die Anwendung für Patientenuntersuchungen angepasst.

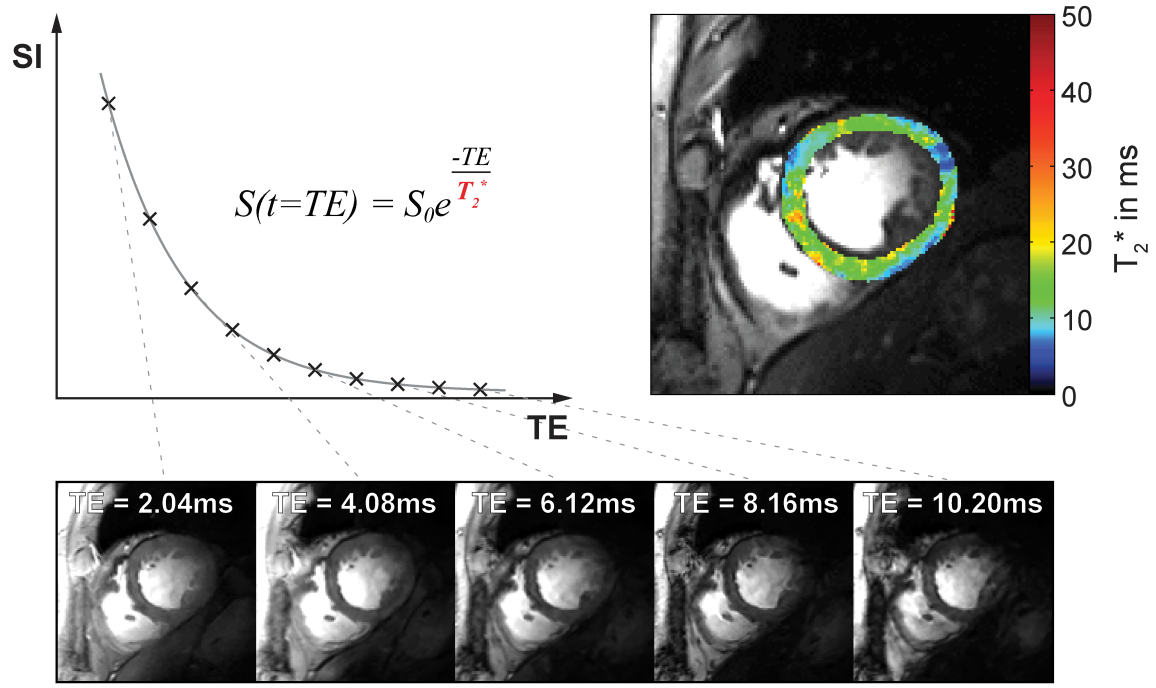

Abbildung 2: *T_2^*-Signalzerfall und T_2^*-Kartierung.* ***Oben links:*** *Zeitlicher Verlauf der Signalintensität in einem Voxel nach einer Hochfrequenzanregung bei Verwendung einer Gradienten-Echo Technik.* ***Unten:*** *Beispiel von mittventrikulären Kurzachsenbildern des menschlichen Herzens mit zunehmender T_2^*-Wichtung.* ***Oben rechts:*** *Zugehörige myokardiale T_2^*-Karte eingefügt in ein anatomisches Bild. [16]*

Im Rahmen dieser Arbeit wurden T_2^*-Messungen an Messphantomen, gesunden Probanden und Patienten mit hypertropher Kardiomyopathie durchgeführt und ausgewertet. Abbildung 3 zeigt ein Beispiel zeitlich aufgelöster T_2^*-Karten des menschlichen Herzens bei 7.0 T

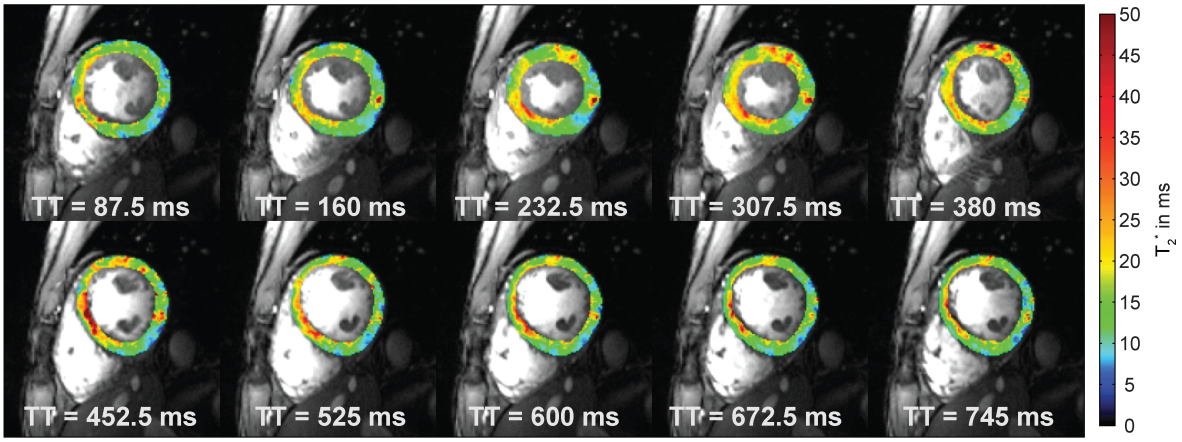

Abbildung 3: *Kurzachsendarstellung zeitlich aufgelöster T_2^* Kartierung des Myokards eines gesunden Probanden bei 7.0 T (10 von 20 Herzphasen dargestellt). Räumliche Auflösung (1.1x1.1x4.0)mm^3. Zeitliche Auflösung 37ms. Zeitliche Veränderungen von T_2^* sind erkennbar. TT bezeichnet den Zeitabstand zum Trigger. [16]*

Einfluss makroskopischer Feldinhomogenitäten auf T_2^*

Die T_2^* Signalabschwächung ist begründet im durch lokale Magnetfeldinhomogenitäten bedingten Verlust der Phasenkohärenz der Spins (Dephasierung). Solche Feldinhomogenitäten können einerseits mikroskopischen und andererseits makroskopischen Ursprungs sein. Mikroskopische Feldeffekte werden von physiologischen Parametern wie unter anderem Blutoxygenierung, Blutvolumenfraktion im Gewebe, Hämatokrit und Mikroarchitektur des Gewebes beeinflusst und sind daher von klinischem Interesse [5,20-22]. Dagegen resultieren makroskopische Feldeffekte und damit verbundene Störfaktoren beispielsweise aus Fertigungstoleranzen der Magneten aber insbesondere aus Wechselwirkungen zwischen Körper und Magnetfeld. Diese treten besonders an starken Suszeptibilitätsübergängen auf.

Eine wesentliche Voraussetzung für eine aussagekräftige T_2^*-Kartierung ist eine möglichst gute Homogenität des äußeren Magnetfeldes, um sicherzustellen, dass die gemessenen T_2^*-Werte ursächlich auf mikroskopische Suszeptibilitätsänderungen zurückgehen und nicht von makroskopischen Feldeffekten dominiert werden. Bedingt durch große Unterschiede in der magnetischen Suszeptibilität zwischen Herzmuskelgewebe und Lunge, treten an den Übergängen vermehrt starke Magnetfeldverzerrungen auf, was die T_2^*-Kartierung des Herzens besonders herausfordernd gestaltet.

Durch Untersuchungen und Optimierungen in Messphantomen wie auch bei *in vivo* Messungen gesunder Probanden konnten reproduzierbar statische Feldhomogenitäten ähnlicher Güte erreicht werden, wie sie auch bei niedrigeren Feldstärken von 1.5 T und 3.0 T berichtet wurden. Dazu wurden Feldkarten aufgenommen und, auf deren Basis, eine Optimierung der Feldhomogenität speziell für das untersuchte Herzvolumen vorgenommen [23].

Für die Untersuchung zeitlicher Änderungen von T_2^* über den Herzzyklus müssen neben statischen Magnetfeldänderungen auch zeitliche Variationen des makroskopischen Magnetfeldes als mögliche Ursache für T_2^*-Änderungen berücksichtigt werden. Durch die starke Verformung der Anatomie und der daraus resultierenden Änderung der Suszeptibilitätsverteilung über den Herzzyklus war eine dadurch bedingte Schwankung des Magnetfeldes nicht auszuschließen.

Zur Untersuchung dieses Zusammenhanges wurden zunächst magnetostatische Simulationen vorgenommen. Auf Basis eines numerischen Voxelmodells eines menschlichen Herzens wurden Feldsimulationen für eine systolische sowie eine dias-

tolische Konfiguration des Herzens durchgeführt. Aus den resultierenden Feldkarten wurden Intravoxel-Magnetfeldgradienten berechnet. Diese Intravoxelgradienten sind ein Maß für den Einfluss der makroskopischen Feldeinflüsse auf den T_2^*-Zerfall. Daraus wurde der Einfluss makroskopischer morphologischer Veränderungen über den Herzzyklus auf T_2^* im ventrikulären Septum abgeschätzt.

Als weiterer Schritt wurden mittels Multi-Echo CINE Gradienten-Echo-Techniken zeitlich aufgelöste Feldkarten im Herzen *in vivo* über den gesamten Herzzyklus akquiriert. Anhand dieser Daten wurden Karten der durch makroskopische Effekte verursachten Intravoxelgradienten bestimmt. Auf Basis dieser Informationen wurden Abschätzungen berechnet, in welchem Maß T_2^* in Abhängigkeit der dynamischen makroskopischen Feldveränderungen variiert.

Daten Vorverarbeitung

Für eine aussagekräftige T_2^*-Kartierung ist ein hohes Signal-zu-Rauschverhältnis (engl. signal to noise ratio, SNR) wünschenswert. Ist das SNR zu gering, besteht die Gefahr ungenauer Ergebnisse und folglich der Ableitung falscher Schlüsse. Die Aufnahme von MR-Bilddaten ist immer ein Kompromiss aus den konkurrierenden Parametern räumliche Auflösung, zeitliche Auflösung, Aufnahmedauer und SNR. Je höher die räumliche und zeitliche Auflösung und je kürzer die Aufnahmedauer sind, umso geringer ist das resultierende SNR.

Die Herzbildgebung stellt hierbei eine besondere Herausforderung dar, da die Aufnahmen häufig bei angehaltenem Atem durchgeführt werden, um Bildartefakte durch Atembewegungen zu vermeiden. Zudem muss die Aufnahme mit der Herzbewegung synchronisiert werden. Diese Randbedingungen limitieren die tatsächlich umsetzbare Aufnahmedauer auf wenige Sekunden und beschränken so das erreichbare SNR. Für Patienten mit kardialen Erkrankungen sind diese Randbedingungen durch die eingeschränkte Fähigkeit die Luft anzuhalten noch verschärft. Um eine ausreichend gute Approximation des Signalzerfalls für eine zuverlässige Bestimmung von T_2^* zu ermöglichen, ist zudem eine hinreichend starke T_2^* Wichtung der Bilder erforderlich (vgl. Abbildung 2). Diese geht ebenfalls mit einer Signalabschwächung einher. Zur Minimierung von makroskopischen Feldeffekten ist des Weiteren eine möglichst geringe Voxelgröße von Vorteil, die wiederum in einem geringeren SNR resultiert.

Trotz des inhärenten SNR Gewinns bei höheren Magnetfeldstärken stellt das begrenzte SNR auch bei einer Magnetfeldstärke von 7.0 T eine Herausforderung für die T_2^*-Kartierung im Myokard dar. Rauschunterdrückungsverfahren bieten eine interessante Möglichkeit, das SNR von Bilddaten im Nachhinein zu erhöhen. So genannte nicht lokale Mittelwertfilter (engl. non local means, NLM) haben sich hierzu als besonders geeignet erwiesen, da sie eine gute Rauschunterdrückung erzielen, gleichzeitig aber feine Bilddetails erhalten.

Im Rahmen dieser Arbeit wurde untersucht, ob sich durch Rauschunterdrückung in den T_2^* gewichteten Bildern präzisere T_2^*-Kartierungen erreichen lassen. Dazu wurde die Anwendung eines sogenannten räumlich angepassten nicht lokalen Mittelwertfilters untersucht (engl. spatially adaptive non local means, SANLM [24]). Wichtige Voraussetzung für eine Verwendung des Filters war, dass durch den Filterungsprozess keine falschen Ergebnisse erzeugt werden. Zu diesem Zweck wurden numerische Simulationen eines definierten Strukturphantoms mit unterschiedlich feinen geometrischen Strukturen durchgeführt. Es wurden für verschiedene Rauschniveaus und T_2^*-Zeiten Signalverläufe simuliert. Anschließend wurden die so erzeugten Bilddaten mittels des Filters entrauscht und T_2^*-Karten aus den verrauschen und entrauschten Daten berechnet. Beide Ergebnisse wurden mit den zuvor definierten wahren T_2^*-Werten verglichen und daraus der Fehler bestimmt. Dieses Vorgehen wurde in Monte-Carlo-Simulationen 500-fach wiederholt und der mittlere Fehler bestimmt [25].

Des Weiteren wurden normale und entrauschte T_2^*-gewichtete *in vivo* Bilddaten des menschlichen Herzens bei 7.0 T analysiert, die Standardabweichung der T_2^*-Kurvenanpassung als Gütemaß bestimmt und verglichen.

Subjektive Akzeptanz von Herz-MRT-Untersuchungen bei 7.0 T

Eine wesentliche Voraussetzung für eine klinische Anwendung der Herz-MRT bei ultrahohen Magnetfeldstärken ist die Sicherstellung der Verträglichkeit und Akzeptanz der Technik durch die zu Untersuchenden. Starke Magnetfelder und Magnetfeldgradienten, wie sie etwa an den Enden der Bohrung von MRT-Geräten auftreten, können potentiell zu Nebenwirkungen wie Schwindel führen. Auch von unwillkürlicher Muskelkontraktion, Wahrnehmung von Lichtblitzen oder metallischem Geschmack im Zusammenhang mit Ultrahochfeld-MRT-Scans wurde berichtet [26-28]. Diese Ergebnisse beziehen sich jedoch überwiegend auf MRTs des Kopfes. Durch die unterschiedliche Positionierung der untersuchten Person während einer Herz-MRT ge-

genüber einer MRT des Kopfes lassen sich die Ergebnisse dieser Studien jedoch nicht ohne weiteres übertragen. In einer Studie wurde in dieser Arbeit gezielt die subjektive Akzeptanz kardialer MRT-Untersuchungen bei 7.0 T untersucht [29]. Mittels eines Fragebogens wurden hierfür 165 Probanden unmittelbar nach einer kardialen MRT-Untersuchung bei 7.0 T zu ihren Erfahrungen vor, während und nach der Untersuchung befragt. Ein korrektes Verständnis der Fragen wurde dabei von einer Aufsichtsperson sichergestellt.

Ergebnisse

Einfluss makroskopischer Feldinhomogenitäten auf T_2^*

Magnetostatische B_0-Feldsimulationen offenbarten einen nur geringen Einfluss der myokardialen Wanddicke auf das Magnetfeld im ventrikulären Septum und die daraus resultierenden Intravoxel-B_0-Gradienten (Abbildung 4). Auch zeitlich aufgelöste Feldkarten des makroskopischen Magnetfeldes *in vivo* zeigten nur sehr geringe Änderungen über den Herzzyklus. Die mittlere absolute Veränderung des Intravoxelgradienten über den Herzzyklus betrug im ventrikulären Septum 0.4 ± 0.3 Hz/voxel.

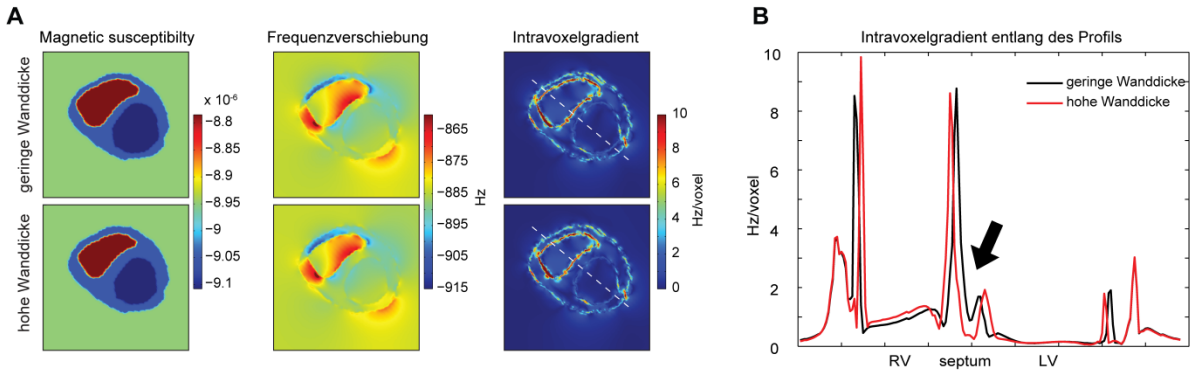

Abbildung 4: *Einfluss der myokardialen Wanddicke auf makroskopische Magnetfeldverzerrungen.* ***A)*** *Magnetostatische Feldsimulationen des menschlichen Herzens für geringe (Diastole) und hohe Wanddicke (Systole). Links: Modellierte Suszeptibilitätsverteilung, Mitte: Feldverschiebung, Rechts Intravoxelgradient.* ***B)*** *Intravoxelgradient entlang des in A rechts gezeigten Profils. Der Intravoxelgradient im Septum (Pfeil) ändert sich nur wenig in Abhängigkeit der Wanddicke. [23]*

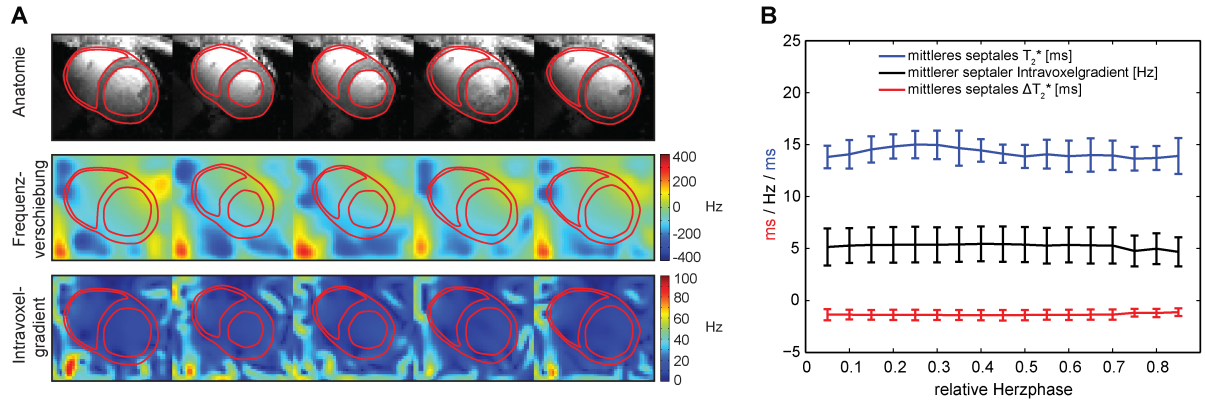

Abbildung 5: *Illustration der räumlichen und zeitlichen Veränderung von Intravoxel-Magnetfeldgradienten im menschlichen Herz bei 7.0T.* ***A)*** *Signalmagnitudenbilder eines mittventrikulären Kurzachsenschnitts im Verlauf über den Herzzyklus (oben) zusammen mit B_0-Feldkarten (Mitte) und Karten des intravoxel B_0 Gradienten (unten).* ***B)*** *Zeitverlauf des mittleren septalen T_2^*, des Intravoxel-B_0-Gradienten und dessen geschätzten Einflusses auf T_2^*. Zeitliche Änderungen des makroskopischen B_0-Feldes und ihr Einfluss auf T_2^* im ventrikulären Septum können als gering betrachtet werden. [23]*

Dieser Wert entspricht einer T_2^* Veränderung von etwa 0.7 ± 0.4 ms (Abbildung 5) und ist gering im Vergleich zu den über den Herzzyklus beobachteten periodischen T_2^* Veränderungen [23].

Daten Vorverarbeitung

Abbildung 6 vergleicht die T_2^* Fit Fehler in einem numerischen 3D Strukturphantom ohne und mit Anwendung eines Rauschfilters. Außer für Strukturen mit Größen von nur wenigen Voxeln und scharfen Kanten bei SNR Werten ≤ 7 konnte in allen Fällen eine deutliche Verbesserung der Kartierungsgenauigkeit erreicht werden [25]. Für die übrigen Fälle war der mittlere T_2^*-Fehler auch ohne eine Rauschunterdrückung schon so hoch, dass eine sinnvolle Auswertung nicht möglich war. Somit war die Anwendung des Filters in keinem Fall nachteilig.

Untersuchungen von T_2^*-Kartierungen des menschlichen Herzens *in vivo* bei 7.0 T zeigten eine durchschnittliche Reduktion der Standardabweichung des Fits im Myokard von etwa 30% [23]. Gleichzeitig wurden in keinem Fall Bildartefakte beobachtet, die auf die Anwendung des Rauschfilters zurückgeführt werden konnten. Als Folge dieser Ergebnisse wurde eine SANLM-Rauschfilterung in den Datenverarbeitungsprozess der T_2^*-Kartierung für alle *in vivo* Bilddaten aufgenommen. Abbildung 7 zeigt ein Beispiel für T_2^*-Kartierung des Myokards ohne und mit Anwendung eines SANLM-Filters.

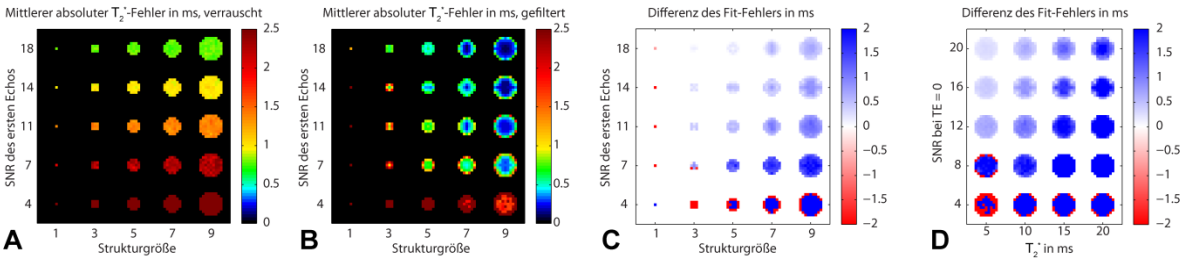

Abbildung 6: *Analyse des Einflusses von Rauschunterdrückung auf den mittleren T_2^*-Fit-Fehler anhand numerischer Simulationen eines Strukturphantoms in Abhängigkeit von Strukturgröße und SNR. Mittlerer T_2^*-Fehler über 500 Simulationen für ungefilterte **(A)** und entrauschte Bilddaten **(B)**. Unterschied des mittleren T_2^*-Fehlers zwischen ungefilterten und gefilterten Daten in Abhängigkeit von Strukturgröße **(C)** und tatsächlicher T_2^*-Zeit **(D)**. Außer für sehr kleine Strukturen und niedrige SNR Werte wird die Genauigkeit der T_2^*-Kartierung durch eine Rauschunterdrückung verbessert. [25]*

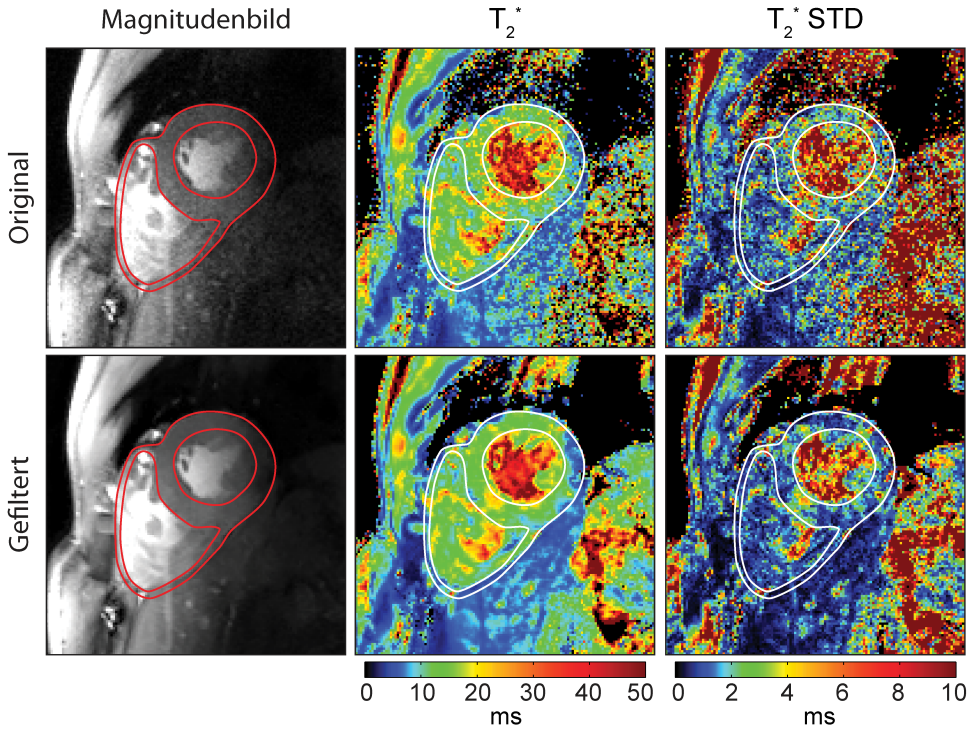

Abbildung 7: *Einfluss von SANLM-Rauschfilterung auf die Genauigkeit der myokardialen T_2^*-Kartierung bei 7.0 T.* ***Links:*** *Originales und SANLM gefiltertes Signalmagnitudenbild des ersten Echos einer Multi-Echo Gradienten-Echo-Bildserie.* ***Mitte:*** *Zugehörige T_2^*-Karten.* ***Rechts:*** *Karten der Fit-Standardabweichung. Durch Rauschunterdrückung konnte die Standardabweichung des Fits im Myokard um etwa 30% reduziert werden. [16]*

Zeitlich aufgelöste myokardiale T_2^*-Kartierung in gesunden Probanden

Die zeitlich Messung von T_2^* in gesunden Probanden ergab eine periodische Veränderung von T_2^* im ventrikulären Septum über den Herzzyklus. T_2^* steigt in der systolischen Phase an und fällt in der diastolischen Phase wieder ab. Diese Variationen korrelieren signifikant (p<0.001) mit Änderungen der septalen Wanddicke sowie des linksventrikulären Innenradius (Abbildung 8A). Die mittleren septale T_2^*-Zeit betrug 15.0 ± 1.4 ms in der endsystolischen Phase gegenüber 13.7 ± 1.2 ms in der enddiastolischen Phase. Die entsprechenden mittleren septalen Wanddicken wurden zu 5.9 ± 0.9 mm in der Enddiastole sowie 9.0 ± 1.3 mm in der Endsystole ermittelt. Das Verhältnis von endsystolischer zu enddiastolischem T_2^* lag bei 1.1 [16]. Die mittlere T_2^*-Schwankung über den Herzzyklus wurde zu 3.5 ± 1.0 ms bestimmt. Dieser Wert ist signifikant höher (p<0.01) als die auf Basis makroskopischer B_0-Feldschwankungen erwartete T_2^*-Änderung von 0.7 ± 0.4 ms. Daher kann ein signifikanter Beitrag von makroskopischen Feldveränderungen auf die Änderungen von T_2^* über den Herzzyklus ausgeschlossen werden [23].

In der Literatur wird T_2^* im Myokard häufig als Maß für die Oxygenierung angesehen [30]. Die Interpretation der systolische T_2^*-Erhöhung als Folge einer Zunahme in der Blutoxygenierung widerspricht jedoch dem aktuellen physiologischen Kenntnisstand und kann daher ebenso als Ursache ausgeschlossen werden.

Die beobachteten periodischen T_2^*-Schwankungen lassen sich stattdessen durch Änderungen in der myokardialen Blutvolumenfraktion über den Herzzyklus erklären. Durch die massive Blutdruckzunahme im linken Ventrikel zu Beginn der Systole werden die intramyokardialen Blutgefäße komprimiert (Abbildung 8B,C). Hierdurch wird die Blutzufuhr ins Myokard reduziert, während gleichzeitig im Muskel enthaltenes Blut aus diesem herausgedrückt wird. Die daraus resultierende Abnahme der Blutvolumenfraktion im Muskel hat eine T_2^*-Erhöhung zur Folge. In der diastolischen Entspannungsphase ist der Prozess umgekehrt [23].

Zeitlich aufgelöste myokardiale T_2^*-Kartierung in HCM-Patienten

Abbildung 9 zeigt systolische und diastolische T_2^*-Karten des Myokards für gesunde Probanden und HCM-Patienten. Ebenso wie in gesunden Probanden wurde auch in

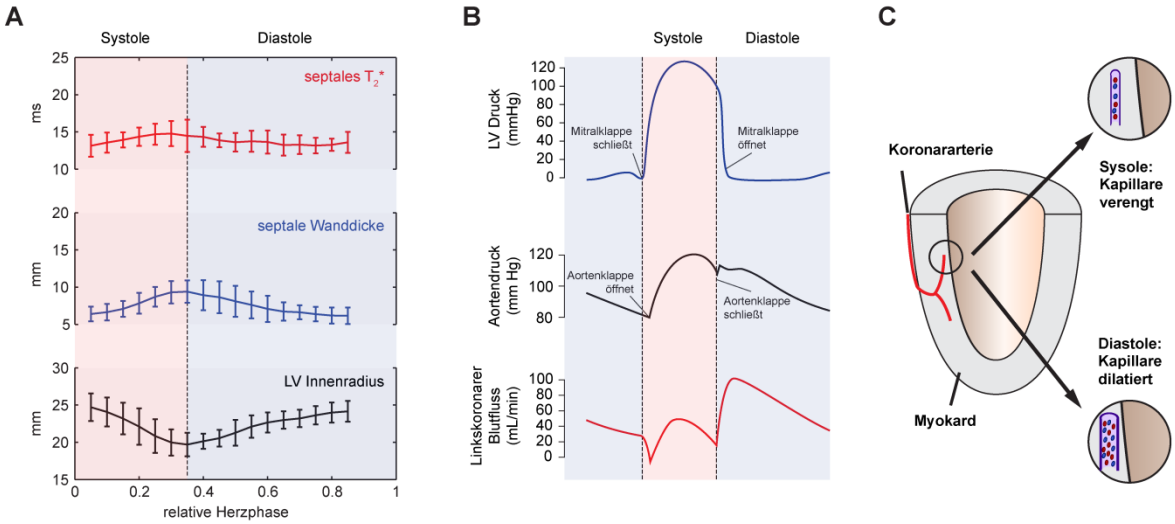

Abbildung 8: *Ergebnis zeitlich aufgelöster T_2^*-Kartierung des Myokards in einer Gruppe gesunder Probanden bei 7.0 T.* ***A)*** *Verlauf von T_2^* und Wanddicke im ventrikulären Septum sowie linksventrikulärem Innenradius über den Herzzyklus. Fehlerbalken repräsentieren den Standardfehler. T_2^* im ventrikulären Septum variiert periodisch über den Herzzyklus, wobei es in der Systole zunimmt und in der Diastole abnimmt.* ***B)*** *Die beobachteten T_2^*-Änderungen lassen sich durch Schwankungen der Blutvolumenfraktion im Herzmuskel erklären.* ***C)*** *Durch die massive Blutdruckzunahme im linken Ventrikel zu Beginn der Systole werden die intramyokardialen Blutgefäße komprimiert, wodurch die Blutzufuhr reduziert wird. Gleichzeitig wird im Muskel enthaltenes Blut aus diesem herausgedrückt. Die resultierende Reduktion der Blutvolumenfraktion im Muskel führt zu einer T_2^*-Erhöhung.*

HCM-Patienten eine periodische Änderung von T_2^* im ventrikulären Septum über den Herzzyklus beobachtet (Abbildung 10). Im Vergleich zu in Alter, Geschlecht und Body-Mass-Index vergleichbaren gesunden Probanden wurde eine signifikante (p<0.001) Erhöhung von T_2^* festgestellt. Die mittleren T_2^*-Werte über den Herzzyklus lagen bei 17.5 ± 1.4 ms in der Patientengruppe im Vergleich zu 13.7 ± 1.1ms in gesunden Probanden. Während die periodischen T_2^*-Veränderung wie bereits in den gesunden Probanden auch in den HCM-Patienten auf Änderungen der Blutvolumenfraktion über den Herzzyklus zurückgeführt wurden, wurden zwei Faktoren als mögliche Ursachen für den Anstieg von T_2^* in HCM-Patienten gegenüber gesunden Probanden identifiziert. Einerseits wurde die transversale Relaxationszeit T_2 in Fällen von HCM als erhöht beschrieben, was mit Entzündungsprozessen assoziiert wurde [31,32]. Eine Erhöhung von T_2 resultiert automatisch auch in einer Erhöhung von T_2^*. Andererseits sind reduzierte Perfusion und Ischämie im Myokard bekannte Phänomene bei HCM [33]. Diese sorgen für eine geringere Blutvolumenfraktion im Myokard und können dadurch auch zu einer T_2^*-Erhöhung beitragen. Eine erhöhte Sauerstoffversorgung im von HCM betroffenen Herz widerspricht gängigem Literaturwissen und wurde als Ursache für die T_2^*-Erhöhung ausgeschlossen.

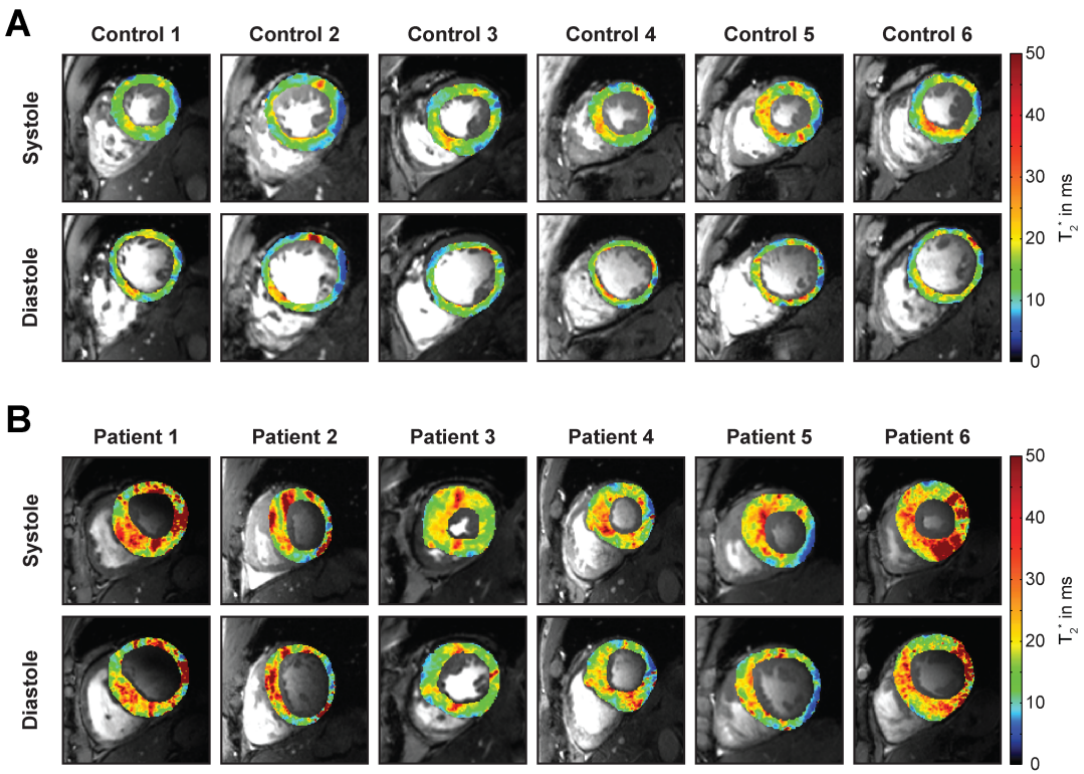

Abbildung 9: *Mittventrikuläre Kurzachsenansichten systolischer und diastolischer myokardialer T_2^*-Karten in gesunden Probanden (A) und HCM-Patienten (B) bei 7.0 T. T_2^*-Unterschiede zwischen Systole und Diastole sind erkennbar. In HCM-Patienten können erhöhte T_2^*-Werte beobachtet werden. [Huelnhagen et al., Sci Rep. 2018 Mar 5;8(1):3974]*

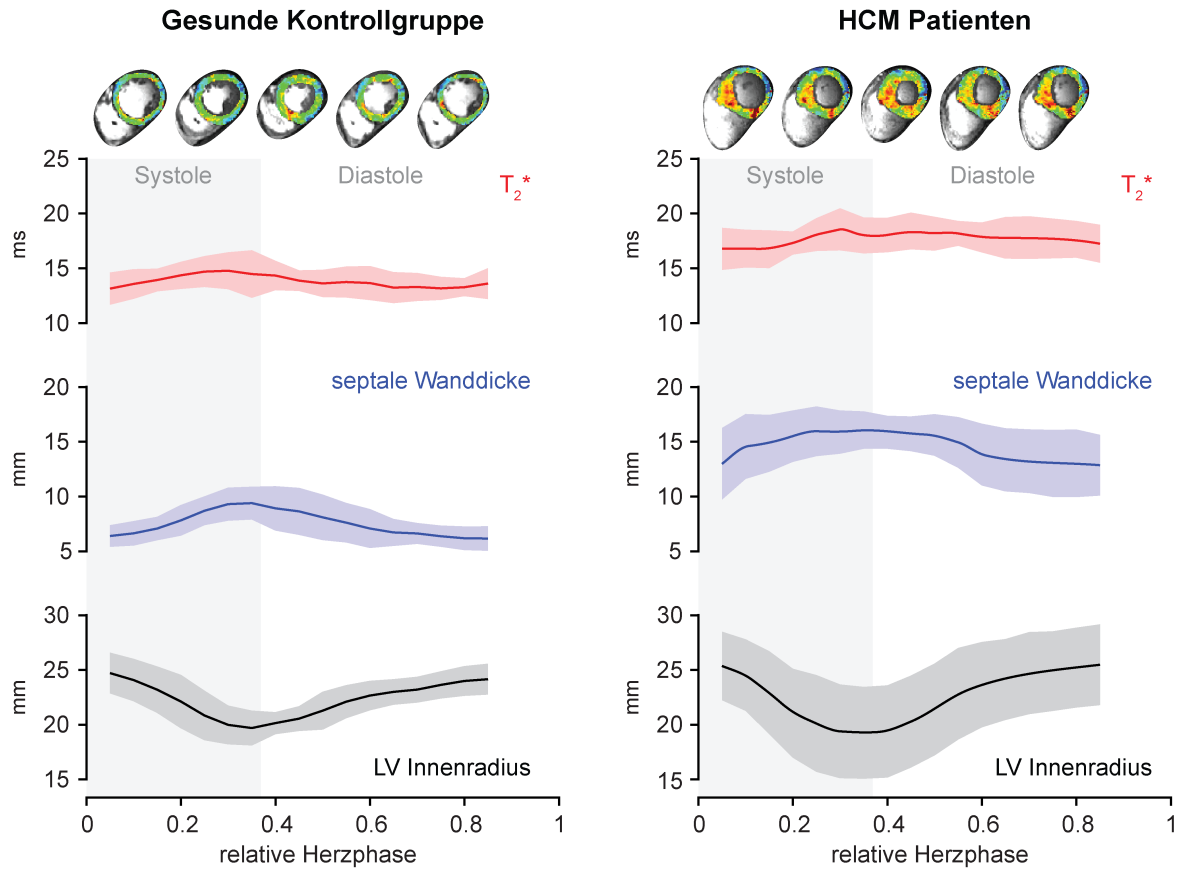

Abbildung 10: *Verlauf von T_2^* und Wanddicke im ventrikulären Septum sowie linksventrikulärem Innenradius über den Herzzyklus in gesunden Probanden und HCM- Patienten bei 7.0 T. Gruppenanalyse von je sechs Probanden und Patienten. Schattierte Bereiche repräsentieren den Standardfehler. T_2^* im ventrikulären Septum ist für HCM- Patienten signifikant erhöht. [Huelnhagen et al., Sci Rep. 2018 Mar 5;8(1):3974.]*

Subjektive Akzeptanz von Herz-MRT-Untersuchungen bei 7.0 T

Jeweils 12.7% der Probanden berichteten in Zusammenhang mit der Herz-MRT-Untersuchung bei 7.0 T über Muskelkontraktion und transienten Schwindel. Diese Effekte wurden am häufigsten beschrieben. 10.1% der Studienteilnehmer berichteten von transientem metallischem Geschmack und 3.6% von der Wahrnehmung von Lichtblitzen. Keiner der Probanden zeigte schwerere Nebenwirkungen wie etwa Erbrechen oder Ohnmacht. Alle beschriebenen Nebenwirkungen waren nur bis maximal 10 Minuten nach Ende der Untersuchung merkbar und danach vollständig abgeklungen. Als wichtiges Ergebnis konnte damit gezeigt werden, dass kardiale MRT-Untersuchungen bei einer Magnetfeldstärke von 7.0 T gut toleriert werden, und die höhere Magnetfeldstärke keine Nebenwirkungen verursacht, welche eine klinische Nutzbarkeit in Frage stellen würden [29].

Diskussion

Die vorliegende Arbeit demonstriert erstmalig die T_2^*-Kartierung des menschlichen Myokards von Patienten hypertropher Kardiomyopathie bei 7.0 T. Mittels zeitlich und räumlich hochaufgelöster suszeptibilitätsgewichteter Magnetresonanztomografie wurde der Verlauf von T_2^* über den Herzzyklus und sein Zusammenhang mit der Morphologie des Herzens in gesunden Probanden und HCM-Patienten systematisch untersucht. Makroskopische Feldeffekte wurden als mögliche Störgröße detailliert betrachtet und ihr Einfluss auf T_2^* analysiert.

Zu diesem Zweck wurden theoretische Überlegungen angestellt, Prozessabläufe entwickelt und Bildgebungstechniken optimiert. Es wurden numerische Simulationen durchgeführt sowie Messungen bei 7.0 T an Phantomen und *in vivo* sowohl an gesunden Probanden als auch an HCM-Patienten vorgenommen und analysiert.

Zur Verbesserung der T_2^*-Messgenauigkeit wurde die Verwendung eines Rauschunterdrückungsverfahrens untersucht und implementiert. Dadurch konnte eine wesentliche Verbesserung der Kartierungsgenauigkeit erreicht werden. Auf diese Weise konnten auch für Patienten tolerierbare Atemanhaltezeiten bei dennoch ausreichender Kartierungsqualität realisiert werden.

Als Ergebnis der Studie konnte gezeigt werden, dass T_2^* sowohl in gesunden Probanden als auch in HCM-Patienten periodisch über den Herzzyklus variiert, wobei es in der Systole ansteigt und in der Diastole sinkt. Es ist eine verbreitete Meinung, dass T_2^* im Myokard die Gewebeoxygenierung widerspiegelt. Während ein Einfluss der Blutoxygenierung auf T_2^* generell unstrittig und gut belegt ist, lassen sich die beobachteten periodischen Änderungen von T_2^* über den Herzzyklus jedoch nicht durch eine veränderte Oxygenierung erklären. Stattdessen konnte hier demonstriert werden, dass die periodischen Variationen von T_2^* über den Herzzyklus maßgeblich auf Änderungen der Blutvolumenfraktion im Herzmuskel zurückzuführen sind. Diese Erkenntnisse stellen ein Novum in der Interpretation von T_2^* im Myokard dar und eröffnen neue Möglichkeiten für die Untersuchung der Physiologie des gesunden und kranken Herzens.

Anhand von numerischen Simulationen und *in vivo* Messungen konnte verifiziert werden, dass die beobachteten zyklischen Änderungen von T_2^* nicht auf makroskopische Feldeffekte in Zusammenhang mit einer veränderten Morphologie des Her-

zens zurückzuführen sind, sondern ihre Ursache in physiologisch bedingen mikroskopischen Suszeptibilitätsänderungen haben.

Weiterhin konnte gezeigt werden, dass T_2^* im Myokard von HCM-Patienten signifikant gegenüber einer gesunden Kontrollgruppe erhöht ist. Als mögliche Ursachen wurden hierfür eine Erhöhung von T_2 im Zusammenhang mit entzündlichen Prozessen sowie eine reduzierte Blutvolumenfraktion identifiziert. Diese beiden Phänomene werden mit einem höheren Risiko für eine ungünstige Krankheitsentwicklung der Patienten in Verbindung gebracht [34,35]. Dies gibt Grund zur Annahme, dass myokardiale T_2^*-Kartierung als zusätzliches Element in der Diagnose und gegebenenfalls in der Risikobewertung von HCM-Patienten genutzt werden könnte.

Durch die gegenüber in der Klinik etablierten Magnetfeldstärken erhöhte räumliche Auflösung in dieser Studie, konnten in anatomischen CINE-Bildern von HCM-Patienten feine Kavitäten im Myokard detektiert werden, die bei 1.5 T und 3.0 T nicht zu sehen waren. Auch diese Informationen könnte zu einem besseren Verständnis und einer verbesserten Diagnostik der Krankheit beitragen [17].

Während bisher aufgrund der permanenten Bewegung des Herzens eine Auswertung von T_2^*-Änderungen über den Herzzyklus nur in größeren Regionen wie etwa dem ventrikulären Septum möglich ist, würde eine Bewegungskompensierung der Bilddaten auch eine lokale Untersuchung von T_2^*-Änderungen zulassen. Erste, vor-

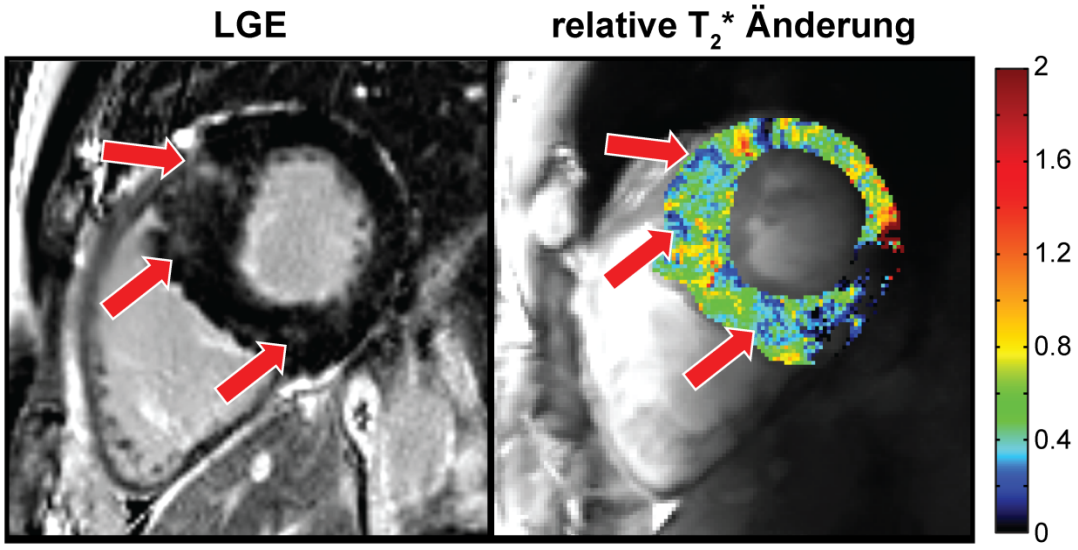

Abbildung 11: *Untersuchung von lokalen T_2^*-Änderungen über den Herzzyklus zur nichtinvasiven kontrastmittelfreien Gewebecharakterisierung. Vergleich von Late Gadolinium Enhancement (LGE) und lokaler relativer T_2^*-Änderung über den Herzzyklus auf Basis bewegungskompensierter Bilddaten.*

läufige Ergebnisse lassen vermuten, dass sich gesundes und erkranktes Herzgewebe anhand der T_2^*-Änderung über den Herzzyklus unterscheiden lassen (Abbildung 11). Damit würde durch zeitlich und räumlich aufgelöste T_2^*-Kartierung eine völlig neuartige Art der nicht-invasiven Gewebecharakterisierung des Herzens möglich. Denkbar sind etwa die Bestimmung von Parametern wie relativer Änderung, Anstieg oder maximaler Amplitude von T_2^*, die als Karten dargestellt werden können.

Die im Rahmen dieser Arbeit vorgestellten Ergebnisse stellen einen wichtigen Schritt auf dem Weg zu einer klinischen Anwendung der Technik als Möglichkeit zur nicht-invasiven Gewebecharakterisierung des Myokards dar. Sie bilden den Ausgangspunkt für weitere, breiter angelegte Studien zur Erforschung der klinischen Anwendbarkeit und des Nutzens der myokardialen Gewebecharakterisierung mittels T_2^*-Kartierung bei ultrahohen Feldstärken. Als wichtige Voraussetzung dafür wurde gezeigt, dass MRT-Untersuchungen des Herzens auch bei ultrahohen Magnetfeldstärken bei den untersuchten Personen eine hohe Akzeptanz erzielen und die höhere Magnetfeldstärke keine Nebenwirkungen verursacht, welche eine Kontraindikation für eine klinische Nutzbarkeit der Technik darstellen würden.

Literaturverzeichnis

[1] Meloni A, Hezel F, Positano V, Keilberg P, Pepe A, Lombardi M, Niendorf T. Detailing magnetic field strength dependence and segmental artifact distribution of myocardial effective transverse relaxation rate at 1.5, 3.0, and 7.0 T. Magnetic Resonance in Medicine. 2014;71:2224-2230.

[2] Yablonskiy DA, Haacke EM. Theory of NMR signal behavior in magnetically inhomogeneous tissues: the static dephasing regime. Magnetic Resonance in Medicine. 1994;32:749-763.

[3] Christen T, Lemasson B, Pannetier N, Farion R, Segebarth C, Rémy C, Barbier EL. Evaluation of a quantitative blood oxygenation level-dependent (qBOLD) approach to map local blood oxygen saturation. NMR Biomed. 2011;24:393-403.

[4] Li TQ, van Gelderen P, Merkle H, Talagala L, Koretsky AP, Duyn J. Extensive heterogeneity in white matter intensity in high-resolution T2*-weighted MRI of the human brain at 7.0 T. Neuroimage. 2006;32:1032-1040.

[5] Lee J, van Gelderen P, Kuo LW, Merkle H, Silva AC, Duyn JH. T2*-based fiber orientation mapping. Neuroimage. 2011;57:225-234.

[6] Wacker CM, Bock M, Hartlep AW, Beck G, van Kaick G, Ertl G, Bauer WR, Schad LR. Changes in myocardial oxygenation and perfusion under pharmacological stress with dipyridamole: assessment using T*2 and T1 measurements. Magnetic Resonance in Medicine. 1999;41:686-695.

[7] Friedrich M, Niendorf T, Schulz-Menger J. Blood oxygen level-dependent magnetic resonance imaging in patients with stress-induced angina. ACC Current Journal Review. 2004;13:30.

[8] Jahnke C, Gebker R, Manka R, Schnackenburg B, Fleck E, Paetsch I. Navigator-gated 3D blood oxygen level–dependent CMR at 3.0-T for detection of stress-induced myocardial ischemic reactions. JACC: Cardiovascular Imaging. 2010;3:375-384.

[9] Utz W, Jordan J, Niendorf T, Stoffels M, Luft FC, Dietz R, Friedrich MG. Blood oxygen level-dependent MRI of tissue oxygenation: relation to endothelium-dependent and endothelium-independent blood flow changes. Arterioscler Thromb Vasc Biol. 2005;25:1408-1413.

[10] Guensch DP, Fischer K, Flewitt JA, Yu J, Lukic R, Friedrich JA, Friedrich MG. Breathing manoeuvre-dependent changes in myocardial oxygenation in healthy humans. Eur Heart J Cardiovasc Imaging. 2014;15:409-414.

[11] Guensch DP, Fischer K, Flewitt JA, Friedrich MG. Impact of intermittent apnea on myocardial tissue oxygenation–a study using oxygenation-sensitive cardiovascular magnetic resonance. PLoS One. 2013;8:e53282.

[12] He T. Cardiovascular magnetic resonance T2* for tissue iron assessment in the heart. Quant Imaging Med Surg. 2014;4:407-412.

[13] Niendorf T, Paul K, Oezerdem C, Graessl A, Klix S, Huelnhagen T, Hezel F, Rieger J, Waiczies H, Frahm J, Nagel AM, Oberacker E, Winter L. W(h)ither human cardiac and body magnetic resonance at ultrahigh fields? technical advances, practical considerations, applications, and clinical opportunities. NMR Biomed. 2016;29:1173-1197.

[14] Niendorf T, Schulz-Menger J, Paul K, Huelnhagen T, Ferrari VA, Hodge R. High Field Cardiac Magnetic Resonance Imaging: A Case for Ultrahigh Field Cardiac Magnetic Resonance. Circ Cardiovasc Imaging. 2017;10.

[15] Hezel F, Thalhammer C, Waiczies S, Schulz-Menger J, Niendorf T. High spatial resolution and temporally resolved T2* mapping of normal human myocardium at 7.0 Tesla: an ultrahigh field magnetic resonance feasibility study. PLoS One. 2012;7:e52324.

[16] Huelnhagen T, Paul K, Ku M-C, Serradas Duarte T, Niendorf T. Myocardial T2* Mapping with Ultrahigh Field Magnetic Resonance: Physics and Frontier Applications Frontiers in Physics. 2017;5.

[17] Prothmann M, von Knobelsdorff-Brenkenhoff F, Topper A, Dieringer MA, Shahid E, Graessl A, Rieger J, Lysiak D, Thalhammer C, Huelnhagen T, Kellman P, Niendorf T, Schulz-Menger J. High Spatial Resolution Cardiovascular Magnetic Resonance at 7.0 Tesla in Patients with Hypertrophic Cardiomyopathy - First Experiences: Lesson Learned from 7.0 Tesla. PLoS One. 2016;11:e0148066.

[18] Mozaffarian D, Benjamin EJ, Go AS, Arnett DK, Blaha MJ, Cushman M, Das SR, de Ferranti S, Després J-P, Fullerton HJ. Heart Disease and Stroke Statistics—2016 Update A Report From the American Heart Association. Circulation. 2015:CIR. 0000000000000350.

[19] Semsarian C, Ingles J, Maron MS, Maron BJ. New perspectives on the prevalence of hypertrophic cardiomyopathy. J Am Coll Cardiol. 2015;65:1249-1254.

[20] Ogawa S, Lee TM, Kay AR, Tank DW. Brain magnetic resonance imaging with contrast dependent on blood oxygenation. Proc Natl Acad Sci USA. 1990;87:9868-9872.

[21] Christen T, Zaharchuk G, Pannetier N, Serduc R, Joudiou N, Vial JC, Remy C, Barbier EL. Quantitative MR estimates of blood oxygenation based on T2*: a numerical study of the impact of model assumptions. Magnetic Resonance in Medicine. 2012;67:1458-1468.

[22] Ziener CH, Kampf T, Melkus G, Jakob PM, Schlemmer HP, Bauer WR. Signal evolution in the local magnetic field of a capillary - analogy to the damped driven harmonic oscillator. Magn Reson Imaging. 2012;30:540-553.

[23] Huelnhagen T, Hezel F, Serradas Duarte T, Pohlmann A, Oezerdem C, Flemming B, Seeliger E, Prothmann M, Schulz-Menger J, Niendorf T. Myocardial Effective Transverse Relaxation Time T2* Correlates With Left Ventricular Wall Thickness: A 7.0 T MRI Study. Magnetic Resonance in Medicine. 2017;77:2381-2389.

[24] Manjon JV, Coupe P, Marti-Bonmati L, Collins DL, Robles M. Adaptive non-local means denoising of MR images with spatially varying noise levels. Journal of Magnetic Resonance Imaging. 2010;31:192-203.

[25] Huelnhagen T, Pohlmann A, Niendorf T. Improving T2* mapping accuracy by spatially adaptive non local means noise filtering. Proc Intl Soc Mag Reson Med 23; 2015; Toronto, Canada. p 3753.

[26] Heilmaier C, Theysohn JM, Maderwald S, Kraff O, Ladd ME, Ladd SC. A large-scale study on subjective perception of discomfort during 7 and 1.5 T MRI examinations. Bioelectromagnetics. 2011;32:610-619.

[27] Versluis MJ, Teeuwisse WM, Kan HE, van Buchem MA, Webb AG, van Osch MJ. Subject tolerance of 7 T MRI examinations. J Magn Reson Imaging. 2013;38:722-725.

[28] Rauschenberg J, Nagel AM, Ladd SC, Theysohn JM, Ladd ME, Moller HE, Trampel R, Turner R, Pohmann R, Scheffler K, Brechmann A, Stadler J, Felder J, Shah NJ, Semmler W. Multicenter study of subjective acceptance during magnetic resonance imaging at 7 and 9.4 T. Invest Radiol. 2014;49:249-259.

[29] Klix S, Els A, Paul K, Graessl A, Oezerdem C, Weinberger O, Winter L, Thalhammer C, Huelnhagen T, Rieger J, Mehling H, Schulz-Menger J, Niendorf T. On the subjective acceptance during cardiovascular magnetic resonance imaging at 7.0 Tesla. PLoS One. 2015;10:e0117095.

[30] Friedrich MG, Karamitsos TD. Oxygenation-sensitive cardiovascular magnetic resonance. J Cardiovasc Magn Reson. 2013;15:43.

[31] Abdel-Aty H, Cocker M, Strohm O, Filipchuk N, Friedrich MG. Abnormalities in T2-weighted cardiovascular magnetic resonance images of hypertrophic cardiomyopathy: regional distribution and relation to late gadolinium enhancement and severity of hypertrophy. J Magn Reson Imaging. 2008;28:242-245.

[32] Hueper K, Zapf A, Skrok J, Pinheiro A, Goldstein TA, Zheng J, Zimmerman SL, Kamel IR, Abraham R, Wacker F, Bluemke DA, Abraham T, Vogel-Claussen J. In hypertrophic cardiomyopathy reduction of relative resting myocardial blood flow is related to late enhancement, T2-signal and LV wall thickness. PLoS One. 2012;7:e41974.

[33] Johansson B, Mörner S, Waldenström A, Stål P. Myocardial capillary supply is limited in hypertrophic cardiomyopathy: a morphological analysis. Int J Cardiol. 2008;126:252-257.

[34] Cecchi F, Olivotto I, Gistri R, Lorenzoni R, Chiriatti G, Camici PG. Coronary microvascular dysfunction and prognosis in hypertrophic cardiomyopathy. New England Journal of Medicine. 2003;349:1027-1035.

[35] Ismail TF, Hsu L-Y, Greve AM, Gonçalves C, Jabbour A, Gulati A, Hewins B, Mistry N, Wage R, Roughton M. Coronary microvascular ischemia in hypertrophic cardiomyopathy-a pixel-wise quantitative cardiovascular magnetic resonance perfusion study. J Cardiovasc Magn Reson. 2014;16:49.

Eidesstattliche Versicherung

„Ich, Till Hülnhagen, versichere an Eides statt durch meine eigenhändige Unterschrift, dass ich die vorgelegte Dissertation mit dem Thema: „Entwicklung und Anwendung suszeptitätsgewichteter Magnetresonanztomografie für die Herzbildgebung bei ultrahohen Magnetfeldstärken“ selbstständig und ohne nicht offengelegte Hilfe Dritter verfasst und keine anderen als die angegebenen Quellen und Hilfsmittel genutzt habe.

Alle Stellen, die wörtlich oder dem Sinne nach auf Publikationen oder Vorträgen anderer Autoren beruhen, sind als solche in korrekter Zitierung (siehe „Uniform Requirements for Manuscripts (URM)“ des ICMJE -*www.**icmje**.org*) kenntlich gemacht. Die Abschnitte zu Methodik (insbesondere praktische Arbeiten, Laborbestimmungen, statistische Aufarbeitung) und Resultaten (insbesondere Abbildungen, Graphiken und Tabellen) entsprechen den URM (s.o) und werden von mir verantwortet.

Meine Anteile an den ausgewählten Publikationen entsprechen denen, die in der untenstehenden gemeinsamen Erklärung mit dem/der Betreuer/in, angegeben sind. Sämtliche Publikationen, die aus dieser Dissertation hervorgegangen sind und bei denen ich Autor bin, entsprechen den URM (s.o) und werden von mir verantwortet.

Die Bedeutung dieser eidesstattlichen Versicherung und die strafrechtlichen Folgen einer unwahren eidesstattlichen Versicherung (§156,161 des Strafgesetzbuches) sind mir bekannt und bewusst.“

_____ _____

Datum Unterschrift

Anteilserklärung an den erfolgten Publikationen

Till Hülnhagen hatte folgenden Anteil an den folgenden Publikationen:

Publikation 1: Klix S, Els A, Paul K, Graessl A, Oezerdem C, Weinberger O, Winter L, Thalhammer C, **Huelnhagen T**, Rieger J, Mehling H, Schulz-Menger J, Niendorf T. On the subjective acceptance during cardiovascular magnetic resonance imaging at 7.0 Tesla. PLoS One 2015;10(1):e0117095. DOI: 10.1371/journal.pone.0117095
Journal Impact Factor 2016: 2.806
Beitrag im Einzelnen:

- Messaufbau und -durchführung für 20% der Teilnehmer
- Messung und Auswertung des Geschwindigkeitsprofils des Patiententisches
- Revision des Manuskripts

Publikation 2: Prothmann M, von Knobelsdorff-Brenkenhoff F, Töpper A, Dieringer MA, Shahid E, Graessl A, Rieger J, Lysiak D, Thalhammer C, **Huelnhagen T**, Kellman P, Niendorf T, Schulz Menger J. High Spatial Resolution Cardiovascular Magnetic Resonance at 7.0 Tesla in Patients with Hypertrophic Cardiomyopathy–First Experiences: Lesson Learned from 7.0 Tesla. PLoS One 2016;11(2):e0148066. DOI: 10.1371/journal.pone.0148066
Journal Impact Factor 2016: 2.806
Beitrag im Einzelnen:

- MR Protokoll Anpassungen
- Durchführung und Kontrolle des Messaufbaus für 90% der Messungen
- Anpassung und Kontrolle des B_0 Shimming für 90% der Messungen
- Revision des Manuskripts

Publikation 3: Niendorf T, Paul K, Oezerdem C, Graessl A, Klix S, **Huelnhagen T**, Hezel F, Rieger J, Waiczies H, Frahm J, Nagel AM, Oberacker E, Winter L. W(h)ither human cardiac and body magnetic resonance at ultrahigh fields? technical advances, practical considerations, applications, and clinical opportunities. NMR Biomed 2016;29(9):1173-1197. DOI: 10.1002/nbm.3268
Journal Impact Factor 2016: 2.872
Beitrag im Einzelnen:

- Abschnitt zu myokardialer T_2* Kartierung
- Erstellung von Abbildungen 7 und 11 und zugehörige Datenverarbeitung
- Überarbeitung Abbildung 14
- Revision des Manuskripts

Publikation 4: Niendorf T, Schulz Menger J, Paul K, **Huelnhagen T**, Ferrari VA, Hodge R. High Field Cardiac Magnetic Resonance Imaging: A Case for Ultrahigh Field Cardiac Magnetic Resonance. Circ Cardiovasc Imaging. 2017. DOI: 10.1161/CIRCIMAGING.116.005460
Journal Impact Factor 2016: 6.803
Beitrag im Einzelnen:

- Abschnitt zu Myocardial Tissue Characterization and Phenotyping
- Erstellung von Abbildung 6

- Überarbeitung Abbildung 1
- Revision des Manuskripts

Publikation 5: **Huelnhagen T**, Paul K, Ku M-C, Serradas Duarte T, Niendorf T. Myocardial T2* Mapping at Ultrahigh Field: Physics and Frontier Applications. Frontiers in Physics. 2017:5. DOI: 10.3389/fphy.2017.00022
Journal Impact Factor: nicht verfügbar
Beitrag im Einzelnen:

- Konzeption
- Literaturrecherche
- Versuchsaufbau und Datenakquisition
- Auswertung und Interpretation der Daten
- Entwurf des Manuskripts und Erstellung der Abbildungen 1,2,5,6,10,11,12,13
- Revision des Manuskripts

Publikation 6: **Huelnhagen T**, Hezel F, Serradas Duarte T, Pohlmann A, Oezerdem C, Flemming B, Seeliger E, Prothmann M, Schulz-Menger J, Niendorf T. Myocardial Effective Transverse Relaxation Time T2* Correlates With Left Ventricular Wall Thickness: A 7.0 T MRI Study. Magn Reson Med 2017;77:2381-2389. DOI: 10.1002/mrm.26312
Journal Impact Factor 2016: 3.924
Beitrag im Einzelnen:

- Konzeption
- Literaturrecherche
- Anpassung der Messsequenzen
- Durchführung von Simulationen
- Versuchsaufbau und Datenakquisition
- Entwicklung der Auswertungsprogramme
- Auswertung und Interpretation der Daten
- Entwurf des Manuskripts und Erstellung der Abbildungen 2,3,4,5,6
- Revision des Manuskripts

Unterschrift, Datum und Stempel des betreuenden Hochschullehrers

_____
Prof. Dr. rer. nat. Thoralf Niendorf

Unterschrift des Doktoranden

_____
Till Hülnhagen

PLOS ONE

RESEARCH ARTICLE

On the Subjective Acceptance during Cardiovascular Magnetic Resonance Imaging at 7.0 Tesla

Sabrina Klix[1], Antje Els[1], Katharina Paul[1], Andreas Graessl[1], Celal Oezerdem[1], Oliver Weinberger[1], Lukas Winter[1], Christof Thalhammer[1], Till Huelnhagen[1], Jan Rieger[1], Heidrun Mehling[2], Jeanette Schulz-Menger[2,3], Thoralf Niendorf[1,2]*

1 Berlin Ultrahigh Field Facility (B.U.F.F.), Max-Delbrueck-Center for Molecular Medicine, Berlin, Germany, **2** Experimental and Clinical Research Center (ECRC), a joint cooperation between the Charité Medical Faculty and the Max-Delbrueck-Center for Molecular Medicine, Berlin, Germany, **3** HELIOS Klinikum Berlin-Buch, Dept. of Cardiology and Nephrology, 13125 Berlin, Germany

* Thoralf.Niendorf@mdc-berlin.de

OPEN ACCESS

Citation: Klix S, Els A, Paul K, Graessl A, Oezerdem C, Weinberger O, et al. (2015) On the Subjective Acceptance during Cardiovascular Magnetic Resonance Imaging at 7.0 Tesla. PLoS ONE 10(1): e0117095. doi:10.1371/journal.pone.0117095

Academic Editor: Sonja Kinner, University Hospital Essen, GERMANY

Received: August 13, 2014

Accepted: December 18, 2014

Published: January 26, 2015

Data Availability Statement: All the relevant data for this study is available from the http://figshare.com database (figshare.com/s/205e6d4a552511e4856c06ec4bbcf141, http://dx.doi.org/10.6084/m9.figshare.1206313.

Funding: This work was supported (in part, C.O.) by the DZHK (German Centre for Cardiovascular Research) and by the BMBF (Federal Ministry of Education and Research). This work was funded (in part, A.G.) by the Helmholtz Alliance ICEMED—Imaging and Curing Environmental Metabolic Diseases, through the Initiative and Network Fund of the Helmholtz Association (ICEMED-Project

Abstract

Purpose

This study examines the subjective acceptance during UHF-CMR in a cohort of healthy volunteers who underwent a cardiac MR examination at 7.0T.

Methods

Within a period of two-and-a-half years (January 2012 to June 2014) a total of 165 healthy volunteers (41 female, 124 male) without any known history of cardiac disease underwent UHF-CMR. For the assessment of the subjective acceptance a questionnaire was used to examine the participants experience prior, during and after the UHF-CMR examination. For this purpose, subjects were asked to respond to the questionnaire in an exit interview held immediately after the completion of the UHF-CMR examination under supervision of a study nurse to ensure accurate understanding of the questions. All questions were answered with “yes” or “no” including space for additional comments.

Results

Transient muscular contraction was documented in 12.7% of the questionnaires. Muscular contraction was reported to occur only during periods of scanning with the magnetic field gradients being rapidly switched. Dizziness during the study was reported by 12.7% of the subjects. Taste of metal was reported by 10.1% of the study population. Light flashes were reported by 3.6% of the entire cohort. 13% of the subjects reported side effects/observations which were not explicitly listed in the questionnaire but covered by the question about other side effects. No severe side effects as vomiting or syncope after scanning occurred. No increase in heart rate was observed during the UHF-CMR exam versus the baseline clinical examination.

1210251). L.W. received support by the BMBF (Federal Ministry of Education and Research, "KMU-innovativ": Medizintechnik MED-373-046). The funders had no role in study design, data collection and analysis, decision to publish, or preparation of the manuscript.

Competing Interests: The authors declare that they have no competing interests with the exception of (i) Christof Thalhammer is currently a contractor and Ph. D. student with Siemens Corporate Technology, München, Germany, and (ii) Thoralf Niendorf and Jan Rieger are founders of MRI.TOOLS GmbH, Berlin, Germany. This does not alter the authors' adherence to PLOS ONE policies on sharing data and materials.

Conclusions

This study adds to the literature by detailing the subjective acceptance of cardiovascular magnetic resonance imaging examinations at a magnetic field strength of 7.0T. Cardiac MR examinations at 7.0T are well tolerated by healthy subjects. Broader observational and multi-center studies including patient cohorts with cardiac diseases are required to gain further insights into the subjective acceptance of UHF-CMR examinations.

Introduction

A growing number of reports refer to explorations into cardiovascular magnetic resonance (CMR) at ultrahigh magnetic field strengths (UHF-CMR, $B_0 \geq 7.0T$) [1–5]. These developments are fueled by the signal-to-noise ratio advantage inherent to higher magnetic field strengths and supported by enabling RF coil technology in conjunction with novel imaging methodology. Pilot studies and early applications of UHF-CMR include cardiac chamber quantification of the left [6–9] and right ventricle [10]. Other studies demonstrated the feasibility of high spatial resolution coronary artery imaging [11–13], temporally resolved myocardial T_2* mapping [14,15], parametric imaging of myocardial T_1 [16,17] and first-pass myocardial perfusion imaging [18]. Explorations into non-proton MR applications involved localized ^{31}P cardiac magnetic resonance spectroscopy [19] and cardiac gated sodium imaging of the heart [20,21]. The implications of these pilot studies feed into a broad spectrum of cardiology, radiology, biomedical engineering and other related fields of clinical research. Arguably, it is too early in the development process to make ultimate statements since UHF-CMR is still in its infancy and the potential of UHF-MR is as yet untapped. It is no secret that the advantages of UHF-CMR are sometimes offset by a number of concomitant physics related phenomena and practical obstacles which can make it a challenge to even compete with the capabilities of CMR at lower fields [2,3]. As UHF-CMR applications become increasingly used for research, they should however help to advance the capabilities of MR for the assessment of cardiovascular diseases but still need to continue to be very carefully validated against CMR applications established at 1.5 T and 3.0 T.

En route to broader UHF-CMR studies it is of relevance to examine how UHF-CMR examinations are tolerated by subjects. Practical concerns evoked by the physical size, the mere bore length of today's 7.0 T MR scanner and the paucity of data about ergonomic constraints, (dis) comfort and sensory side effects are driving the notion that UHF-MR constitutes a challenge for subject tolerance of 7.0 T examinations *per se*. Recognizing this potential, UHF-MR institutions observe subjective acceptance during UHF-MR examinations very carefully [22–25]. The lack of data prompted research into human exposure to ultrahigh magnetic fields and related biophysical and biological effects [26–28], vital signs [29,30], cognitive function [30–34], and stress [35]. Explorations into subject tolerance, subjective perception and sensory side effects during UHF-MR examinations include pioneering single- and multi-centre studies covering static magnetic fields of 7.0 T and higher, RF power deposition induced temperature sensations and spatially varying or rapidly switching magnetic field gradients as potential root causes for discomfort [22–25].

While being very important and valuable the results obtained from these pioneering studies are largely constrained to brain imaging [22–25] so that the conclusions drawn on subjective acceptance do not involve the specific characteristics of UHF-CMR. These particularities include the use of local cardiac-optimized transceiver RF coil arrays covering the upper torso by

means of anterior and posterior coil sections rather than volume RF coils surrounding the head. This difference in the setup has implications for subjective discomfort and distress potentially caused by space constraints and the weight of the anterior RF coil section, as well as for RF power deposition considerations and for thermal isolation of the upper torso induced by the relatively large-area RF coil covers. It is common in brain MRI to attach a mirror to the head coil, which enhances subject comfort by allowing a view out of the magnet bore or onto a display featuring animations; an approach which is not common in CMR. Unlike brain MRI the head is not positioned in the magnet's iso-center for UHF-CMR which might affect the propensity to vertigo, dizziness, metallic taste and light flashes. Likewise, the travel distance of the subject being positioned on the patient table from the home position to the target position is pronounced for UHF-CMR versus brain imaging. With the upper torso being positioned in the magnet's iso-center for an UHF-CMR examination rapidly switching magnetic field gradients bear the potential to provoke peripheral nerve stimulations (PNS) rates owing to induced electric currents in the body which might differ from PNS rates and regions reported for brain UHF-MR. Extra sensors, ancillary hardware and cabling used to record and track physiological motion for gating/triggering might provide another factor that governs subjective tolerance during UHF-CMR.

Realizing the limitations of previous reports on subjective tolerance during UHF-MR and recognizing the particularities of cardiac MR this study examines the subjective acceptance during UHF-CMR examinations. To meet this goal, a cohort of healthy 165 subjects who underwent a cardiac MR examination at 7.0 T in our institution was asked to fill out a questionnaire under supervision of a study nurse.

Materials and Methods

Subjects and subject preparation

Within the period January 2012 to June 2014 a total of 165 healthy volunteers without any known history of cardiac disease underwent UHF-CMR. All volunteers underwent a medical informed consent discussion including a basic clinical examination prior to the UHF-CMR session. Medical history was taken by a clinician. The basic clinical examination included the recording and documentation of height, body weight, body mass index, heart rate, blood pressure, temperature, sex and date of birth in a Case Report Form (CRF). Female subjects underwent a pregnancy test. If this test indicated pregnancy subjects were excluded. Contraindications for UHF-MR were observed very carefully. Subjects with cardiac pacemakers, tattoos, conducting implants or metal clips were excluded. Prior to the actual MR investigation subjects were informed about potential side effects covering vertigo, nausea, dizziness, metallic taste, light flashes, peripheral nerve stimulation and feeling of cold or heat. This standardized information was provided by the same study nurse. No mention was made that these sensations might be more pronounced versus clinical 1.5 T or 3.0 T MR scanners. All subjects were advised that the MR images acquired during the UHF-CMR session are not used for diagnostic purposes. To meet data protection requirements, data were rendered pseudoanonymized.

Each subject was asked to wear MR safe clothes without zippers or snaps provided by our institution. During the examination, the heart rate of each subject was monitored using pulse oximetry and a MR compatible stethoscope (EasyACT, MRI.TOOLS GmbH, Berlin, Germany). The latter was used for cardiac gating and triggering [36–39]. To ensure communication with the research staff operating the scanner, each subject was able to communicate via a two way speaker system and was equipped with an emergency squeeze bulb. For acoustic noise protection each subject received earplugs (3M^{TM} earplugs 1100, Neuss, Germany, noise reduction = -37dB) and headphones (Siemens Healthcare, Erlangen, German, noise

reduction = -14dB). Each subject was covered with a blanket reaching up to the torso. The subjects' head was not fixated but placed on a pad which conveniently conforms to the shape of the head.

Ethics Statement

For the entire cohort, 165 healthy subjects without known history of cardiac diseases (41 female, 124 male, mean age: 36 ± 12 years, mean BMI: 23.6 ± 3.3 kg/m^2, mean heart rate: 69 ± 12 bpm) were included after due approval by the local ethical committee (registration number DE/CA73/5550/09; Landesamt für Arbeitsschutz, Gesundheitsschutz und technische Sicherheit, Berlin, Germany). Informed written consent was obtained from each volunteer prior to the study.

MR equipment at 7 T

All cardiac MR experiments were conducted on a 7.0 T whole body MR scanner (Magnetom, Siemens Healthcare, Erlangen, Germany), with a bore size of 60 cm and a magnet length of 337 cm. The scanner was equipped with a gradient system offering a maximum slew rate of 170 mT/m/ms and a maximum gradient strength of 26 mT/m per axis (Siemens Healthcare, Erlangen, Germany) and an 8-kW single channel RF amplifier (Stolberg HF-Technik AG, Stolberg-Vicht, Germany). A synopsis of the MR system characteristics is listed in Table 1.

Subjects were positioned supine and head-first in the magnet. To reduce if not eliminate side effects caused by spatially-varying magnetic fields the 7.0 T system is equipped with a logic that controls the patient table speed profile. Our measurements showed that a table speed of v_{poti} = 25 mm/s is used when moving the table from its home position towards the magnet's isocenter. This includes regions with pronounced $B_0*(\mathrm{grad}(B_0))$ ranging from approximately 60 cm to approximately 200 cm from the magnet's isocenter. With the subject being positioned head first our measurements revealed that the table speed changes into v_{iso} = 60 mm/s at a head position of approximately 45 cm from the isocenter. This speed is maintained until the head or heart is positioned in the isocenter.

Table 1. Synopsis of the characteristics of the 7.0 T whole body MR system used.

systems characteristics	
magnet bore	whole-body magnet
magnet length without cover	337 cm
scanner length including cover	400 cm
inner diameter	60 cm
diameter of flared opening	120 cm
length of flared opening	35 cm
patient table	
max. patient weight	200 kg
max. range	325 cm
patient table speed	(25–60) mm/s
patient comfort	
effective inner A-P diameter with patient table in the isocenter position	40 cm
in bore ventilation	can be set to 3 different levels
in bore intercom	including loudspeaker, microphone and earphones

doi:10.1371/journal.pone.0117095.t001

Table 2. Overview of the transceiver RF coil arrays (^{1}H, f = 298 MHz) coils employed.

RF coil design	number of RF coil elements	RF coil size head-feet x left-right (cm2)	RF coil weight (kg)	max local SAR (10g average) @ 1W input power in (W/kg)	subjects under-going an UHF-CMR examina-tion (n = 165)
four channel transmit/ receive loop coil array	2 anterior and 2 posterior loop elements	34x30 anterior 35x30 posterior	1.8 anterior 1.7 posterior	0.57	3
eight channel transmit/ receive loop coil array	5 anterior and 3 posterior loop elements	21x31 anterior 21x31 posterior	2.1 anterior 1.8 posterior	0.43	1
sixteen channel transmit/receive loop coil array	8 anterior and 8 posterior loop elements	33x33 anterior 45x34 posterior	2.1 anterior 2.7 posterior	0.36	50
modular 32-channel transmit/receive loop coil array	16 anterior and 16 posterior loop elements	32x37 anterior 32x37 posterior	1.6 anterior 1.6 posterior	0.9	40
8 channel transmit/ receive bow tie antenna array	4 anterior and 4 posterior bow tie antennas	15x32 anterior 15x32 posterior	2.6 anterior 2.6 posterior	0.6	26
16 channel transmit/ receive bow tie antenna array	8 anterior and 8 posterior bow tie antennas	31x32 anterior 31x32 posterior	5.3 anterior 5.3 posterior	0.34	45

doi:10.1371/journal.pone.0117095.t002

For signal excitation and reception local surface transmit/receive RF coil configurations tailored for ^{1}H cardiac MR were employed including (see Table 2 for details):

- a four channel transmit/receive loop coil array [40]
- an eight channel transmit/receive loop coil array [41]
- a sixteen channel transmit/receive loop coil array [9,42]
- a modular 32-channel transmit/receive loop coil array [43]
- an eight channel transmit/receive bow tie antenna array [44]
- a sixteen channel transmit/receive bow tie antenna array [45]

Prior to the volunteer study the RF coil configurations underwent safety assessment to confirm compliance with the relevant sections of IEC 60601–2–33:2010 Ed.3 and IEC 60601–1:2005 Ed.3 [46]. This procedure included numerical electromagnetic field (EMF) simulations together with specific absorption rate (SAR) assessment plus risk assessment and risk management procedures. For EMF simulations a finite integration technique of CST Studio Suite 2011 (CST AG, Darmstadt, Germany) and human voxel models Duke (BMI: 23.1) and Ella (BMI: 22) from the Virtual Family [47] were used to calculate the EMF fields and SAR. A single feeding RF power amplifier transmission mode was used together with fixed phase settings specific for each RF coil [9,40–45].

Cardiac imaging at 7.0 T

The UHF-CMR protocol included the following protocol as a minimum. Slice positioning was carried out following international consensus [48,49] based upon our previous report [7] For this purpose the heart was localized in three orthogonal thoracic slices placed along each main axis of the upper torso using single breath-hold, low spatial resolution 2D gradient echo acquisitions (matrix = 132 x 192, in-plane spatial resolution = (2.5 x 1.9)mm^2, slice thickness = 8mm, TR = 6.7 ms, TE = 1.35 ms , FOV = 360 mm, bandwidth = 651Hz/pixel). The long axis

Table 3. Overview of the parameters used for 2D CINE FLASH imaging of the heart at 7.0 T.

RF coils	spatial resolution (mm^3)	matrix size	FOV (mm^2)	TE (ms)	TR (ms)	receiver bandwidth (Hz/pixel)	acceleration factor
four channel TX/RX loop coil array	(1.4x1.4x4)	256x232	360x326	2.7	5.6	444	1–4
eight channel TX/RX loop coil array	(1.4x1.4x4)	256x232	360x326	2.7	5.6	444	1–4
sixteen channel TX/RX loop coil array	(1.4x1.4x4)	256x232	360x326	2.8	6.3	444	1–4
modular 32 channel TX/RX loop coil array	(1.1x1.1x2.5) (1.4x1.4x4) (1.8x1.8x6)	320x264 232x256 160x176	360x326	3.3 2.7 2.4	6.7 5.6 5.1	446 444 441	1–5
8 channel TX/RX bow tie antenna array	(1.4x1.4x4)	256x256	360x360	2.7	5.6	444	2
16 channel TX/RX bow tie antenna array	(0.8x0.8x2.5) (1.1x1.1x2.5) (1.4x1.4x4) (1.8x1.8x6)	380x464 260x320 208x256 170x208	360x326	2.2 2.1 1.7 1.7	4.8 4.6 4.2 4.0	445 446 444 431	1–6

doi:10.1371/journal.pone.0117095.t003

of the left ventricle (LV) was dissected twice, and finally a stack of short axis views was obtained. These slices provided the basis for planning standard long axis views (four-chamber, three-chamber and two-chamber view) derived from 2D CINE FLASH imaging.

Based on the four-chamber view, a mid-ventricular short axis view positioned parallel to the mitral valve plane was planned as a minimum for high spatial resolution CINE imaging. Alternatively a stack of mid-ventricular short axes views covering the complete LV in diastole was positioned parallel to the mitral valve plane. Short axis and long axis CINE views were acquired using single breath-hold 2D CINE FLASH imaging. Imaging parameters are summarized in Table 3.

Since these examinations were part of our development process the minimum protocol was supplemented by further research sequences on a case-by case basis. These efforts included localized B_0 shimming for the assessment of field dispersion across the heart, transmission field mapping, myocardial T_2* mapping, examination of parallel imaging performance, signal-to-noise ratio assessment, noise correlation measurements and fat-water imaging using methodology and parameters described in [9,10,14,15,42,43]. For all subjects the total duration of the UHF-CMR examination was recorded.

Assessment of subjective acceptance

For the assessment of the subjective acceptance a questionnaire was used to examine the participant's experience prior, during and after the UHF-CMR examination. The questionnaire is part of the documents included in our ethics approval. The subjects were kindly asked to respond to the questionnaire in an exit interview held immediately after the completion of the UHF-CMR examination under supervision of a study nurse to ensure accurate understanding of the questions. The questionnaire was setup by strictly following the guidelines given by our IRB approval. All questions were answered with "yes" or "no" including extra space for additional comments as shown in Table 4.

Statistical significance in the differences (i) between male and female subjects, (ii) between the coil configurations used and (iii) between 30 subjects covering the low end of the age range and 30 subjects covering the high end of the age range involved in this study was analyzed using IBM SPSS Statistics 22 (IBM, Ehningen, Germany). Pearson's analysis (Chi-square test) was applied [50]. A p-value $p<0.05$ was considered to be statistically relevant significant.

Table 4. Questionnaire which was completed by all subjects immediately after the completion of the UHF-CMR examination.

#	Question	yes	no	Comments
1	Did you feel dizziness prior to the study?			
2	Did you feel dizziness during the study?			
3	Did you feel dizziness after the study?			
4	Did you see light flashes?			
5	Did you feel heating?			
6	Did you feel cold?			
7	Did you feel unease?			
8	Did you recognize muscular contraction?			
9	Have you perceived a metallic taste?			
10	Have you noticed other side effects?			

doi:10.1371/journal.pone.0117095.t004

Results

The subject characteristics are listed in Table 5. During the UHF-CMR examination, a mean heart rate of 64 ± 7 bpm (min: 46 bpm, max: 91 bpm) was observed. In comparison, the clinical examination performed prior to the UHF-CMR exam yielded a mean heart rate of 69 ± 12 bpm (min: 47 bpm, max: 115 bpm). The mean scan time per subject was 64 ± 27min. Examples of short axis views acquired with the 6 RF coil configurations are demonstrated in Fig. 1.

Table 5. Overview of subject (n = 165) characteristics.

	total	female	male
number of questionnaires	165	41	124
mean age	36 ± 12	33 ± 11	37 ± 12
age range min	23	25	23
age range max	72	67	72
mean height (cm)	176 ± 9	167 ± 7	179 ± 7
height range min (cm)	158	158	165
height range max (cm)	196	183	196
mean weight (kg)	72.9 ± 11.8	63 ± 7.3	76.2 ± 11.1
weight range min (kg)	47.6	47.6	60.5
weight range max (kg)	114.0	83	114.0
mean BMI (kg/m^2)	23.6 ± 3.3	22.7 ± 2.7	23.9 ± 3.5
BMI range min (kg/m^2)	16.9	18.5	16.9
BMI range max (kg/m^2)	33.5	32	33.5
mean blood pressure (mmHg)	127/79 ± 14/11	123/76 ±14/10	129/80 ± 14/12
blood pressure range min (mmHg)	96/55	96/55	100/55
blood pressure range min (mmHg)	180/119	166/111	180/119
mean RR-interval (ms) (prior to UHF-MR exam)	892 ± 149	833 ± 136	912 ± 148
RR-interval range min (ms)	522	618	522
RR-interval range max (ms)	1277	1071	1277
mean heart rate (bpm) (prior to UHF-MR exam)	69 ± 12	74 ± 12	68 ± 12
heart rate range min (bpm)	47	56	47
heart rate range max (bpm)	115	97	115

(*Continued*)

Table 5. (*Continued*)

	total	female	male
mean RR-interval (ms) (during UHF-CMR exam)	945 ± 106	827 ± 78	985 ± 82
RR-interval range min (ms)	657	657	726
RR-interval range max (ms)	1296	1077	1296
mean heart rate (bpm) (during UHF-CMR exam)	64 ± 7	73 ± 7	61 ± 5
heart rate range min (bpm)	46	55	46
heart rate range max (bpm)	91	91	82
mean body temperature (°C)	36.4 ± 0.5	36.6 ± 0.4	36.3 ± 0.5
temperature range min (°C)	34.5	35.6	34.5
temperature range max (°C)	37.6	37.5	37.6
mean examination time (min)	64 ± 27	63 ± 17	65± 27
examination time min (min)	34	45	34
examination time max (min)	124	85	124

doi:10.1371/journal.pone.0117095.t005

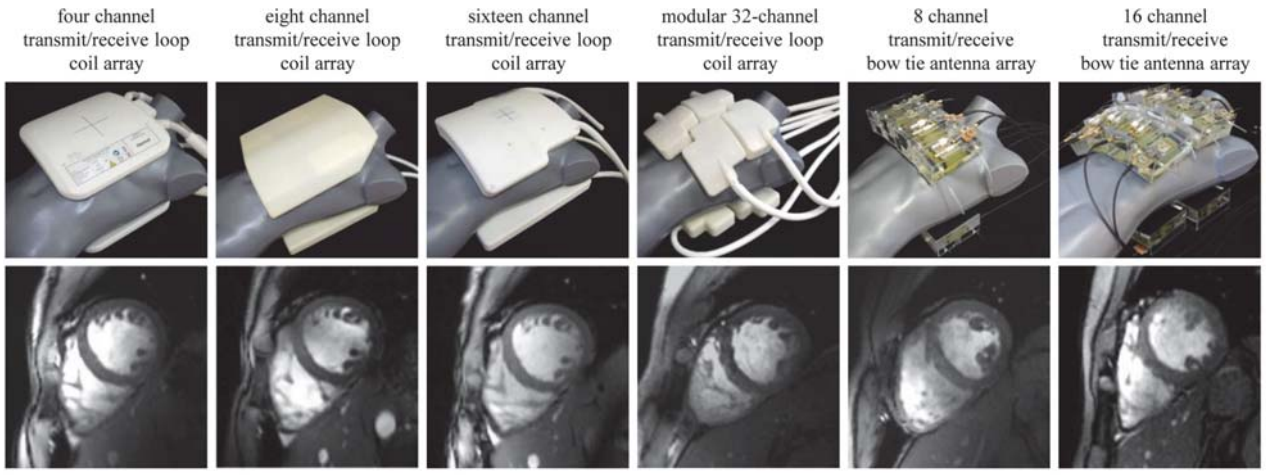

Figure 1. Synopsis of RF coil configurations used in this study. Top: Photographs of the cardiac optimized 7.0 T transceiver RF coil arrays to illustrate the coil design and the coil geometry together with the coil positioning used in the UHF-CMR setting. The RF coils employed include a four channel [40], an eight channel [41], a 16 channel [9,42] and a 32 channel loop coil [43] configuration and an eight channel [44] and 16 channel bow tie antenna array configuration [45]. **Bottom:** Short axis views of the heart derived from 2D CINE FLASH acquisitions using the RF coil configurations in the top row and a spatial resolution of (1.4 x 1.4 x 4) mm^3 and parallel imaging (R = 2, GRAPPA reconstruction).

doi:10.1371/journal.pone.0117095.g001

No subject aborted the UHF-CMR examination. Throughout the study, there were no injuries or other incidents. A total of 165 questionnaires (male 124, female 41) were completed and included into the analysis.

A synopsis of the evaluation of the questionnaires is provided in Fig. 2. The gender distribution of the reported sensory side effects is shown in detail in Fig. 3. Major differences in response to question 1–9 were not observed for the RF coil configurations used; with the exception of question 8 for which Pearson's analysis provided p = 0.015.

The analysis of the questionnaires showed that muscular contraction during scanning was found to be among the two most frequently reported side effects. This peripheral nerve

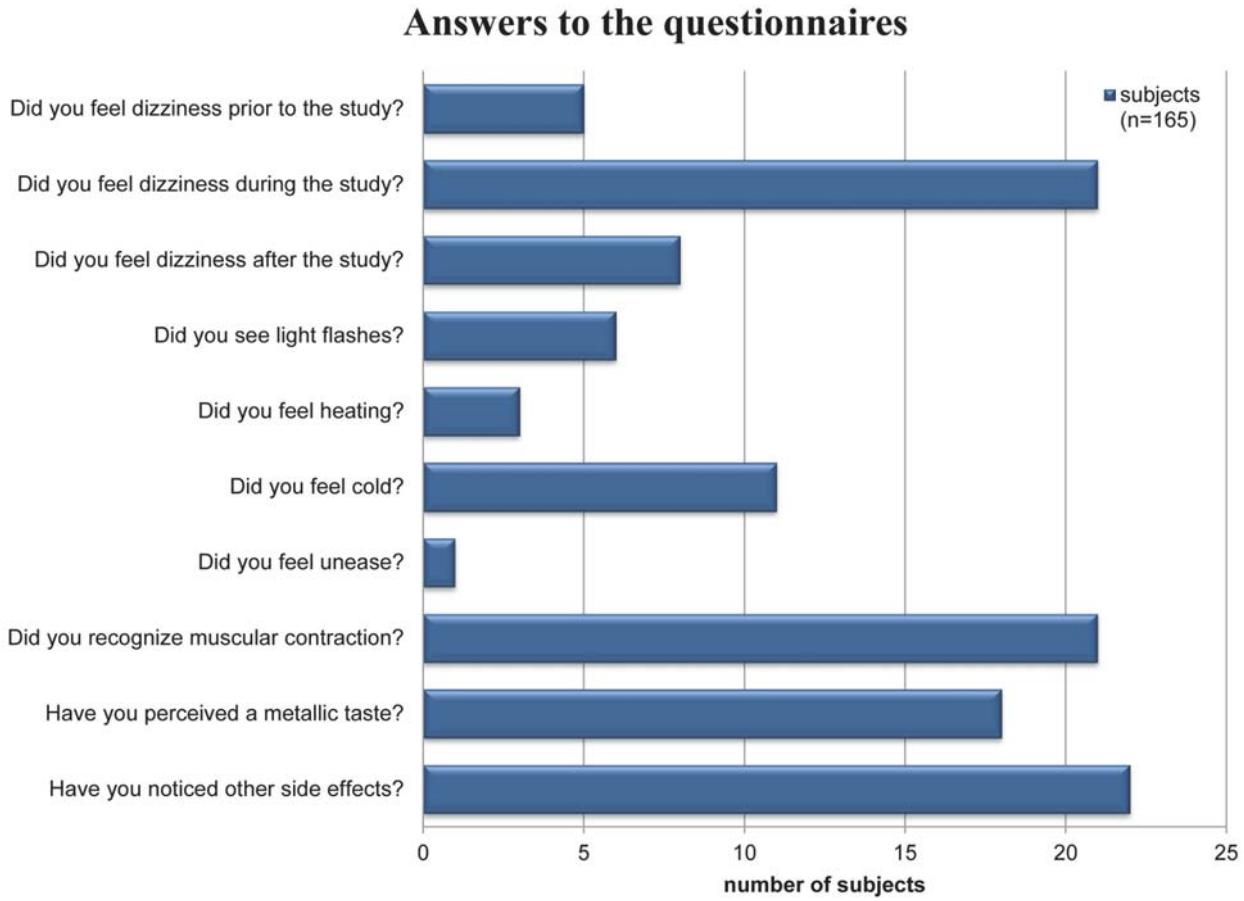

Figure 2. Results derived from the completed questionnaires. Synopsis of the results reported by 165 subjects on subjective acceptance of UHF-CMR. The most mentioned side effects reported were transient muscular contraction during scanning (12.7%) and dizziness experienced during the study (12.7%).

doi:10.1371/journal.pone.0117095.g002

stimulation induced sensation was reported by 21 out of 165 subjects which represents 12.7% of the cohort investigated. A closer examination revealed that this phenomenon was reported by one female and 20 male subjects, which corresponds to 2.4% out of all female and 16.1% out of all male subjects. Pearson's analysis provided $p = 0.023$ for the gender dependence of muscular contraction. Muscular contraction was reported as a transient symptom. In most cases transient muscular contraction symptoms occurred in the leg, but also in the shoulder or in the abdomen and pelvis. Muscular contraction occurred only during periods of scanning with the magnetic fields gradients being rapidly switched while strictly staying within the specifications and limits for gradient duty cycle, slew rates and maximum gradient amplitudes given by the MR manufacturer.

Dizziness during the study was reported with the same frequency as muscular contraction. A total of 21 subjects (12.7%) documented dizziness experienced during the UHF-CMR examination. This effect was noticed by 4 female (9.8% of female subjects) and 17 male (13.7% of male subjects) subjects. In comparison, 5 subjects (2.4% of female subjects and 3.2% of male subjects) outlined the occurrence of dizziness prior to the UHF-CMR examination. eight subjects (in total 4.8%, 3 female, 5 male) affirmed that dizziness occurred after completion of the

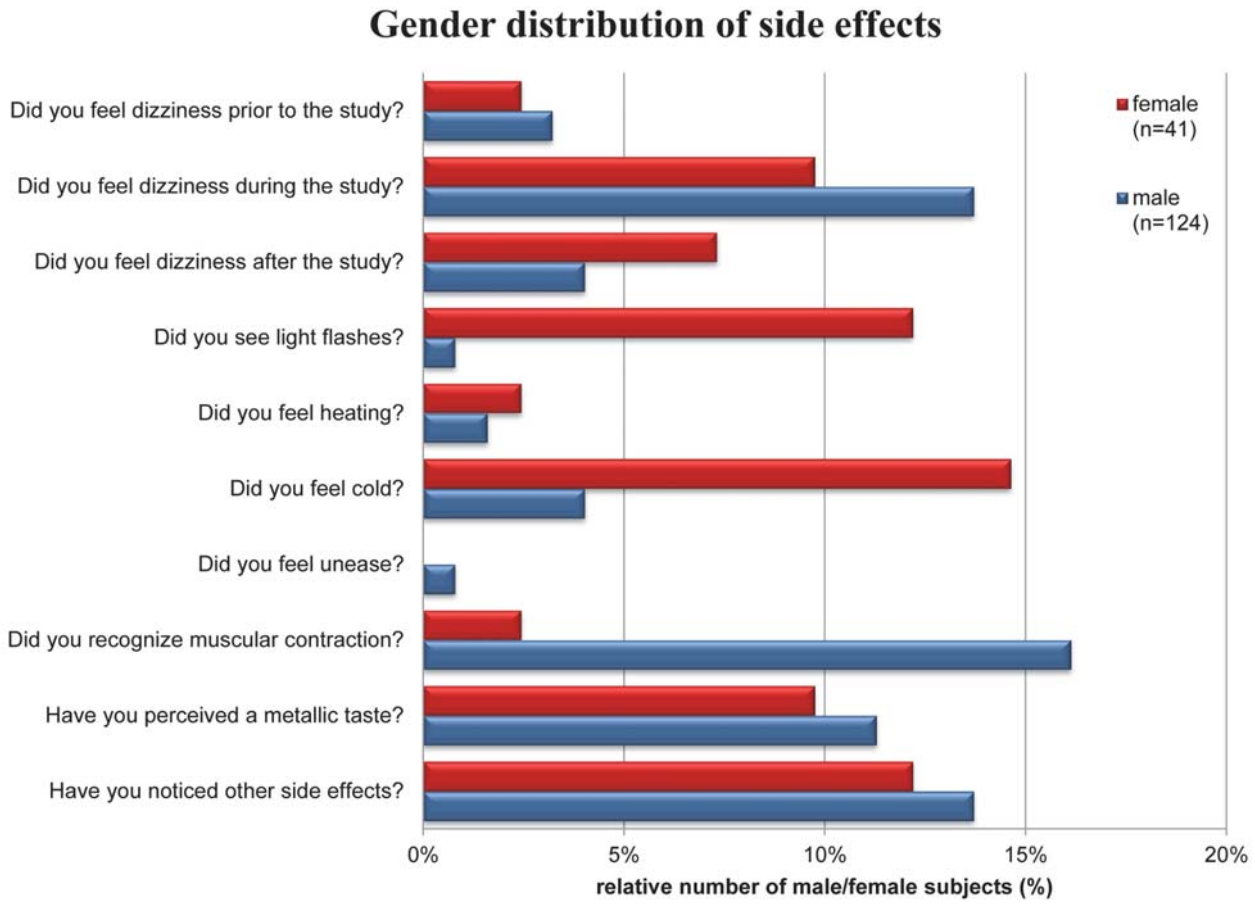

Figure 3. Gender distribution of reasons of discomfort. Synopsis of reasons of discomfort reported by female and male subjects who underwent an UHF-CMR examination.

doi:10.1371/journal.pone.0117095.g003

UHF-CMR exam. After completion of the study the symptoms were completely resolved within a maximum period of 10 minutes. The subjects which reported dizziness showed an average blood pressure of 135/72 mmHg and an average heart rate of 73 bpm.

Taste of metal was mentioned by 18 subjects which represents 10.1% of the study population. In detail, taste of metal was pointed out by 4/41 female and 14/124 male subjects. Further sensations documented by the subjects in the questionnaires were light flashes which were reported by 6 out of 165 subjects, which correspond to 3.6% of the entire cohort. This includes 5 female (12.2%) and one male (0.8%) subject. Pearson's analysis provided $p = 0.001$ for the gender dependence of reports on light flashes.

Feeling of heat was reported by 3 subjects (female: 2.4%, male 1.6%). Feeling of cold was outlined by 11 subjects, which represents 6.6% of the study population. In detail, cold was pointed out by 14.6% of the female and by 4% of the male subjects. Pearson's analysis provided $p = 0.018$ for the gender dependence of feeling of cold.

Out of 165 subjects, 22 subjects reported side effects/observations which were not explicitly listed in the questionnaire but covered by the question about other side effects and observations. These comments are summarized in Table 6. We noted that 30% of the subjects belonging to a sub-group of 30 subjects covering the high end of the age range (age 51–72) reported

Table 6. Summary of other side effects revealed by the question: "Have you noticed other side effects".

other side effects (in response to question 10)	total	female	male
arm fell asleep	1	-	1
cough	2	-	2
dry lips	1	-	1
dry mouth	7	1	6
feeling of a caressing on stomach	1	-	1
feet and thighs fell asleep	1	-	1
back pain from lying down with projection into the kidney region	1	1	-
pain in the left ear	1	1	-
seeing shadows	1	-	1
sensory illusions	1	-	1
sensory loss in hip joints	1	-	1
stiff neck	1	1	-
sweating attacks	1	-	1
tingling in both arms	1	1	-
tingling on the forehead	1	-	1
tiredness	1	1	-
vibration at the hip	1	-	1

doi:10.1371/journal.pone.0117095.t006

other side effects and observations covered by question 10. In comparison, 6% of the subjects assigned to a sub-group of 30 subjects covering the low end of the age range (age 24–28) reported other side effects and observations covered by question 10. Pearson's analysis yielded $p = 0.034$ for the assessment of the age dependence of other side effects and observations covered by question 10.

Seven subjects reported a dry mouth during the UHF-CMR examination. Two subjects reported cough. One subject mentioned that his arm fell asleep during the UHF-CMR examination. One subject was feeling tired and one subject had dry lips. A feeling of a caressing on stomach was mentioned by one male. Feet and thighs fell asleep in one subject. Back pain with projection into the kidney region due to lying on the table was mentioned by one subject. One subject recognized a pain in the left ear, another one saw shadows. Sensory illusion and a sensory loss in the hip joints were reported by one subject in each case. A stiff neck was documented by one subject. One subject reported vegetative symptoms (sweating). Tingling on both arms, and also on the forehead was described once. One subject reported a vibration at the hips. None of the subjects reported claustrophobia. Acoustic noise was not reported as a reason for discomfort. The total UHF-CMR examination time was not reported as a cause for discomfort. None of the subjects reported discomfort induced by the local RF coils placed on the anterior chest.

Discussion

This study adds to the literature by detailing the subjective acceptance of cardiac magnetic resonance imaging examinations at a magnetic field strength of 7.0 T. Among the two most common experiences that generated discomfort was transient muscular contraction or involuntary muscle twitching due to peripheral nerve stimulation induced by switching of magnetic field gradients. This observation does not accord with previous reports on the subjective tolerance

obtained for brain imaging at 7.0 T and at 9.4 T [22,24], which outlined lower incidence rates of transient symptoms of muscular contraction and peripheral nerve stimulation. Notwithstanding this difference these reports included the same gradient coil and technical specifications for maximum slew rate, maximum gradient amplitude and maximum duty cycle used here [22,24]. Even if more powerful gradient coils were used for brain MRI including maximum gradient amplitudes of up to 70 mT/m and slew rates of 400 mT/m/ms twitching and muscular contraction was less frequently reported as a cause of discomfort versus dizziness [24]. It should be noted that the switching frequencies used for CMR are commonly ranging between 300–600 Hz and hence are similar or even below the switching frequencies generally employed for anatomical (approximately 200–600 Hz) and functional brain imaging (approximately 1000–3000 Hz). Also, it is fair to assume that the peak integrals of the magnetic field gradients are smaller for CMR versus brain imaging due to the use of larger slice thicknesses and field of views. However, to meet the speed constraints of CMR it is common that the maximum gradient amplitudes used for slice selection, phase encoding, dephasing read-out and spoiler gradients are larger for CMR versus brain MRI. Our data suggest that male subjects are more strongly affected by involuntary muscle contraction due to peripheral nerve stimulation. This difference might be related to differences in body cross-section which effects the size of the current loops, and hence the magnitude of the current density. An experimental study at a lower magnetic field strength noted that the gender of the subject affects the magnitude of the peripheral nerve stimulation threshold but not the position of the stimulation [51]. Mean stimulation thresholds of healthy male subjects were found to be lower than those of healthy female subjects [51]. This observation was attributed to the larger stature of males [51]. To this end it should be noted, that the average height of the male subjects involved in our study was 7% larger than the average height of the female subjects.

Vertigo was found to be the second effect among the two most frequent causes for discomfort in our UHF-CMR study cohort. Magnetic field related vertigo like sensations are thought to result from magnetic susceptibility differences between vestibular organs and surrounding fluid, and from induced currents acting on the vestibular hair cells [52]. Thresholds for motion induced vertigo have been estimated to be around 1 T/s for greater than 1 s [53]. This translates into a recommendation derived from numerical simulations that a moving speed of 1 m/s should not be exceeded when accessing an area closer than 1 m to the front/rear ends of a 7.0 T magnet [54]. The recent ICNIRP guidelines for limiting exposure to electric fields induced by movement of the human body in a static magnetic field and by time-varying fields below 1Hz recommends that the change of the magnetic flux density B should not exceed 2 T during any 3 s period [55]. For the same reason there is a need to ensure that subjects are moved slowly into the 7.0 T magnet bore resulting in a recommendation that patient table motion is set to be lower than 0.66 T/s. To meet this requirement the speed profile of the table motion is adjusted to $B_0*(\mathrm{grad}(B_0))$ by some vendors including the MR system used in our UHF-CMR study. This might explain why previous brain UHF-MR studies reported an incidence rate of approximately 25–34% for vertigo and dizziness [23,56], which is more pronounced than the 12.7% rate observed in our UHF-MR study. In the previous studies subjects were positioned on a non-motorized table and were moved manually into the scanner bore at a constant speed [23,24]. Alternatively, a constant speed was used for automatic table motion [25]. Unlike our UHF-CMR study no attempt was made to reduce the table speed in the vicinity of the highest gradient of the magnetic field [23–25]. The 12.7% incidence rate of vertigo observed in our UHF-MR study is in line with a very recent publication which reported vertigo for 10.5% out of 504 subjects enrolled into UHF-MR examinations [57]. For this study a constant table speed of 20 mm/s [57] was used which is similar to v_{poti} = 25 mm/s used in our study. Our data do

not match a very recent report that women are more strongly affected by dizziness in static magnetic fields of 7.0 T [58].

It should be also noted that it is common to use extra pads to reduce bulk head motion in brain UHF-MR. This measure should work in favor of reducing motion induced vertigo. On the other hand, pillows or full size pads that conveniently conform to the shape of the head commonly used in CMR might provide enhanced comfort versus thin layer pads commonly used in brain imaging and hence might contribute to a lower incidence of magnetic field induced vertigo.

In addition to vertigo and nausea being potentially induced by movement in a static magnetic field, a direct interaction of the magnetic field with the vestibular system cannot be excluded [55]. Glover et.al. reported an altered sense of balance for subjects positioned stationary in proximity to a 7.0 T MR magnet [52]. Notwithstanding the potential role of spatially-varying magnetic fields for induction of vertigo, important recent findings provide strong evidence that static magnetic fields stimulate rotational sensors in the brain resulting in involuntary slow-phase eye movements, designated as nystagmus [59] which is thought to share a common mechanism with static magnetic field evoked vertigo [60]. This indicates that magnetic vestibular stimulation makes magnetic field induced nystagmus and vertigo possible while simply lying in the static magnetic field of an MR scanner [59,61]. Nystagmus strength depends on the static magnetic field strength, not motion through the magnetic field. Eye movement measurements using infrared video cameras while the subjects laid still in a 7.0 T MR scanner showed that horizontal nystagmus direction is related to the static head pitch angle, which describes the angulation of the chin towards the chest [59]. For a head pitch angle of approximately 10° to 30°—which resembles a static head pitch commonly used in a CMR setup—a horizontal slow phase eye motion velocity close to zero was observed [59]. In comparison, the largest slow phase eye motion velocity was observed for a head patch angle of approximately -10°; an arrangement which approximately resembles the positioning of the head in a head RF coil [59] used for brain MRI. This phenomenon might provide another plausible interpretation for the decreased occurrence of vertigo reported in our UHF-CMR study versus previous ultrahigh field brain imaging examinations.

Five percent of the 165 volunteers reported that dizziness persisted after the UHF-MR examination but disappeared within 10 min after completion of the study. This observation was underscored by a very recent study, which carefully examined the duration of such effects by quantitatively assessing the vestibular performance including measurements of postural instability and rotational divergences [27]. To this end, a recent report demonstrated that Diphenhydramine—a medication used to prevent motion sickness—reduces the strength of vertigo and nausea in UHF-MR—even at a low dose—and may be even used preventively [62]. Yet, this application should be considered very carefully on a case-by-case basis, taking potential side effects and interactions into account.

Approximately 10% of the study population reported metallic taste which accords very well with previous studies [23]. A similar accordance was found for the occurrences of electromagnetically-induced visual flashes of light due to retina stimulation reported in our study with previous UHF-MR brain imaging studies [24]. None of the subjects reported claustrophobia, which is in agreement with recent UHF-MR studies that reported seven scan abortions due to claustrophobia out of 3467 examinations [24]. This rate might appear to be rather low when compared to previous observations at clinical field strengths of 1.5 T and 3.0 T but can be explained by the solely voluntarily nature of the subject recruitment and the careful preparation of the volunteers.

Acoustic noise was not reported as a reason for discomfort in our study. This observation seems to contradict recent results derived from brain imaging at ultrahigh fields, which showed

acoustic noise as the second frequent cause for discomfort with incidence rates of up to 33% of the study population [23,24]. This difference is not as much of a surprise as it appears to be at first glance. Sophisticated UHF brain MR includes anatomical and functional scans with scans times of 10 min and even much longer running at sound pressure levels of up to 112 dB. This setup bears the potential to constitute acoustic noise induced discomfort. In comparison, short breath-hold, cardiac gated scans were used in our UHF-CMR study, which offsets the potential for acoustic noise related discomfort. Another reason for the difference between the rates reported for acoustic noise induced discomfort in our study and previous brain imaging studies might be the use of different acoustic noise protection approaches. In this study earplugs plus headphones were used for acoustic noise protection. Space constraints dictated by the RF coil configurations tailored for brain imaging—where it is common to use a helmet design that closely fits to the head for signal reception—render the use of headphones unsuitable so that acoustic noise protection is primarily accomplished with earplugs [23,24].

The requirements of patient comfort are likely to pave the way for further advances in technology tailored for CMR at 7.0 Tesla, including novel safety concepts [63] and innovative RF coil designs. Though the broad spectrum of applications makes it somewhat challenging to identify a single optimal RF coil design for UHF-CMR, the selected design should meet certain minimum requirements. This should include RF coil casings that afford thermal exchange to offset heat related sensory effects as a root cause for subjective discomfort. These efforts might go as far as printing circuits onto T-shirts or vests that fit the upper torso [64,65]. One could also envision flexible coil designs attached to vacuum pillows, which hold the promise to provide a subject specific fit to the torso while ensuring customized, semi-permanent stabilization. Another important development is the move towards shorter 7.0 T MR systems, which will be far more compatible with installations in clinical imaging suites but which will also help to improve the subjective acceptance during UHF-CMR examinations.

It is a recognized limitation of this study, that only 165 subjects were involved. Taking into account that cardiac MR at 7.0 T is a field in a state of creative flux we felt that it is important to begin by reporting on the details and on the implications of subjective acceptance of UHF-CMR for clinical imaging before the new technology will be placed in the hands of a broader group of clinical colleagues. Also, the study is constrained to subjects undergoing UHF-MR examinations without considering side effects and transient symptoms due to occupational exposure of research and healthcare staff to static or varying magnetic stray fields [66].

Conclusions

This study adds to the literature by detailing the subjective acceptance of cardiac magnetic resonance imaging examinations at a magnetic field strength of 7.0 T. The most important finding is that all subjects tolerated the UHF-CMR examinations, which is confirmed by no volunteer aborting the examination. Transient muscular contraction and dizziness during the study were the most frequent side effects reported in this study. To conclude, 7.0 T cardiac MR examinations are well tolerated by healthy subjects. Broader observational and multi-center studies including patient cohorts with cardiac diseases together with the use of consistent and simple questionnaires harmonized among UHF-MR institutions [24] are required to provide further insights into the subjective acceptance of UHF-CMR examinations.

Acknowledgments

The authors wish to thank Heiko Kallert, Martin Schröder and Valentin Darlau (Siemens Healthcare, Erlangen, Germany) for technical assistance.

Author Contributions

Conceived and designed the experiments: SK KP AG CO OW LW CT TH JR AE JSM TN. Performed the experiments: AE SK KP AG CO OW LW CT TH JR. Analyzed the data: SK KP AG CO OW LW CT TH JR AE JSM TN. Contributed reagents/materials/analysis tools: SK KP AG CO OW LW CT TH JR AE HM JSM TN. Wrote the paper: TN SK KP AG CO OW LW CT TH JR AE JSM HM. Helped to draft the questionnaire: JSM. Performed the medical informed consent discussion including a basic clinical examination prior to the UHF-CMR session: HM.

References

1. Vaughan JT, Snyder CJ, DelaBarre LJ, Bolan PJ, Tian J, et al. (2009) Whole-body imaging at 7T: preliminary results. Magn Reson Med 61: 244–248. doi: 10.1002/mrm.21751 PMID: 19097214
2. Niendorf T, Sodickson DK, Krombach GA, Schulz-Menger J (2010) Toward cardiovascular MRI at 7 T: clinical needs, technical solutions and research promises. Eur Radiol 20: 2806–2816. doi: 10.1007/s00330-010-1902-8 PMID: 20676653
3. Niendorf T, Graessl A, Thalhammer C, Dieringer MA, Kraus O, et al. (2013) Progress and promises of human cardiac magnetic resonance at ultrahigh fields: a physics perspective. J Magn Reson 229: 208–222. doi: 10.1016/j.jmr.2012.11.015 PMID: 23290625
4. Niendorf T, Schulz-Menger J (2013) [Cardiovascular ultrahigh field magnetic resonance imaging: challenges, technical solutions and opportunities]. Radiologe 53: 422–428. doi: 10.1007/s00117-012-2348-6 PMID: 23613023
5. Kraff O, Fischer A, Nagel AM, Monninghoff C, Ladd ME (2015) MRI at 7 tesla and above: Demonstrated and potential capabilities. J Magn Reson Imaging 41: 13–33. doi: 10.1002/jmri.24573 PMID: 24478137
6. Brandts A, Westenberg JJ, Versluis MJ, Kroft LJ, Smith NB, et al. (2010) Quantitative assessment of left ventricular function in humans at 7 T. Magn Reson Med 64: 1471–1477. doi: 10.1002/mrm.22529 PMID: 20593368
7. von Knobelsdorff-Brenkenhoff F, Frauenrath T, Prothmann M, Dieringer MA, Hezel F, et al. (2010) Cardiac chamber quantification using magnetic resonance imaging at 7 Tesla—a pilot study. Eur Radiol 20: 2844–2852. doi: 10.1007/s00330-010-1888-2 PMID: 20640427
8. Suttie JJ, Delabarre L, Pitcher A, van de Moortele PF, Dass S, et al. (2012) 7 Tesla (T) human cardiovascular magnetic resonance imaging using FLASH and SSFP to assess cardiac function: validation against 1.5 T and 3 T. NMR Biomed 25: 27–34. doi: 10.1002/nbm.1708 PMID: 21774009
9. Winter L, Kellman P, Renz W, Grassl A, Hezel F, et al. (2012) Comparison of three multichannel transmit/receive radiofrequency coil configurations for anatomic and functional cardiac MRI at 7.0T: implications for clinical imaging. Eur Radiol 22: 2211–2220. doi: 10.1007/s00330-012-2487-1 PMID: 22653280
10. von Knobelsdorff-Brenkenhoff F, Tkachenko V, Winter L, Rieger J, Thalhammer C, et al. (2013) Assessment of the right ventricle with cardiovascular magnetic resonance at 7 Tesla. J Cardiovasc Magn Reson 15: 23. doi: 10.1186/1532-429X-15-23 PMID: 23497030
11. van Elderen SG, Versluis MJ, Webb AG, Westenberg JJ, Doornbos J, et al. (2009) Initial results on in vivo human coronary MR angiography at 7 T. Magn Reson Med 62: 1379–1384. doi: 10.1002/mrm.22168 PMID: 19859918
12. van Elderen SG, Versluis MJ, Westenberg JJ, Agarwal H, Smith NB, et al. (2010) Right coronary MR angiography at 7 T: a direct quantitative and qualitative comparison with 3 T in young healthy volunteers. Radiology 257: 254–259. doi: 10.1148/radiol.100615 PMID: 20851943
13. Bizino MB, Bonetti C, van der Geest RJ, Versluis MJ, Webb AG, et al. (2014) High spatial resolution coronary magnetic resonance angiography at 7 T: comparison with low spatial resolution bright blood imaging. Invest Radiol 49: 326–330. doi: 10.1097/RLI.0000000000000047 PMID: 24637588
14. Hezel F, Thalhammer C, Waiczies S, Schulz-Menger J, Niendorf T (2012) High spatial resolution and temporally resolved T2* mapping of normal human myocardium at 7.0 Tesla: an ultrahigh field magnetic resonance feasibility study. PLoS One 7: e52324. doi: 10.1371/journal.pone.0052324 PMID: 23251708
15. Meloni A, Hezel F, Positano V, Keilberg P, Pepe A, et al. (2014) Detailing magnetic field strength dependence and segmental artifact distribution of myocardial effective transverse relaxation rate at 1.5, 3.0, and 7.0 T. Magn Reson Med 71: 2224–2230. doi: 10.1002/mrm.24856 PMID: 23813553
16. Rodgers CT, Piechnik SK, Delabarre L, Van de Moortele PF, Snyder CJ, et al. (2012) Human cardiac T1 mapping in vivo at 7T: quantifying and correcting for partial inversion; Melbourne, AUS. pp. 3780.

17. Rodgers CT, Piechnik SK, Delabarre LJ, Van de Moortele PF, Snyder CJ, et al. (2013) Inversion recovery at 7 T in the human myocardium: measurement of T(1), inversion efficiency and B(1) (+). Magn Reson Med 70: 1038–1046. doi: 10.1002/mrm.24548 PMID: 23197329

18. Tao Y, Hess AT, Keith GA, Rodgers CT, Liu A, et al. (2014) [Epub ahead of print]) Optimized saturation pulse train for human first-pass myocardial perfusion imaging at 7T. Magn Reson Med. doi: 10.1002/mrm.25522 PMID: 25537578

19. Rodgers CT, Clarke WT, Snyder C, Vaughan JT, Neubauer S, et al. (2014) Human cardiac (31) P magnetic resonance spectroscopy at 7 tesla. Magn Reson Med 72: 304–315. doi: 10.1002/mrm.24922 PMID: 24006267

20. Ruehle A, Renz W, Winter L, Pfeiffer H, Ruff J, et al. (2012) Sodium Imaging of the Heart at 7T: Design, Evaluation and Application of a Four-Channel Transmit/Receive Surface Coil Array; Melbourne, Australia. pp. 82.

21. Resetar A, Hoffmann SH, Graessl A, Waiczies H, Niendorf T, et al. (2014) Retrospectively gated CINE 23Na imaging of the heart at 7.0 T using density-adapted 3D projection reconstruction; Milan, Italy. pp. 436.

22. Heilmaier C, Theysohn JM, Maderwald S, Kraff O, Ladd ME, et al. (2011) A large-scale study on subjective perception of discomfort during 7 and 1.5 T MRI examinations. Bioelectromagnetics. doi: 10.1002/bem.20695 PMID: 22389196

23. Versluis MJ, Teeuwisse WM, Kan HE, van Buchem MA, Webb AG, et al. (2013) Subject tolerance of 7 T MRI examinations. J Magn Reson Imaging 38: 722–725. doi: 10.1002/jmri.23904 PMID: 23150466

24. Rauschenberg J, Nagel AM, Ladd SC, Theysohn JM, Ladd ME, et al. (2014) Multicenter study of subjective acceptance during magnetic resonance imaging at 7 and 9.4 T. Invest Radiol 49: 249–259. doi: 10.1097/RLI.0000000000000035 PMID: 24637589

25. Cosottini M, Frosini D, Biagi L, Pesaresi I, Costagli M, et al. (2014) Short-term side-effects of brain MR examination at 7 T: a single-centre experience. Eur Radiol 24: 1923–1928. doi: 10.1007/s00330-014-3177-y PMID: 24816933

26. Chakeres DW, de Vocht F (2005) Static magnetic field effects on human subjects related to magnetic resonance imaging systems. Prog Biophys Mol Biol 87: 255–265. PMID: 15556664

27. Theysohn JM, Kraff O, Eilers K, Andrade D, Gerwig M, et al. (2014) Vestibular effects of a 7 Tesla MRI examination compared to 1.5 T and 0 T in healthy volunteers. PLoS One 9: e92104. doi: 10.1371/journal.pone.0092104 PMID: 24658179

28. van Nierop LE, Slottje P, Kingma H, Kromhout H (2013) MRI-related static magnetic stray fields and postural body sway: a double-blind randomized crossover study. Magn Reson Med 70: 232–240. doi: 10.1002/mrm.24454 PMID: 22886724

29. Atkinson IC, Renteria L, Burd H, Pliskin NH, Thulborn KR (2007) Safety of human MRI at static fields above the FDA 8 T guideline: sodium imaging at 9.4 T does not affect vital signs or cognitive ability. J Magn Reson Imaging 26: 1222–1227. PMID: 17969172

30. Atkinson IC, Sonstegaard R, Pliskin NH, Thulborn KR (2010) Vital signs and cognitive function are not affected by 23-sodium and 17-oxygen magnetic resonance imaging of the human brain at 9.4 T. J Magn Reson Imaging 32: 82–87. doi: 10.1002/jmri.22221 PMID: 20578014

31. van Nierop LE, Slottje P, van Zandvoort MJ, de Vocht F, Kromhout H (2012) Effects of magnetic stray fields from a 7 tesla MRI scanner on neurocognition: a double-blind randomised crossover study. Occup Environ Med 69: 759–766. doi: 10.1136/oemed-2011-100468 PMID: 22930737

32. Schlamann M, Voigt MA, Maderwald S, Bitz AK, Kraff O, et al. (2010) Exposure to high-field MRI does not affect cognitive function. J Magn Reson Imaging 31: 1061–1066. doi: 10.1002/jmri.22065 PMID: 20432339

33. Schlamann M, Yoon MS, Maderwald S, Pietrzyk T, Bitz AK, et al. (2010) Short term effects of magnetic resonance imaging on excitability of the motor cortex at 1.5T and 7T. Acad Radiol 17: 277–281. doi: 10.1016/j.acra.2009.10.004 PMID: 20036585

34. Heinrich A, Szostek A, Meyer P, Nees F, Rauschenberg J, et al. (2013) Cognition and sensation in very high static magnetic fields: a randomized case-crossover study with different field strengths. Radiology 266: 236–245. doi: 10.1148/radiol.12112172 PMID: 23091174

35. Gilles M, Paslakis G, Heinrich A, Szostek A, Meyer P, et al. (2013) A cross-over study of effects on the hypothalamus-pituitary-adrenal (HPA) axis and the sympathoadrenergic system in magnetic field strength exposure from 0 to 7 T. Stress 16: 172–180. doi: 10.3109/10253890.2012.708949 PMID: 22775799

36. Frauenrath T, Hezel F, Renz W, d'Orth Tde G, Dieringer M, et al. (2010) Acoustic cardiac triggering: a practical solution for synchronization and gating of cardiovascular magnetic resonance at 7 Tesla. J Cardiovasc Magn Reson 12: 67. doi: 10.1186/1532-429X-12-67 PMID: 21080933

37. Becker M, Frauenrath T, Hezel F, Krombach GA, Kremer U, et al. (2010) Comparison of left ventricular function assessment using phonocardiogram- and electrocardiogram-triggered 2D SSFP CINE MR imaging at 1.5 T and 3.0 T. Eur Radiol 20: 1344–1355. doi: 10.1007/s00330-009-1676-z PMID: 20013275

38. Frauenrath T, Hezel F, Heinrichs U, Kozerke S, Utting JF, et al. (2009) Feasibility of cardiac gating free of interference with electro-magnetic fields at 1.5 Tesla, 3.0 Tesla and 7.0 Tesla using an MR-stethoscope. Invest Radiol 44: 539–547. doi: 10.1097/RLI.0b013e3181b4c15e PMID: 19652614

39. Frauenrath T, Niendorf T, Kob M (2008) Acoustic method for synchronization of Magnetic Resonance Imaging (MRI). Acta Acustica united with Acustica: 148–155.

40. Dieringer MA, Renz W, Lindel T, Seifert F, Frauenrath T, et al. (2011) Design and application of a four-channel transmit/receive surface coil for functional cardiac imaging at 7T. J Magn Reson Imaging 33: 736–741. doi: 10.1002/jmri.22451 PMID: 21438067

41. Grassl A, Winter L, Thalhammer C, Renz W, Kellman P, et al. (2013) Design, evaluation and application of an eight channel transmit/receive coil array for cardiac MRI at 7.0 T. Eur J Radiol 82: 752–759. doi: 10.1016/j.ejrad.2011.08.002 PMID: 21920683

42. Thalhammer C, Renz W, Winter L, Hezel F, Rieger J, et al. (2012) Two-dimensional sixteen channel transmit/receive coil array for cardiac MRI at 7.0 T: design, evaluation, and application. J Magn Reson Imaging 36: 847–857. doi: 10.1002/jmri.23724 PMID: 22706727

43. Graessl A, Renz W, Hezel F, Dieringer MA, Winter L, et al. (2014) Modular 32-channel transceiver coil array for cardiac MRI at 7.0T. Magn Reson Med 72: 276–290. doi: 10.1002/mrm.24903 PMID: 23904404

44. Winter L, Ozerdem C, Hoffmann W, Santoro D, Muller A, et al. (2013) Design and evaluation of a hybrid radiofrequency applicator for magnetic resonance imaging and rf induced hyperthermia: electromagnetic field simulations up to 14.0 Tesla and proof-of-concept at 7.0 Tesla. PLoS One 8: e61661. doi: 10.1371/journal.pone.0061661 PMID: 23613896

45. Graessl A, Winter L, Oezerdem C, Hezel F, Fuchs K, et al. (2013) A two-dimensional 16 Channel Dipole Transceiver Array for Cardiac MR at 7.0T: Design, Evaluation of RF Shimming Behavior and Application in CINE Imaging. Salt Lake City, Utah, USA. pp. 136.

46. IEC (2010) 60601–2–33 Medical electrical equipment—Part 2–33: Particular requirements for the basic safety and essential performance of magnetic resonance equipment for medical diagnosis. 3.0 ed.

47. Christ A, Kainz W, Hahn EG, Honegger K, Zefferer M, et al. (2010) The Virtual Family—development of surface-based anatomical models of two adults and two children for dosimetric simulations. Physics in medicine and biology 55: N23. doi: 10.1088/0031-9155/55/2/N01 PMID: 20019402

48. Kramer CM, Barkhausen J, Flamm SD, Kim RJ, Nagel E (2008) Standardized cardiovascular magnetic resonance imaging (CMR) protocols, society for cardiovascular magnetic resonance: board of trustees task force on standardized protocols. J Cardiovasc Magn Reson 10: 35. doi: 10.1186/1532-429X-10-35 PMID: 18605997

49. Kramer CM, Barkhausen J, Flamm SD, Kim RJ, Nagel E (2013) Standardized cardiovascular magnetic resonance (CMR) protocols 2013 update. J Cardiovasc Magn Reson 15: 91. doi: 10.1186/1532-429X-15-91 PMID: 24103764

50. Plackett RL (1983) Pearson,Karl and the Chi-Squared Test. International Statistical Review 51: 59–72.

51. Faber SC, Hoffmann A, Ruedig C, Reiser M (2003) MRI-induced stimulation of peripheral nerves: dependency of stimulation threshold on patient positioning. Magn Reson Imaging 21: 715–724. PMID: 14559335

52. Glover PM, Cavin I, Qian W, Bowtell R, Gowland PA (2007) Magnetic-field-induced vertigo: a theoretical and experimental investigation. Bioelectromagnetics 28: 349–361. PMID: 17427890

53. ICNIRP (2009) Amendment to the ICNIRP "Statement on Medical Magnetic Resonance (MR) Procedures: Protection of Patients". Health Physics 97: 259–261. doi: 10.1097/HP.0b013e3181aff9eb PMID: 19667810

54. Crozier S, Wang H, Trakic A, Liu F (2007) Exposure of workers to pulsed gradients in MRI. J Magn Reson Imaging 26: 1236–1254. PMID: 17969133

55. (2014) ICNIRP guidelines for limiting exposure to electric fields induced by movement of the human body in a static magnetic field and by time-varying fields below 1Hz. HEALTH PHYSICS 106: 8.

56. Theysohn JM, Maderwald S, Kraff O, Moenninghoff C, Ladd ME, et al. (2008) Subjective acceptance of 7 Tesla MRI for human imaging. MAGMA 21: 63–72. PMID: 18064501

57. Uwano I, Metoki T, Sendai F, Yoshida R, Kudo K, et al. (2014) Assessment of Sensations Experienced by Subjects during MR Imaging Examination at 7T. Magn Reson Med Sci; [Epub ahead of print]. doi: 102463/mrms2014-0004 PMID: 25500782

58. Heinrich A, Szostek A, Meyer P, Reinhard I, Gilles M, et al. (2014) Women are more strongly affected by dizziness in static magnetic fields of magnetic resonance imaging scanners. Neuroreport 25: 1081–1084. doi: 10.1097/WNR.0000000000000225 PMID: 25089803

59. Roberts DC, Marcelli V, Gillen JS, Carey JP, Della Santina CC, et al. (2011) MRI magnetic field stimulates rotational sensors of the brain. Curr Biol 21: 1635–1640. doi: 10.1016/j.cub.2011.08.029 PMID: 21945276

60. Mian OS, Li Y, Antunes A, Glover PM, Day BL (2013) On the vertigo due to static magnetic fields. PLoS One 8: e78748. doi: 10.1371/journal.pone.0078748 PMID: 24205304

61. Ward BK, Roberts DC, Della Santina CC, Carey JP, Zee DS (2014) Magnetic vestibular stimulation in subjects with unilateral labyrinthine disorders. Front Neurol 5: 28. doi: 10.3389/fneur.2014.00028 PMID: 24659983

62. Thormann M, Amthauer H, Adolf D, Wollrab A, Ricke J, et al. (2013) Efficacy of diphenhydramine in the prevention of vertigo and nausea at 7 T MRI. Eur J Radiol 82: 768–772. doi: 10.1016/j.ejrad.2011.08.001 PMID: 21945402

63. Winter L, Oberacker E, Ozerdem C, Ji Y, von Knobelsdorff-Brenkenhoff F, et al. (2014) On the RF heating of coronary stents at 7.0 Tesla MRI. Magn Reson Med; [Epub ahead of print]. doi: doi: 101002/mrm25483 PMID: 25537578

64. Lattanzi R, Sodickson DK (2012) Ideal current patterns yielding optimal signal-to-noise ratio and specific absorption rate in magnetic resonance imaging: computational methods and physical insights. Magn Reson Med 68: 286–304. doi: 10.1002/mrm.23198 PMID: 22127735

65. Corea J, Flynn A, Scott G, Arias A, Lustig M (2012) Bespoke Coils: Screen-Printed, Tailored Flexible MRI Receiver Coils; Melbourne, Australia. pp. 434.

66. Schaap K, Christopher-de Vries Y, Mason CK, de Vocht F, Portengen L, et al. (2014) Occupational exposure of healthcare and research staff to static magnetic stray fields from 1.5–7 Tesla MRI scanners is associated with reporting of transient symptoms. Occup Environ Med 71: 423–429. doi: 10.1136/oemed-2013-101890 PMID: 24714654

PLOS ONE

RESEARCH ARTICLE

High Spatial Resolution Cardiovascular Magnetic Resonance at 7.0 Tesla in Patients with Hypertrophic Cardiomyopathy – First Experiences: Lesson Learned from 7.0 Tesla

Marcel Prothmann[1,2], Florian von Knobelsdorff-Brenkenhoff[1,2], Agnieszka Töpper[1,2], Matthias A. Dieringer[1,2], Etham Shahid[1,2], Andreas Graessl[1], Jan Rieger[3], Darius Lysiak[1,3], C. Thalhammer[1], Till Huelnhagen[1], Peter Kellman[4], Thoralf Niendorf[1,3,5], Jeanette Schulz-Menger[1,2,5]*

1 Berlin Ultrahigh Field Facility (B.U.F.F.), Max-Delbrueck Center for Molecular Medicine, Berlin, Germany, **2** Working Group on Cardiovascular Magnetic Resonance, Experimental and Clinical Research Center, a joint cooperation between the Charité Medical Faculty of the Humboldt University of Berlin and the Max-Delbrueck Center for Molecular Medicine, and HELIOS Klinikum Berlin Buch, Department of Cardiology and Nephrology, Berlin, Germany, **3** MRI.TOOLS GmbH, Berlin, Germany, **4** National Institutes of Health / NHLBI, Bethesda, Maryland, United States of America, **5** DZHK (German Centre for Cardiovascular Research), partner site Berlin, Germany

* Jeanette.Schulz-Menger@charite.de

OPEN ACCESS

Citation: Prothmann M, von Knobelsdorff-Brenkenhoff F, Töpper A, Dieringer MA, Shahid E, Graessl A, et al. (2016) High Spatial Resolution Cardiovascular Magnetic Resonance at 7.0 Tesla in Patients with Hypertrophic Cardiomyopathy – First Experiences: Lesson Learned from 7.0 Tesla. PLoS ONE 11(2): e0148066. doi:10.1371/journal.pone.0148066

Editor: Joshua M. Hare, University of Miami Miller School of Medicine, UNITED STATES

Received: July 29, 2015

Accepted: January 12, 2016

Published: February 10, 2016

Data Availability Statement: Ethical restrictions prevent public sharing of the data. Interested readers may send requests for data access to Jeanette Schulz- Menger (jeanette.schulz-menger@charite.de) or Marcel Prothmann (marcel.prothmann@charite.de). Data will be available upon request to all interested researchers.

Funding: The study was supported by university funds (Charité) hold by Prof. Dr. med. Jeanette Schulz Menger. Thoralf Niendorf is founder and CEO

Abstract

Background

Cardiovascular Magnetic Resonance (CMR) provides valuable information in patients with hypertrophic cardiomyopathy (HCM) based on myocardial tissue differentiation and the detection of small morphological details. CMR at 7.0T improves spatial resolution versus today's clinical protocols. This capability is as yet untapped in HCM patients. We aimed to examine the feasibility of CMR at 7.0T in HCM patients and to demonstrate its capability for the visualization of subtle morphological details.

Methods

We screened 131 patients with HCM. 13 patients (9 males, 56 ±31 years) and 13 healthy age- and gender-matched subjects (9 males, 55 ±31years) underwent CMR at 7.0T and 3.0T (Siemens, Erlangen, Germany). For the assessment of cardiac function and morphology, 2D CINE imaging was performed (voxel size at 7.0T: (1.4x1.4x2.5) mm^3 and (1.4x1.4x4.0) mm^3; at 3.0T: (1.8x1.8x6.0) mm^3). Late gadolinium enhancement (LGE) was performed at 3.0T for detection of fibrosis.

Results

All scans were successful and evaluable. At 3.0T, quantification of the left ventricle (LV) showed similar results in short axis view vs. the biplane approach (LVEDV, LVESV, LVMASS, LVEF) ($p = 0.286$; $p = 0.534$; $p = 0.155$; $p = 0.131$). The LV-parameters obtained

of MRI.TOOLS GmbH, Berlin, Germany. Jan Rieger is founder and CTO of MRI.TOOLS GmbH, Berlin, Germany. Darius Lysiak is currently employee of MRI.TOOLS GmbH, Berlin, Germany. MRI.TOOLS GmbH provided support in the form of salaries for authors Jan Rieger and Darius Lysiak, but did not have any additional role in the study design, data collection and analysis, decision to publish, or preparation of the manuscript. The specific roles of these authors are articulated in the 'author contributions' section.

Competing Interests: Thoralf Niendorf is founder and CEO of MRI.TOOLS GmbH, Berlin, Germany. Jan Rieger is founder and CTO of MRI.TOOLS GmbH, Berlin, Germany. Darius Lysiak is currently an employee of MRI.TOOLS GmbH, Berlin, Germany. Thoralf Niendorf, Jan Rieger and Darius Lysiak from MRI.TOOLS GmbH provided the easyACT (an acoustic a triggering/gating device) together with the RF coil array used in this study. There are no patents, products in development or marketed products to declare. This does not alter the authors' adherence to all the PLOS ONE policies on sharing data and materials.

at 7.0T where in accordance with the 3.0T data (p_{LVEDV} = 0.110; p_{LVESV} = 0.091; p_{LVMASS} = 0.131; p_{LVEF} = 0.182). LGE was detectable in 12/13 (92%) of the HCM patients. High spatial resolution CINE imaging at 7.0T revealed hyperintense regions, identifying myocardial crypts in 7/13 (54%) of the HCM patients. All crypts were located in the LGE-positive regions. The crypts were not detectable at 3.0T using a clinical protocol.

Conclusions

CMR at 7.0T is feasible in patients with HCM. High spatial resolution gradient echo 2D CINE imaging at 7.0T allowed the detection of subtle morphological details in regions of extended hypertrophy and LGE.

Introduction

Cardiovascular magnetic resonance (CMR) is known to offer additional morphologic information in hypertrophic cardiomyopathy (HCM). Accurate phenotyping is essential for the diagnosis and risk stratification of HCM [1]. Echocardiography is currently the most important basic imaging modality in the diagnostic work-up of patients and relatives [2]. CMR is able to provide information beyond myocardial function based on CINE-imaging by detecting fibrosis based on Late Gadolinium Enhancement (LGE) imaging [3]. Fibrosis imaging plays an important role in risk stratification of HCM. It is accepted as a "modifier" in the HCM guidelines [1]. In a comprehensive evaluation of HCM, CMR-based myocardial tissue differentiation with assessment of perfusion and fibrosis provides important information [4,5]. An ongoing multicenter international trial (Hypertrophic Cardiomyopathie Registry-HCMR) includes fibrosis imaging based on LGE and T_1-mapping and will help to define the role of CMR in risk stratification [6].

Furthermore, CMR allows the identification of focal hypertrophy in atypical regions. In particular the apical and the anterolateral region may be underestimated with echocardiography [7]. In recent years, small morphological features such as myocardial crypts or clefts have come to awareness. They have been described increasingly in different genotypes, but are not specific for HCM [8,9]. The detection of small myocardial structures goes along with the improvement of clinically available imaging technology, mainly with an increased spatial resolution.

Currently, experimental MRI at 7.0 Tesla (T) is under evaluation in a human setting, mainly covering neuroscience. Neurovascular ultrahigh field (UHF)-MR has been successfully performed in different clinical entities. Based on the increased spatial resolution MRI at 7.0T was superior to 3.0T [10]. Early applications of UHF-CMR manifest the enhancements in spatial resolution, but were limited to healthy volunteer studies [11–15].

The aim of our study was to prove the feasibility of CMR at 7.0T in HCM and investigate its capability for the detection of subtle morphological changes in comparison to standardized clinical protocols.

Methods

The ethics committee (Charite Campus Mitte EA1/54/09) approved the study and all participants provided written informed consent prior to the study. (Ethics committee: Ethicausschuss 1 am Campus Charite Mitte head: Prof. Dr. R Uebelhack Charitéplatz 1, 10117 Berlin phone: +4030450–517222 Ethics approval number: EA1/054/09, Renewal number: NI 532/6-2)

Study population

We prospectively screened patients with HCM. As a reference group healthy volunteers were identified for eligibility for 7.0T.

Exclusion criteria

Usual MR-exclusion criteria such as claustrophobia and implanted devices were applied. In particular at 7.0T, all metallic implants and tattoos led to an exclusion. Furthermore, all patients with any evidence of other cardiovascular diseases, severe arrhythmias and renal failure based on the estimation of glomerular filtration reserve < 60ml/min were excluded.

Patients

The diagnosis of HCM was based on clinical parameters including echocardiography following the guidelines [1].

Healthy volunteers

Healthy volunteer was defined based on clinical investigation and a negative history of any diseases. There were no ECG-abnormalities and cardiac function was normal.

CMR-protocol

CMR at 7.0 Tesla. A whole body 7.0T MR-system (Magnetom, Siemens Healthcare, Erlangen, Germany, equipped with a gradient system providing a maximum gradient strength of 38 mT/m and a maximum slew rate of 170 mT/m/ms (Siemens Healthcare, Erlangen, Germany) were used. For signal reception and transmission, a 16-channel radio-frequency (RF) transceiver array tailored for CMR at 7.0T was employed [14]. Prior to the study, the RF coil underwent thorough safety assessment in line with the technical standards given by IEC 60601-2-33:2010 Ed.3 and IEC 60601–1:2005 Ed.3 [16]. The safety assessment, the implemented safety measures, the technical documentation and the risk management file for the coil were evaluated and duly approved for implementation in clinical studies following conformity declaration provided by a notified body.

The basic scan protocol was described recently [11,12]. In brief, 2D CINE FLASH images were acquired using a high resolution fast gradient echo (FGRE) technique in end-expiratory breath-holds. Imaging parameters were: echo time (TE) = 2.7 ms, repetition time (TR) = 5.5 ms, nominal flip angle (FA) = 32°, field of view (FOV) typically (360x360) mm^2, FOV phase = 73%, acquisition matrix size = 256×186, bandwidth (BW) = 445 Hz/pixel, 30 phases per heart cycle, parallel imaging using two-fold acceleration and GRAPPA reconstruction (R = 2). We acquired three long-axis views of the left ventricle ((slice thickness (slth) = 4.0mm)) corresponding to the standard procedure in clinical routine. Additionally, three short axes views (slth 4.0mm and 2.5mm) were acquired in the LGE-positive region as identified at 3.0T. Specific slices were acquired to enhance regions with noticeable structure as identified in clinical scans at 3.0T. Cardiac gating was performed with acoustic cardiac triggering (easyACT, MRI.TOOLS GmbH, Berlin, Germany) [17] or pulse oximetry.

CMR at 3.0 Tesla. A 3.0T MR system (Magnetom Verio, Siemens Healthcare, Erlangen, Germany) was used. For signal transmission, a whole body RF coil was applied. For signal reception a 32-channel RF coil dedicated for CMR was employed.

According to the established clinical protocol, 2D steady-state free precession (SSFP) CINE imaging was applied for cardiac chamber quantification. We acquired four-, two—and three chamber views and a stack of short axis views covering the whole left ventricle without a gap (slth:

6.0mm, TR: 3.1ms, TE: 1.3ms FA: 45°, FOV: (340 x 276) mm^2, matrix: 192x156, BW: 704Hz/px, 30 phases per heart cycle, GRAPPA reconstruction, acceleration factor 2 [18]. LGE images were acquired 10 to 15 minutes after application of gadobutrol (0.2mmol/kg body weight) using fast low angle shot (FLASH) inversion recovery gradient echo to detect fibrosis. Imaging parameters were: TR = 10.5ms, TE = 5.4ms, FA = 30°, FOV (350 x 262) mm^2, matrix 256 x162, slth 6.0mm, BW 140Hz/px, GRAPPA acceleration factor 2. Cardiac gating was performed using ECG.

CMR at 1.5 Tesla. A subgroup of our study population (n = 2) underwent an additional scan at 1.5T (MAGNETOM Avanto, Siemens Healthcare, Erlangen, Germany) using a 12-channel RF body array coil for signal reception. 2D CINE images were acquired using SSFP following our routine protocol. Imaging parameters were: TE = 2.7 ms, TR = 5.5 ms, FA = 80°, FOV typically (340x340) mm^2, matrix 192×156, slth 7.0mm, 30 phases per heart cycle, parallel imaging with two-fold acceleration and GRAPPA reconstruction. Pre-contrast multi–echo fat–water–separated imaging was applied as following: bandwidth = 977 Hz/pixel, matrix = 256×126, TR = 11.2 ms, TE = 1.64, 4.17, 6.7, and 9.23 ms, flip angle = 20–25° [19].

Image analysis

Quantitative analysis. LV morphology was quantified using CVI[42] version 4.15 (Circle Cardiovascular Imaging, Calgary, Canada). LV myocardium was delineated by semi-automatically contouring the endocardial and epicardial borders. For LV quantification, both biplanar (3.0T, 7.0T) and short axis data were analyzed (3.0T). The papillary muscles were excluded from LV-mass and counted as blood in the biplanar approach reflecting the area-length method as published, whereas the LV quantification based on the short axis stack regarded the papillary muscles as myocardium [20].

Qualitative analysis. Image quality of the CINE images at 7.0T was analyzed qualitatively. Artifacts and anatomical particularities were assessed as published recently [12]. Quality score were 0 = non-diagnostic, 1 = good, and 2 = excellent. The artifact-score was as following: 2 = major artifacts, 1 = mild artifacts, 0 = no artifacts. Two experienced observers (FVK > 10000 CMR scans, MP > 1500 CMR scans) evaluated a mid-ventricular short axis view with different slice thicknesses (4.0 and 2.5mm) and a three chamber view (4mm). Visual assessment of pericardial effusion was based on CINE imaging evaluating the pericardial bright signal following clinical criteria. Wall motion abnormalities were visually scored following established criteria (normo-, hypo-, a- and dyskinesia).

All images were systematically screened for subtle morphological abnormalities such as the myocardial structure itself and papillary muscles. The visual evaluation was slice based and an evaluation of the perpendicular slices using a cross-reference tool was allowed. The definition of myocardial crypts was based on previous studies [9].

Statistics

Results are presented as mean ± standard deviation. The Wilcoxon matched pairs test was used to compare the results in HCM patients. The Mann-Whitney test was used to compare the results between healthy volunteers and patients. Statistical significance was accepted as $p<0.05$. Statistical analyses were performed using SPSS version 20.0 (IBM, Armonk) and Prism version 5.0 (graphpad, San Diego).

Results

Study population

We screened 131 patients with HCM between 2011 and 2014. Main reasons for exclusion at 7.0 T were implants like cardiac devices (n = 16), significant cardiac-morbidity (n = 32), other co-

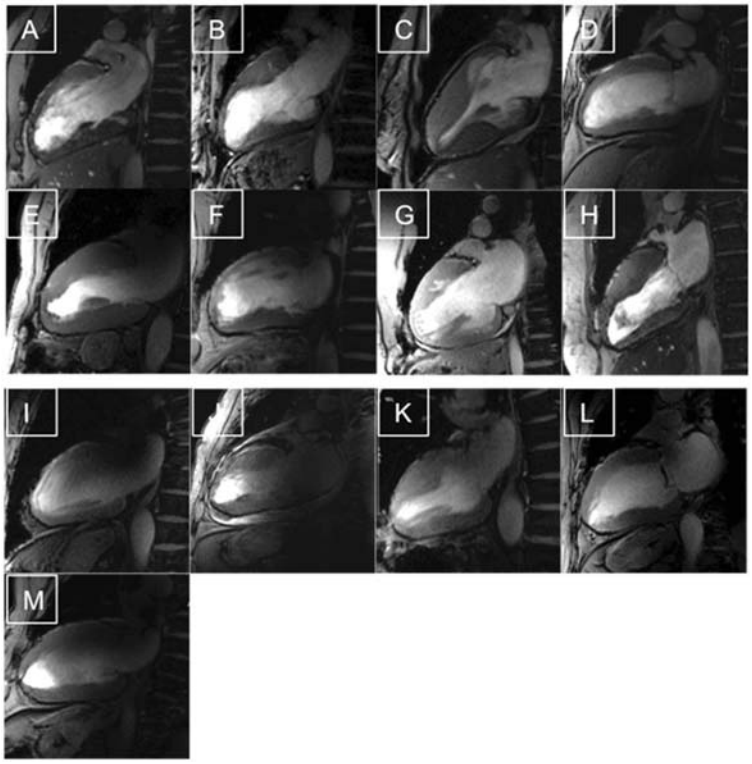

Fig 1. Feasibility of CMR in HCM patients at 7.0T. High Resolution CINE images of each patient (slice thickness 2.5 mm) All images were evaluable as shown by these two-chamber views, but the quality scoring revealed differences. A-H) Examples with a good images quality and mild artifacts. I-M) Images with different types of artifacts

doi:10.1371/journal.pone.0148066.g001

morbidities (35) and arrhythmias (n = 7). Because of the rigorous exclusion criteria we had to exclude patients with dental implants (n = 16), tattoos (7). Some patients refused to participate in the 7.0 T study (n = 18).

26 participants (13 HCM patients) were included and successfully scanned at 7.0T and at clinical scanners (mean time interval 29 days) (Fig 1). Mean scan time at 7.0T assessing the LV-morphology was 22±13 minutes. All scans could be performed without any complication. Only temporary dizziness, temperature sensations and metallic taste were reported in 6 cases at 7.0T.

HCM-Patients

We examined 9 males (mean age: 56 ±31) and 4 females (mean age: 54 ±12) at 7.0T (Table 1). No relevant symptoms were reported during or after the 7.0T-scan.

All patients underwent also CMR at clinical field strengths. Eleven patients were investigated at 3.0T, two patients refused the examination. In these cases we evaluated the clinical scan at 1.5 T. The clinical CMR protocol at 1.5T assessing LV function and fibrosis was similar to the 3.0T-protocol.

Healthy Volunteers

Nine male and four female healthy volunteers completed the scan at 7.0T. They were age- and gender-matched to HCM (Table 1). No relevant symptoms during or after the 7.0T-scan were reported.

Table 1. Clinical characteristics and left ventricular assessment for healthy volunteers and HCM patients at 7.0 T. BMI—Body Mass Index, LVEDV—Left Ventricular End-Diastolic Volume, LVEF—Left Ventricular Ejection Fraction, LVESV—Left Ventricular End-Systolic Volume, PE—Pericardial Effusion, WMA—Wall Motion Abnormalities.

	patients with HCM	healthy volunteers
gender	13 (9 male)	13 (9 male)
age (years)	56 (25–71)	55 (24–71)
BMI (kg/m^2)	27 (22–36)	24 (19–29)
Dental wires(n)	11	4
WMA(n)	1	-
PE(n)	1	-
Crypts(n)		-
- absolute	7	
- average/patient	1	
- maximum/patient	3	
LGE(n)	12	-
LVmass (g)	174.9 (112.8–273.5)	100.3 (75.2–134.5)
LVEDV (ml)	136.7 (68.5–231.2)	127.2 (94.9–186.8)
LVEF (%)	59.9 (50.2–76.0)	58.5 (49.8–71.6)
LVESV (ml)	51.2 (26.3–71.3)	55.4 (35.8–75.8)

doi:10.1371/journal.pone.0148066.t001

Qualitative image analysis

The image quality score of 7.0T 2D CINE FGRE data reflected a good quality. The quality was scored as"good" with a mean of 1.1±0.3 by observer 1 and 1.3±0.2 by observer 2 (FvK,MP). Artifacts were identified in six patients, but they did not influence the evaluation of the cardiac function. The mean artifact score was classified as mild reflected by a score of 1.2±0.2 given by observer 1 and 1.4±0.3 by observer 2.

The visual evaluation of the 7.0T CINE images acquired with a slice thickness of 2.5mm and 4.0mm and an in-plane spatial resolution of (1.4x1.4) mm^2 revealed unexpected results of the myocardial structure in the areas of LGE depicted at 3.0T (distribution of LGE see Fig 2). At

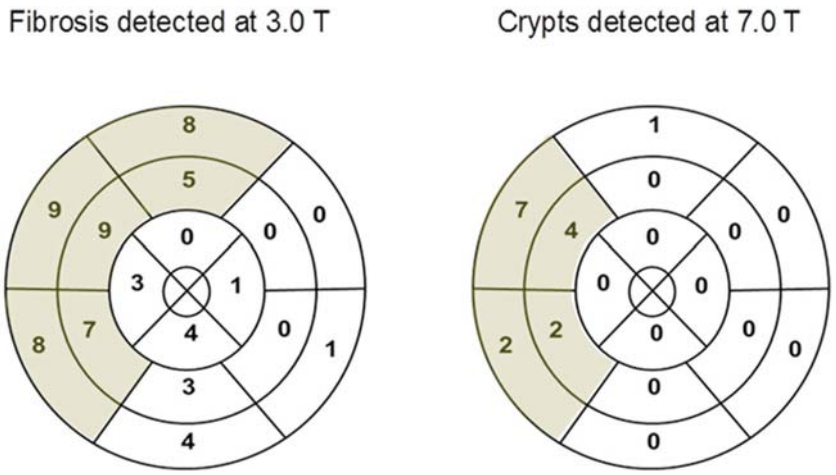

Fig 2. Distribution and prevalence of fibrosis and crypts. Myocardial crypts were only located in the regions with fibrosis as identified by LGE at 3.0T

doi:10.1371/journal.pone.0148066.g002

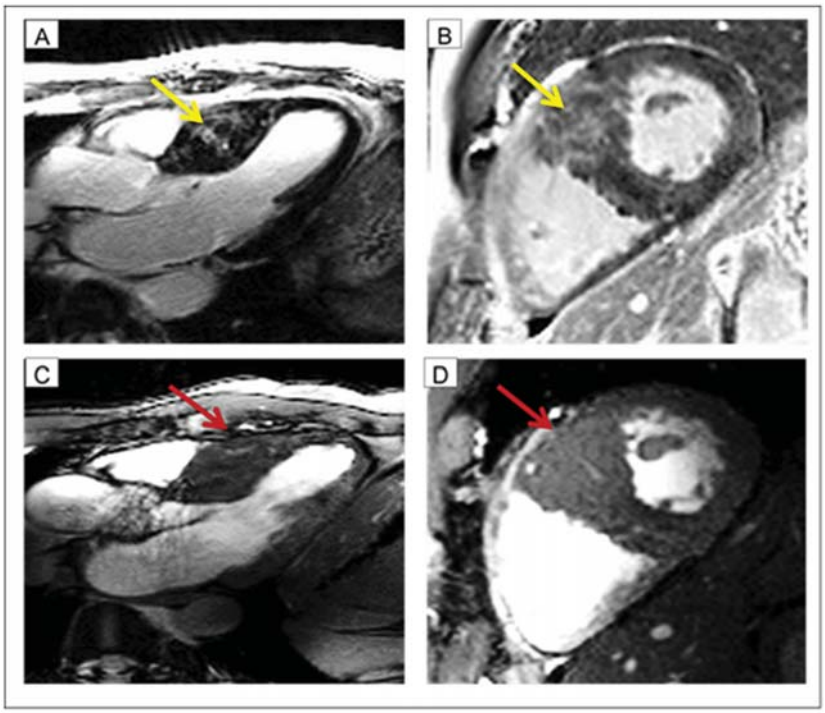

Fig 3. Case example: Patient with myocardial crypts. In the top row fibrosis imaging (LGE at 3.0T) is shown. The yellow arrow indicates the fibrosis (A long axis view B short axis view). In the bottom row cine imaging at 7.0T is shown The red arrow indicates the myocardial crypts (A long axis view B short axis view). Remarkable, fibrosis and crypts have a certain overlap. One may assume, that the bright signal at 3.0T might be also induced by blood within the crypts.

doi:10.1371/journal.pone.0148066.g003

7.0T, we detected small hyperintense regions in the myocardium mainly in the hypertrophied anteroseptal region. Most of them had access to the blood of the left ventricle. The visibility of the hyperintense regions was related to the cardiac phase. The structures were best detectable during diastole. The findings could be identified as myocardial crypts (Fig 3 and S1 File). To exclude the theoretical possibility of fatty infiltration as the cause of the hyperintense signal, we re-scanned two patients at 1.5T applying multi–echo fat–water–separated imaging. No fat was detectable in the respective regions (Fig 4).

Myocardial crypts were observed in 7/13 (54%) of HCM patients at 7.0T. The agreement of two experienced (MP and FvK) readers was 92%. Prospective and retrospective analysis of the corresponding CINE images at the clinical field strengths did not allow the detection of intra-myocardial hyperintense structures. No myocardial crypts were detected in healthy volunteers.

Quantitative analysis of the left ventricle

There were no significant differences between short axis and long axis assessment at 3.0T: LVEDV ($p = 0.286$), LVESV ($p = 0.534$), LVEF ($p = 0.131$) and LV-Mass ($p = 0.155$). The long axis comparison between 3.0T and 7.0T also revealed no significant differences: LVEDV ($p = 0.110$), LVESV ($p = 0.091$), LVEF ($p = 0.182$) and LV-MASS ($p = 0.131$) (Table 2). Plots are shown in Fig 5.

Quantitative analysis of LV function at 7.0T in healthy volunteers is shown in Table 1.

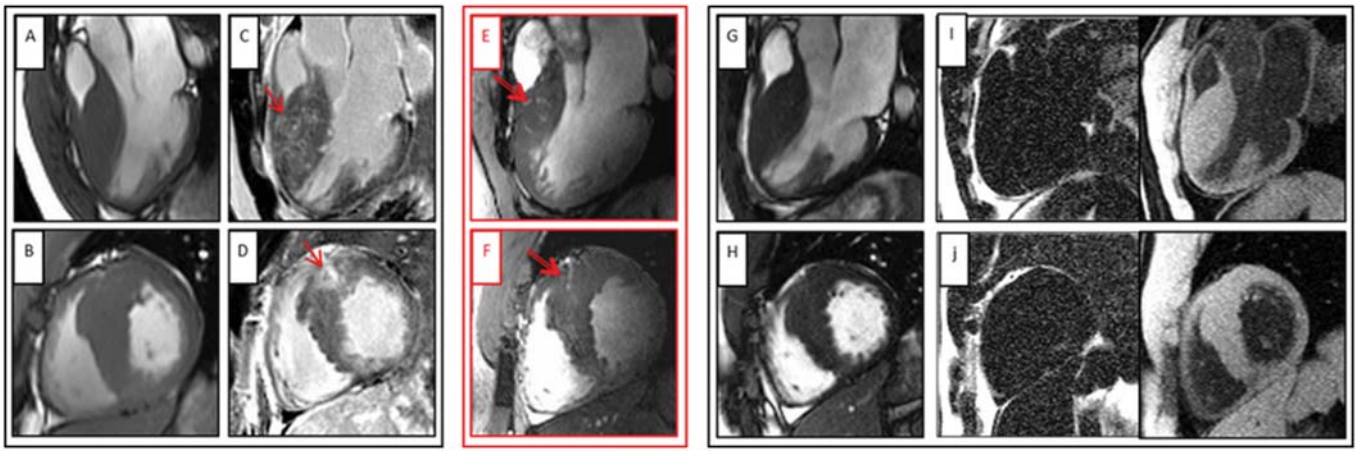

Fig 4. HCM patient with myocardial crypts in the anteroseptal region. Upper row: 3-chamber view with different techniques, Bottom row: short axis view using the same techniques, A and B CINE images at 3.0T, C and D Late Gadolinium Enhancement at 3.0T, E and F CINE images at 7.0T, G and H CINE images at 1.5 T CMR, I and J Fat-Water images, Single arrows indicates LGE at 3.0T, Double arrow displays myocardial crypt at 7.0T.

doi:10.1371/journal.pone.0148066.g004

Table 2. Left ventricular assessment of HCM patients at different field strengths. SAX = Short axis

	7.0T(biplanar)	3.0T(biplanar)	3.0T(sax)	p-value(3.0T biplanar vs. 3.0T sax)	p-value(7.0T biplanar vs 3.0T biplanar)
LVEDV (ml)Mean	**136.7**	**139.9**	**148.0**	**0.286**	**0.110**
Min-Max	**68.5–231.2**	**86.3–256.5**	**81.93–240.4**		
LVESV (ml)Mean	**51.2**	**53.0**	**50.0**	**0.534**	**0.091**
Min-Max	**26.3–71.3**	**25.3–85.9**	**26.0–75.3**		
LVM (g)Mean	**174.9**	**187.0**	**183.8**	**0.155**	**0.131**
Min-Max	**112.8–273.5**	**112.6–319.4**	**105.3–314.6**		
LVEF (%)Mean	**59.9**	**62.9**	**65.7**	**0.131**	**0.182**
Min-Max	**50.2–76.0**	**53.6–70.7**	**59.0–76.7**		

doi:10.1371/journal.pone.0148066.t002

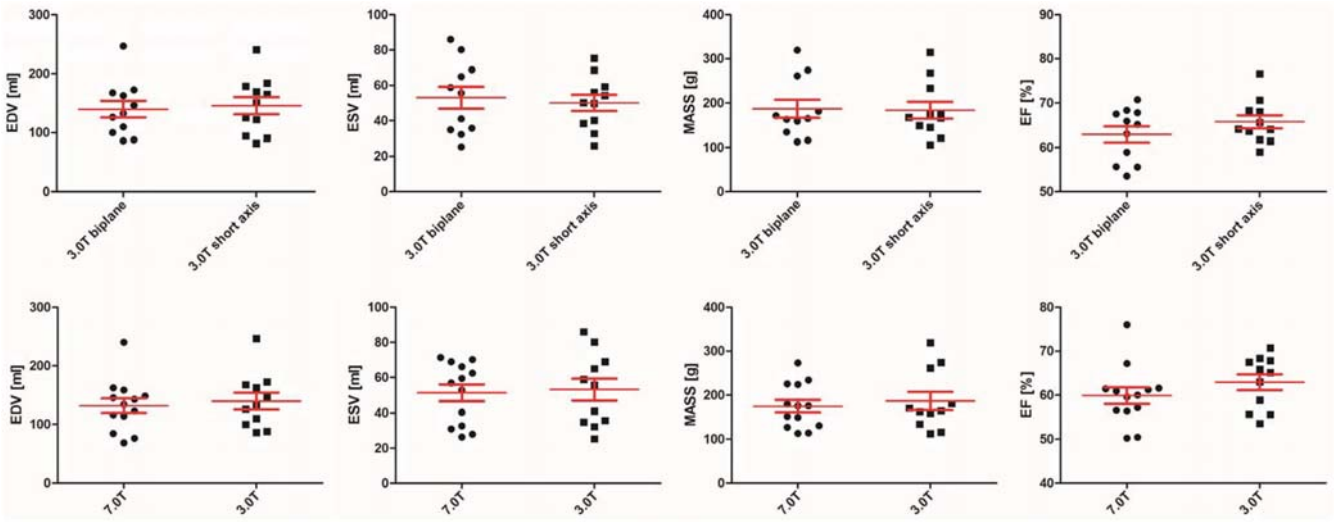

Fig 5. Comparison of left ventricular function between the different field strengths. The comparison of left ventricular function revealed no ignificant differences between the field strengths, Top: Left ventricular function at 3.0 T (biplanar versus short axis). Bottom: Left ventricular function at 7.0 T compared to 3.0 T (both biplanar).

doi:10.1371/journal.pone.0148066.g005

As expected, LV-mass differed significantly between healthy volunteers and HCM patients ($p = 0.001$). There were no significant differences in LVEDV ($p = 0.541$), LVESV ($p = 0.316$) and LVEF ($p = 0.451$) between field strength.

Technical aspects

Magnetic field inhomogeneity did not influence the assessment of the cardiac structures. Cardiac gating was successful in all participants. In six volunteers we had to switch from acoustic gating to pulse oxymetry (four HCM patients and two healthy volunteers).

Discussion

To the best of our knowledge, this is the first study showing the feasibility of CMR at 7.0T in a larger group of cardiac patients. Besides the successful implementation of 7.0T in HCM, we were able to identify unexpected subtle crypts in hypertrophied regions, which were not detectable at clinical field strengths in a routine setting [4,21]. The detection of various morphological changes may have impact on advanced non-invasive phenotyping of HCM.

Quantitative assessment of left ventricle

The assessment of the left ventricular function is a basic requisite of a CMR scan. In our setting we could confirm that the LV-function obtained at 7.0T accords with the 3.0T data. Our findings are in line with previous results, that the assessment of cardiac function is reliable at 7.0T [11]. So far the assessment of cardiac function is not an obstacle to further application developments at ultrahigh field strengths.

Qualitative assessment of left ventricle

Based on high-resolution CINE imaging, we have identified myocardial crypts at 7.0T. They were detectable in regions with hypertrophy and fibrotic changes as indicated by LGE. We detected the crypts in more than 50% of our HCM-patients applying high spatial resolution CINE imaging at 7.0T. Theoretically, the incidence of crypts could be even higher, as in our setting full coverage including different slice positions or high resolution 3D cine imaging was not applicable. The detected crypts were not observed at 3.0T or 1.5 T using standardized 2D CINE SSFP imaging. The findings may lead to new insights into the bright regions seen with LGE imaging (Fig 4). LGE itself is associated with an impaired clinical outcome based on heart failure and arrhythmias [4]. A further differentiation could enhance the prediction of different outcomes. The interpretation of hyperintense signal in non-contrast CINE imaging can be difficult, as it can be caused by fat or fluid [19]. We could exclude that the bright signal is caused by fat by using fat-water imaging at 1.5 T.

Crypts have already been described in HCM applying CMR [22,23]. Interestingly, they were found in HCM patients with LV-hypertrophy, but also in genotype-positive patients without LV-hypertrophy [9]. One group detected the crypts more often in non-hypertrophied regions and explained that by the remodeling process [9].

One could assume that the myocardial crypts are compressed by the hypertrophied myocardium. The currently used image spatial resolution at lower field strength is not good enough to depict them. During the time course of disease while developing heart failure, they could be detectable. The prevalence of myocardial crypts as detected at 7.0T seems to be as high as described in pre hypertrophy stages of HCM [8]. Systematic CMR based follow-up would offer the chance to depict this and to elucidate the underlying mechanisms. The description of subtle

myocardial structural changes, such as crypts, may help to predict the disease development and the differentiation between risk of sudden cardiac death and development of heart failure.

Petryka et al reported a prevalence of crypts in HCM of 15.6% using both 1.5T and 3.0T. Crypts were mainly identified in the non-hypertrophied inferior wall [24]. In our study, the prevalence of crypts was 54%. In post-mortem studies, crypts were identified in up to 32% and were mostly localized in the anteroseptal region [25], matching our findings. Hence, the increased spatial resolution of 7.0T may lead to an improvement in the identification of small structures. Currently, the clinical advantage of myocardial crypt detection is unclear. There is first evidence, that the identification of ≥ 2 crypts had a 100% positive predictive value to identify carriers [8]. Another group could show that deep basal inferoseptal crypts are more common in patients with HCM with disease-causing mutations than in patients with genotype-negative HCM [22]. Assessment of family members is one of the most challenging and responsible tasks in a clinical setting. Detection of multiple crypts may add additional information.

The definition of crypts was based on access to the blood of the ventricles. All but one structure could be verified in perpendicular slices. In one patient (Fig 4f) we were not able to exclude, that this hyperintense region is related to a septal branch. But it is very unlikely, as the larger coronaries were not visible in the same intensity. A whole heart coverage would have been helpful to assess all anatomical details with 2D CINE imaging and should be used in future trials.

The detection of the inferobasal myocardial crypts is usually detectable in the two- chamber view, sometimes better in a modified one [8]. The assessment of additional crypts may depend on slice positioning. In the current trial we have focused on the most hypertrophied myocardial segments.

Safety and technical aspects

All volunteers completed the CMR examination; no severe adverse events occurred matching pervious experiences [11]. The rate of minor subjective events was similar to recently published data [26]. Safety data about metallic implants are rare for 7.0T. At least dental wires, which many of the participants of the present study had, did not cause any problems. Other safety issues have to be addressed in the future to expand the use of 7.0T in cardiac patients. For example coronary stents are frequent in patients with coronary artery disease. The prevalence in US patients aged 20 and over is about 6.5% [27]. Currently the safety of CMR at ultrahigh fields ($B_0 \geq 7.0$ T) for patients with stents is under investigation. Recently, electro-magnetic field simulations and heating experiments at 7.0T demonstrated that radiofrequency (RF)-induced stent heating did not exceed limits given by the IEC guidelines for RF power deposition [28]. Another study scrutinized RF induced heating of coronary stents at 7.0T for a broad range of stent configurations [29].

Following the success of neuroradiology by detecting subtle focal lesions in the brain [30], CMR at ultrahigh fields may also allow us to detect histopathological structures of the heart. We were able to detect subtle myocardial structures at 7.0 T thanks to the spatial resolution which is superior to the capabilities of clinical field strengths. The differentiation of fibrotic areas in HCM might be helpful to identify prospectively patients with further development of systolic heart failure, but this was not a part of this pilot study. We anticipate, that CMR at 7.0T can also provide information on fibrotic tissue changes without any contrast application. First results have indicated, that at least assessment of changes in blood oxygenation could be possible [31].

Conclusion

7.0T MRI is feasible in patients with HCM. High spatial resolution CINE imaging at 7.0T allows the identification of subtle morphological details in regions of extended hypertrophy

and fibrosis. These structures were not detectable at clinical field strength and may allow new insights into the development of remodeling.

Limitation

In this pilot trial the number of patients was limited; therefore a genotype/phenotype correlation is missing. This study has addressed the potential advantage of higher spatial resolution, whereas the challenges of acquisition time and systematic evaluation of magnetic field inhomogeneity have to be elucidated in next studies. RF power deposition was not a limiting factor in this setting, but could impact other CMR techniques such as fast spin-echo imaging.

In our setting we did not perform coverage of the entire LV by CINE-imaging due to examination time constraints. That may impact the assessment of further small structures. The use of high-resolution 3D cine application would help to overcome this limitation.

Supporting Information

S1 File. HCM patient with myocardial crypts at 7.0T.
(MP4)

Acknowledgments

The authors wish to thank the technicians Kerstin Kretschel, Evelyn Polzin, Denise Kleindienst and Antje Els for their dedication and support during the CMR examinations. We thank the study nurses Elke Nickel-Szczech and Annette Köhler for their help in patient recruitment. The study was supported by university funds (Charité) hold by JSM.

Author Contributions

Conceived and designed the experiments: JSM MP. Performed the experiments: JSM MP AT FvK. Analyzed the data: MP ES FvK JSM. Contributed reagents/materials/analysis tools: TN PK CT TH MD AG DL JR. Wrote the paper: MP JSM TN.

References

1. Authors/Task Force m, Elliott PM, Anastasakis A, Borger MA, Borggrefe M, et al. (2014) 2014 ESC Guidelines on diagnosis and management of hypertrophic cardiomyopathy: The Task Force for the Diagnosis and Management of Hypertrophic Cardiomyopathy of the European Society of Cardiology (ESC). Eur Heart J.
2. Gersh BJ, Maron BJ, Bonow RO, Dearani JA, Fifer MA, et al. (2011) 2011 ACCF/AHA Guideline for the Diagnosis and Treatment of Hypertrophic Cardiomyopathy: a report of the American College of Cardiology Foundation/American Heart Association Task Force on Practice Guidelines. Developed in collaboration with the American Association for Thoracic Surgery, American Society of Echocardiography, American Society of Nuclear Cardiology, Heart Failure Society of America, Heart Rhythm Society, Society for Cardiovascular Angiography and Interventions, and Society of Thoracic Surgeons. J Am Coll Cardiol 58: e212–260. doi: 10.1016/j.jacc.2011.06.011 PMID: 22075469
3. Moon JC, Reed E, Sheppard MN, Elkington AG, Ho SY, et al. (2004) The histologic basis of late gadolinium enhancement cardiovascular magnetic resonance in hypertrophic cardiomyopathy. J Am Coll Cardiol 43: 2260–2264. PMID: 15193690
4. O'Hanlon R, Grasso A, Roughton M, Moon JC, Clark S, et al. (2010) Prognostic significance of myocardial fibrosis in hypertrophic cardiomyopathy. J Am Coll Cardiol 56: 867–874. doi: 10.1016/j.jacc.2010.05.010 PMID: 20688032
5. Bruder O, Wagner A, Jensen CJ, Schneider S, Ong P, et al. (2010) Myocardial scar visualized by cardiovascular magnetic resonance imaging predicts major adverse events in patients with hypertrophic cardiomyopathy. J Am Coll Cardiol 56: 875–887. doi: 10.1016/j.jacc.2010.05.007 PMID: 20667520

6. Kramer CM, Appelbaum E, Desai MY, Desvigne-Nickens P, DiMarco JP, et al. (2015) Hypertrophic Cardiomyopathy Registry: The rationale and design of an international, observational study of hypertrophic cardiomyopathy. Am Heart J 170: 223–230. doi: 10.1016/j.ahj.2015.05.013 PMID: 26299218
7. Rickers C, Wilke NM, Jerosch-Herold M, Casey SA, Panse P, et al. (2005) Utility of cardiac magnetic resonance imaging in the diagnosis of hypertrophic cardiomyopathy. Circulation 112: 855–861. PMID: 16087809
8. Brouwer WP, Germans T, Head MC, van der Velden J, Heymans MW, et al. (2012) Multiple myocardial crypts on modified long-axis view are a specific finding in pre-hypertrophic HCM mutation carriers. Eur Heart J Cardiovasc Imaging 13: 292–297. doi: 10.1093/ehjci/jes005 PMID: 22277119
9. Maron MS, Rowin EJ, Lin D, Appelbaum E, Chan RH, et al. (2012) Prevalence and clinical profile of myocardial crypts in hypertrophic cardiomyopathy. Circ Cardiovasc Imaging 5: 441–447. doi: 10.1161/CIRCIMAGING.112.972760 PMID: 22563033
10. Sinnecker T, Mittelstaedt P, Dorr J, Pfueller CF, Harms L, et al. (2012) Multiple sclerosis lesions and irreversible brain tissue damage: a comparative ultrahigh-field strength magnetic resonance imaging study. Arch Neurol 69: 739–745. doi: 10.1001/archneurol.2011.2450 PMID: 22351849
11. von Knobelsdorff-Brenkenhoff F, Frauenrath T, Prothmann M, Dieringer MA, Hezel F, et al. (2010) Cardiac chamber quantification using magnetic resonance imaging at 7 Tesla—a pilot study. Eur Radiol 20: 2844–2852. doi: 10.1007/s00330-010-1888-2 PMID: 20640427
12. von Knobelsdorff-Brenkenhoff F, Tkachenko V, Winter L, Rieger J, Thalhammer C, et al. (2013) Assessment of the right ventricle with cardiovascular magnetic resonance at 7 Tesla. J Cardiovasc Magn Reson 15: 23. doi: 10.1186/1532-429X-15-23 PMID: 23497030
13. van Elderen SG, Versluis MJ, Webb AG, Westenberg JJ, Doornbos J, et al. (2009) Initial results on in vivo human coronary MR angiography at 7 T. Magn Reson Med 62: 1379–1384. doi: 10.1002/mrm.22168 PMID: 19859918
14. Thalhammer C, Renz W, Winter L, Hezel F, Rieger J, et al. (2012) Two-dimensional sixteen channel transmit/receive coil array for cardiac MRI at 7.0 T: design, evaluation, and application. J Magn Reson Imaging 36: 847–857. doi: 10.1002/jmri.23724 PMID: 22706727
15. Graessl A, Renz W, Hezel F, Dieringer MA, Winter L, et al. (2014) Modular 32-channel transceiver coil array for cardiac MRI at 7.0T. Magn Reson Med 72: 276–290. doi: 10.1002/mrm.24903 PMID: 23904404
16. IEC (2010) 60601-2-33 Medical electrical equipment—Part 2–33: Particular requirements for the basic safety and essential performance of magnetic resonance equipment for medical diagnosis. 3.0 ed.
17. Frauenrath T, Hezel F, Renz W, d'Orth Tde G, Dieringer M, et al. (2010) Acoustic cardiac triggering: a practical solution for synchronization and gating of cardiovascular magnetic resonance at 7 Tesla. J Cardiovasc Magn Reson 12: 67. doi: 10.1186/1532-429X-12-67 PMID: 21080933
18. von Knobelsdorff-Brenkenhoff F, Prothmann M, Dieringer MA, Wassmuth R, Greiser A, et al. (2013) Myocardial T1 and T2 mapping at 3 T: reference values, influencing factors and implications. J Cardiovasc Magn Reson 15: 53. doi: 10.1186/1532-429X-15-53 PMID: 23777327
19. Kellman P, Hernando D, Shah S, Zuehlsdorff S, Jerecic R, et al. (2009) Multiecho dixon fat and water separation method for detecting fibrofatty infiltration in the myocardium. Magn Reson Med 61: 215–221. doi: 10.1002/mrm.21657 PMID: 19097213
20. Schulz-Menger J, Bluemke DA, Bremerich J, Flamm SD, Fogel MA, et al. (2013) Standardized image interpretation and post processing in cardiovascular magnetic resonance: Society for Cardiovascular Magnetic Resonance (SCMR) board of trustees task force on standardized post processing. J Cardiovasc Magn Reson 15: 35. doi: 10.1186/1532-429X-15-35 PMID: 23634753
21. Rudolph A, Abdel-Aty H, Bohl S, Boye P, Zagrosek A, et al. (2009) Noninvasive detection of fibrosis applying contrast-enhanced cardiac magnetic resonance in different forms of left ventricular hypertrophy relation to remodeling. J Am Coll Cardiol 53: 284–291. doi: 10.1016/j.jacc.2008.08.064 PMID: 19147047
22. Deva DP, Williams LK, Care M, Siminovitch KA, Moshonov H, et al. (2013) Deep basal inferoseptal crypts occur more commonly in patients with hypertrophic cardiomyopathy due to disease-causing myofilament mutations. Radiology 269: 68–76. doi: 10.1148/radiol.13122344 PMID: 23771913
23. Child N, Muhr T, Sammut E, Dabir D, Ucar E, et al. (2014) Prevalence of myocardial crypts in a large retrospective cohort study by cardiovascular magnetic resonance. J Cardiovasc Magn Reson 16: 66. doi: 10.1186/s12968-014-0066-0 PMID: 25231729
24. Petryka J, Baksi AJ, Prasad SK, Pennell DJ, Kilner PJ (2014) Prevalence of inferobasal myocardial crypts among patients referred for cardiovascular magnetic resonance. Circ Cardiovasc Imaging 7: 259–264. doi: 10.1161/CIRCIMAGING.113.001241 PMID: 24508667

25. Kuribayashi T, Roberts WC (1992) Myocardial disarray at junction of ventricular septum and left and right ventricular free walls in hypertrophic cardiomyopathy. Am J Cardiol 70: 1333–1340. PMID: 1442587

26. Klix S, Els A, Paul K, Graessl A, Oezerdem C, et al. (2015) On the subjective acceptance during cardiovascular magnetic resonance imaging at 7.0 Tesla. PLoS One 10: e0117095. doi: 10.1371/journal.pone.0117095 PMID: 25621491

27. Go AS, Mozaffarian D, Roger VL, Benjamin EJ, Berry JD, et al. (2014) Heart disease and stroke statistics—2014 update: a report from the American Heart Association. Circulation 129: e28–e292. doi: 10.1161/01.cir.0000441139.02102.80 PMID: 24352519

28. Santoro D, Winter L, Muller A, Vogt J, Renz W, et al. (2012) Detailing radio frequency heating induced by coronary stents: a 7.0 Tesla magnetic resonance study. PLoS One 7: e49963. doi: 10.1371/journal.pone.0049963 PMID: 23185498

29. Winter L, Oberacker E, Ozerdem C, Ji Y, von Knobelsdorff-Brenkenhoff F, et al. (2015) On the RF heating of coronary stents at 7.0 Tesla MRI. Magn Reson Med 74: 999–1010. doi: 10.1002/mrm.25483 PMID: 25293952

30. Mainero C, Benner T, Radding A, van der Kouwe A, Jensen R, et al. (2009) In vivo imaging of cortical pathology in multiple sclerosis using ultra-high field MRI. Neurology 73: 941–948. doi: 10.1212/WNL.0b013e3181b64bf7 PMID: 19641168

31. Hezel F, Thalhammer C, Waiczies S, Schulz-Menger J, Niendorf T (2012) High spatial resolution and temporally resolved T2* mapping of normal human myocardium at 7.0 Tesla: an ultrahigh field magnetic resonance feasibility study. PLoS One 7: e52324. doi: 10.1371/journal.pone.0052324 PMID: 23251708

W(h)ither human cardiac and body magnetic resonance at ultrahigh fields? Technical advances, practical considerations, applications, and clinical opportunities

Thoralf Niendorf, Katharina Paul, Celal Oezerdem, Andreas Graessl, Sabrina Klix, Till Huelnhagen, Fabian Hezel, Jan Rieger, Helmar Waiczies, Jens Frahm, Armin M. Nagel, Eva Oberacker and Lukas Winter

NMR Biomed. 2016 Sep;29(9):1173-97

https://doi.org/10.1002/nbm.3268

High Field Cardiac Magnetic Resonance Imaging: A Case for Ultra-high Field Cardiac Magnetic Resonance.

Thoralf Niendorf, PhD; Jeanette Schulz-Menger, MD; Katharina Paul, PhD; Till Huelnhagen, Dipl Ing; Victor A. Ferrari, MD, PhD; Russell Hodge, MA

Circ Cardiovasc Imaging. 2017;10:e005460.

https://doi.org/10.1161/CIRCIMAGING.116.005460

frontiers in Physics

TECHNOLOGY REPORT
published: 14 June 2017
doi: 10.3389/fphy.2017.00022

Myocardial T_2* Mapping with Ultrahigh Field Magnetic Resonance: Physics and Frontier Applications

Till Huelnhagen[1], *Katharina Paul*[1], *Min-Chi Ku*[1,2], *Teresa Serradas Duarte*[1] *and Thoralf Niendorf*[1,2,3]*

[1] Berlin Ultrahigh Field Facility, Max Delbrück Center for Molecular Medicine in the Helmholtz Association, Berlin, Germany, [2] DZHK (German Centre for Cardiovascular Research), Berlin, Germany, [3] MRI.TOOLS GmbH, Berlin, Germany

Cardiovascular magnetic resonance imaging (CMR) has become an indispensable clinical tool for the assessment of morphology, function and structure of the heart muscle. By exploiting quantification of the effective transverse relaxation time (T_2*) CMR also affords myocardial tissue characterization and probing of cardiac physiology, both being in the focus of ongoing research. These developments are fueled by the move to ultrahigh magnetic field strengths, which permits enhanced sensitivity and spatial resolution that help to overcome limitations of current clinical MR systems with the goal to contribute to a better understanding of myocardial (patho)physiology *in vivo*. In this context, the aim of this report is to introduce myocardial T_2* mapping at ultrahigh magnetic fields as a promising technique to non-invasively assess myocardial (patho)physiology. For this purpose the basic principles of T_2* assessment, the biophysical mechanisms determining T_2* and (pre)clinical applications of myocardial T_2* mapping are presented. Technological challenges and solutions for T_2* sensitized CMR at ultrahigh magnetic field strengths are discussed followed by a review of acquisition techniques and post-processing approaches. Preliminary results derived from myocardial T_2* mapping in healthy subjects and cardiac patients at 7.0 T are presented. A concluding section discusses remaining questions and challenges and provides an outlook on future developments and potential clinical applications.

Keywords: magnetic resonance, MRI, ultrahigh field, magnetic susceptibility, MR technology, cardiac physiology, cardiovascular imaging, myocardial tissue characterization

OPEN ACCESS

Edited by:
Ewald Moser,
Medical University of Vienna, Austria

Reviewed by:
Bernhard Gruber,
University Medical Center Utrecht, Netherlands
Albrecht Ingo Schmid,
Medical University of Vienna, Austria

***Correspondence:**
Thoralf Niendorf
thoralf.niendorf@mdc-berlin.de

Specialty section:
This article was submitted to Biomedical Physics, a section of the journal Frontiers in Physics

Received: *24 March 2017*
Accepted: *30 May 2017*
Published: *14 June 2017*

Citation:
Huelnhagen T, Paul K, Ku M-C, Serradas Duarte T and Niendorf T (2017) Myocardial T_2 Mapping with Ultrahigh Field Magnetic Resonance: Physics and Frontier Applications. Front. Phys. 5:22. doi: 10.3389/fphy.2017.00022*

INTRODUCTION

T_2* Sensitized Cardiovascular Magnetic Resonance

Myocardial tissue characterization plays an important role in the diagnosis and treatment of cardiac diseases. Thanks to its soft tissue contrast and versatility, cardiovascular magnetic resonance imaging (CMR) has become a vital clinical tool for diagnosis and for guiding therapy of cardiac diseases [1, 2]. CMR can provide morphologic and functional information as well as insights into microstructural changes of the heart muscle [2]. Quantitative mapping of MR relaxation times which govern the MR signal evolution offers the potential of non-invasive myocardial tissue characterization without the need of exogenous contrast agents. Mapping of the effective transverse relaxation time T_2* is the subject of intense clinical interest in CMR. By exploiting the blood oxygenation level-dependent (BOLD) effect [3], T_2* sensitized CMR has been proposed as a

means of assessing myocardial tissue oxygenation and perfusion. T_2* mapping has been shown to be capable of detecting myocardial ischemia caused by coronary artery stenosis [4], to reveal myocardial perfusion deficits under pharmacological stress [5–10], to study endothelial function [11] or to assess breathing maneuver-dependent oxygenation changes in the myocardium [12–15]. Preclinical studies have also demonstrated the potential of T_2* mapping to detect structural changes in the infarcted heart muscle and even to distinguish between focal and diffuse fibrosis [16–18]. In clinical application T_2* mapping is the method of choice for quantification of myocardial iron content, an essential parameter for guiding therapy in patients with myocardial iron overload [19–23].

The linear increase of susceptibility effects with magnetic field strength together with the availability of ultrahigh field ($B_0 \geq$ 7.0 T) whole body human MR systems has fueled explorations into myocardial T_2* mapping at 7.0 T. In this context, the aim of this report is to introduce the biophysical background of T_2* as a promising MR biomarker, present challenges and technical solutions for myocardial T_2* assessment at ultrahigh magnetic field strengths, discuss its merits and current limitations, as well as to show early applications in healthy volunteers and cardiac patients along with providing a look beyond the horizon.

Biophysics of the Effective Transverse Relaxation Time T_2*

The fundamental principle behind T_2* relaxation is the loss of phase coherence of an ensemble of spins contained within a volume of interest or voxel after a radio frequency (RF) excitation. Unlike T_1 relaxation which is based on spin-lattice interactions or T_2 relaxation which is caused by spin-spin interactions both being inherent properties of tissues in a magnetic field, T_2* relaxation includes a tissue inherent part as well as contributions from external magnetic field perturbations [24]. These magnetic field inhomogeneities influence the effective transversal MR relaxation time T_2* [25, 26]. T_2* is defined as:

$$\frac{1}{T_2^*} = \frac{1}{T_2} + \frac{1}{T_2'} \tag{1}$$

with T_2 being the transverse relaxation time and T_2' representing magnetic susceptibility related contributions [27].

The most common way of T_2*-weighted imaging is gradient recalled echo (GRE) imaging. The MR signal magnitude $S_m(\theta)$ created by a spoiled GRE pulse sequence is:

$$S_m(\theta) = S_0 sin(\theta) exp\left(-TE/T_2^*\right) \frac{\left[1 - exp\left(-TR/T_1\right)\right]}{\left[1 - cos\left(\theta\right) exp\left(-TR/T_1\right)\right]} \tag{2}$$

with S_0 representing the spin density, TR the repetition time, TE the echo time defined by the time between MR signal excitation and MR signal readout [28], T_1 and T_2* are tissue specific longitudinal and effective transversal relaxation time constants and θ is the flip angle about which the magnetization is deflected by the excitation RF pulse. If TR and T_1 are being kept constant Equation (2) can be simplified to:

$$S_m(\theta) \propto exp\left(-TE/T_2^*\right) \tag{3}$$

Exploiting this relationship T_2* can be estimated by acquiring a series of images at different echo times TE followed by an exponential fit of the measured signal intensity vs. the echo time TE. This is commonly realized by using multi echo gradient echo (MEGRE) pulse sequences, which employ a series of dephasing and refocusing gradients to quickly acquire a series of T_2* sensitized images at several echo times as illustrated in **Figure 1**. T_2* weighted MRI is most sensitive to field perturbations when TE is equal to T_2* [29]. Exponential fitting of the signal decay can be done either for each voxel individually or for the mean signal within a region of interest. Single voxel fitting is more prone to noise but provides spatially resolved information in the form of relaxation maps (**Figure 1**). Besides mono-exponential fitting also multi-exponential fitting can be applied, if multiple signal compartments with different T_2* relaxation times are expected within an imaging voxel.

$$\begin{aligned} S_m(\theta) \propto\ & S_1 exp\left(-TE/{}^1T_2^*\right) + S_2 exp\left(-TE/{}^2T_2^*\right) + \ldots \\ & + S_n exp\left(-TE/{}^nT_2^*\right) \end{aligned} \tag{4}$$

Here S_1, S_2, S_n represent the relative volume fractions of the different compartments with their corresponding effective transverse relaxation times ${}^1T_2$*, ${}^2T_2$*, and ${}^nT_2$*.

T_2* relaxation is blood oxygenation level dependent and provides a functional MR contrast which serves as the basis of functional brain mapping [3, 26]. The effect results from a change of the magnetic susceptibility of hemoglobin (Hb) depending on its oxygenation state. Oxygenated hemoglobin is diamagnetic and has minor effect on magnetic field homogeneity. Deoxygenated hemoglobin in contrast is paramagnetic and causes magnetic field perturbations on a microscopic level resulting in spin dephasing and signal loss. T_2*-weighted MRI is sensitive to changes in the amount of deoxygenated Hb (deoxy Hb) per tissue volume element (voxel). T_2* changes and corresponding signal attenuation in T_2*-weighted MR images can hence result from a change in hemoglobin oxygenation or a change of the tissue blood volume fraction. The discovery of the BOLD phenomenon led to the development of functional MRI for mapping of human brain function, but also inspired research into BOLD imaging and T_2* mapping of the heart [9, 30].

T_2* sensitized imaging and mapping are widely assumed to provide a surrogate of oxygenation. Yet the factors impacting the transverse relaxation rate other than oxygenation are numerous including macroscopic magnetic field inhomogeneities, blood volume fraction and hematocrit [31]. Considering a biologic tissue with a specific blood volume fraction BVf, a hematocrit Hct, and a local blood oxygen saturation So_2, T_2* can be modeled as:

$$\begin{aligned} \frac{1}{T_2^*} = \frac{1}{T_2} + \gamma \left|\Delta B\right| = & \frac{1}{T_2} \\ & + BVf \cdot \gamma \cdot \frac{4}{3} \cdot \pi \cdot \Delta\chi_0 \cdot Hct \cdot (1 - So_2)\, B_0 + \gamma \left|\Delta B_{other}\right| \end{aligned} \tag{5}$$

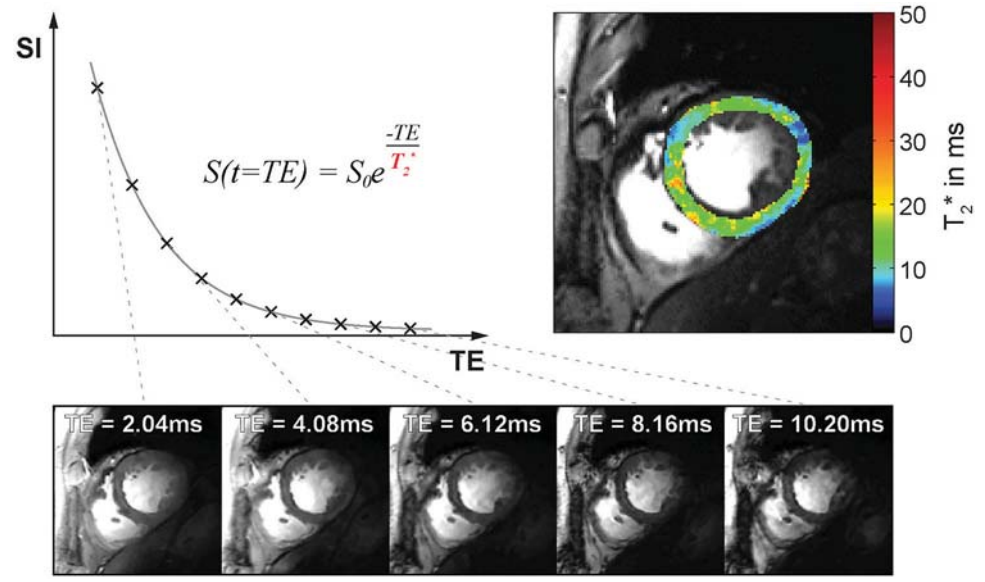

FIGURE 1 | T_2^* decay and T_2^*-weighted image contrast. Top left: Plot of signal intensity over echo time for T_2^* weighted imaging. Bottom: Example of mid-ventricular short axis views of the human heart obtained at 7.0 T. Images were acquired with increasing T_2^*-weighting (from left to right). Top right: Corresponding myocardial T_2^* map superimposed to a FLASH CINE image.

with $\gamma\,|\Delta B_{other}|$ representing additional magnetic field inhomogeneities such as macroscopic field changes [32, 33] and $\Delta\chi_0 = 3.318$ ppm being the magnetic susceptibility difference of fully oxygenated and fully deoxygenated hemoglobin (in SI units) [34]. When tissue blood volume fraction, hematocrit level and macroscopic B_0 contributions are known and echo times are greater than a characteristic time Equation (5) can be employed to non-invasively estimate tissue oxygenation using MRI [33]. It should be noted that a reduction in the tissue blood volume fraction can result in a T_2* increase which could be misinterpreted as an oxygenation increase and hence result in premature conclusions if the effect of blood volume fraction is not taken into account [35]. If all the parameters are considered correctly, T_2* can serve as a non-invasive means to probe physiology *in vivo*. It should be noted that T_2 changes, e.g., caused by alterations in tissue water content or distribution are also reflected in T_2* and hence should be considered as potential confounders.

Benefits of Myocardial T_2* Mapping at Higher Magnetic Field Strengths

The magnetization M of a material in response to an applied magnetic field is given by its magnetic susceptibility χ and the strength of the applied magnetic field H:

$$M = \chi H \tag{6}$$

This relationship results in a linear increase of magnetic field perturbations induced by microscopic susceptibility changes—the main driving force behind T_2* decay—when moving to higher magnetic fields. The effect has been confirmed for myocardial R_2* ($R_2^* = 1/T_2^*$) *in vivo* rendering T_2* mapping at ultrahigh magnetic fields ($B_0 \geq 7.0$ T) particularly appealing [36] (**Figure 2**). The enhanced susceptibility effects at 7.0 T may be useful to extend the dynamic range of the sensitivity for monitoring T_2* changes and to lower their detection level. Another advantage of performing T_2* weighted imaging and mapping at ultrahigh magnetic field strengths (UHF) is that the signal-to-noise ratio (SNR) gain achieved at higher fields can be used to improve the spatial resolution [37, 38]. This reduction in voxel sizes lowers the impact of macroscopic magnetic field gradients on intra-voxel dephasing and hence T_2* which otherwise can be a concern especially in the vicinity of strong susceptibility transitions. Transitioning to higher magnetic field strengths runs the additional benefit that the in-phase inter-echo time governed by the fat-water phase shift between the water and main fat peak of about 3.5 ppm is reduced from approximately 4.5 ms (223 Hz) at 1.5 T to 0.96 ms (1,043 Hz) at 7.0 T. This enables rapid acquisition of multiple echoes with different T_2* sensitization and facilitates high spatio-temporally resolved myocardial CINE T_2* mapping of the human heart [39]. Taking advantage of this technique, T_2* mapping at ultrahigh magnetic fields has been suggested as a means to probe myocardial physiology and to advance myocardial tissue characterization.

CHALLENGES AND TECHNICAL SOLUTIONS FOR CARDIAC MRI AT ULTRAHIGH MAGNETIC FIELDS

Enabling Radio Frequency Antenna Technology

Imaging the heart—a deep-lying target region surrounded by the lung within the large volume of the thorax—at ultrahigh magnetic field strengths poses a severe challenge due to the

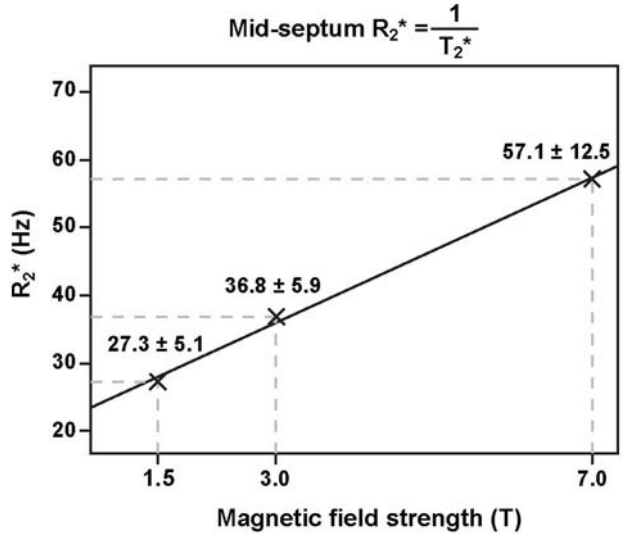

FIGURE 2 | Relation of ventricular septal R_2^* and static magnetic field strength. Myocardial R_2^* increases linearly with magnetic field strength (adapted from Meloni et al. [36] with permission from John Wiley and Sons).

short wavelength of the proton resonance frequency in tissue ($\lambda_{myocardium} \approx 12$ cm at 7.0 T). As a result, non-uniformities in the transmission field (B_1^+) can cause shading, massive signal drop-off or signal void in the images up to non-diagnostic image quality. These constraints were reported being a concern in CMR at 3.0 T [40] and were to be expected to pose a major obstacle for CMR at UHF.

A plethora of reports have evolved during the past years introducing technical innovations in RF antenna design to overcome non-uniform transmission fields. Local transceiver (TX/RX) and multi-channel transmission arrays in conjunction with multi-channel local receive arrays have been suggested as possible solutions. Eminent developments put building blocks to use consisting of stripline elements [41–45], electrical dipoles [45–51], dielectric resonant antennas [52], slot antennas [53], and loop elements [54–59]. Rigid, flexible and modular configurations have been exploited. Irrespective of the building block technology, a trend toward higher numbers of transmit and receive elements can be observed with the purpose to advance anatomic coverage [47, 54–59] and to add degrees of freedom for transmission field shaping [60].

Figure 3 compiles developments of loop element based transceiver configurations optimized for CMR at 7.0 T. A 4-channel TX/RX [55] (**Figure 3A**) and an 8-channel TX/RX [58] (**Figure 3B**) one-dimensional array were reported and extended to a 16-channel two-dimensional design [56] (**Figure 3C**). A modular 32-channel TX/RX [59] (**Figure 3D**) array further exploited the two-dimensional building block layout.

Electric dipoles hold the benefit of a linearly polarized current pattern with the RF energy being directed perpendicular to the dipole along the Poynting vector to the subject. As a consequence, the excitation field is symmetrical and uniform and comes with ample depth penetration [48] which renders electric dipoles particularly promising for MR of the upper torso and the heart. This property formed the starting point for explorations into electric dipole configurations [46–48, 50, 51]. Due to their length straight dipole elements are unfavorable if not unfeasible for high density multi-dimensional transceiver coil arrays [48]. To address this issue, the fractionated dipole concept splits the dipole's legs into segments interconnected by capacitors or inductors to achieve dipole shortening. Reduced SAR levels, moderate coupling and homogeneous B_1^+ have been reported for prostate imaging using an eight-element array consisting of fractionated dipoles [51]. A combined 16-channel loop-dipole transceiver array exploiting the fractionated dipole antenna design provided cardiac images acquired at 7.0 T exhibiting high SNR and B_1^+ transmit efficiency [50]. As an alternative, shortening of the effective antenna length can be achieved for a bow tie shaped λ/2-dipole antenna by immersing it in D_2O. Following this achievement electric dipole configurations optimized for UHF-CMR have been reported using 8 or 16 bow tie antenna building blocks [47] (**Figures 3E,F**). As a result of these research efforts, dedicated RF antenna arrays are now available which facilitate cardiac MRI at 7.0 T with rather uniform signal intensities across the heart.

In summary, explorations into enabling RF antenna technology underlined the benefits of many-channel high-density arrays for UHF-CMR.

Ancillary Devices for Cardiac Synchronization

Imaging the heart requires synchronization of the data acquisition with the cardiac cycle. Magneto hydrodynamic (MHD) effects severely disturb the electrocardiogram (ECG) [61–63] commonly applied for cardiac triggering and gating at clinical field strengths [64–66] (**Figure 4**). Distortions of the ECG's S-T segment are caused by the increased MHD impact during systolic aortic flow [67]. The S-T elevation might be mis-interpreted as an R-wave. Consequently, image quality is impaired due to the mis-detected onset of a cardiac cycle. The propensity to MHD effects is pronounced at ultrahigh magnetic field strengths [42, 68, 69]. An MR-stethoscope has been proposed as an alternative to ECG gating and triggering putting acoustic signals to use which have been reported to be immune to interferences with electromagnetic fields. With this practical solution the first heart tone of the phonocardiogram is detected, which marks the onset of the acoustic cardiac cycle. The minor latency between the onset of the electrophysiological cardiac activity and the onset of the acoustic cardiac activity allows prospectively triggered and retrospectively gated acquisitions. Acoustic triggering can hence be used with all pulse sequences that support ECG triggering without the need of sequence adjustments. Reliable trigger information has been demonstrated when using acoustic cardiac triggering and gating for UHF-CMR (**Figure 4**) [61, 68, 70]. Further alternatives for cardiac synchronization include post-processing of the ECG signal to reduce MHD induced distortions of the ECG trace [71, 72]. Wideband radar, magnetic field probes or optical systems have been proposed for physiological monitoring [73–75].

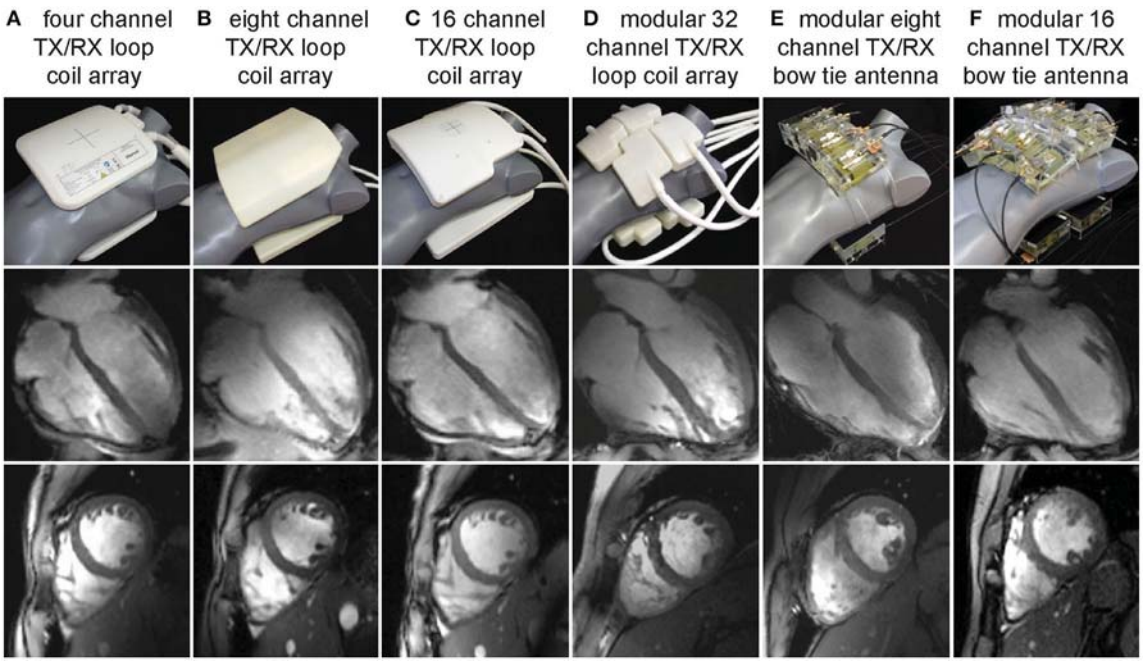

FIGURE 3 | Examples of multi-channel transceiver arrays tailored for cardiac MR at 7.0 T. Top: Photographs of cardiac optimized 7.0 T transceiver coil arrays including (left to right) **(A)** a four-channel, **(B)** an eight channel, **(C)** a 16 channel and **(D)** a 32 channel loop array configuration together with an **(E)** eight channel and **(F)** 16 channel bow tie antenna array. For all configurations the RF elements are used for transmission and reception. Center and bottom: Four chamber and short axis views of the heart derived from 2D CINE FLASH acquisitions using the RF coil arrays shown on the left and a spatial resolution of (1.4 × 1.4. × 4.0) mm^3 (from Niendorf et al. [113] with permission from John Wiley and Sons).

T_2* Imaging Techniques

T_2* sensitized imaging and mapping is commonly performed employing gradient echo imaging independent of magnetic field strength. To decrease acquisition times multi echo gradient echo techniques (MEGRE) acquiring multiple echoes after each RF excitation instead of only one echo per repetition time *TR* are recommended for fast T_2* mapping (**Figure 5A**, top). For myocardial T_2* mapping cardiac triggered segmented acquisitions are commonly performed in end-expiratory breath hold conditions to avoid respiratory and cardiac motion and to reduce related macroscopic B_0 field fluctuations.

The used echo times should be adapted to sufficiently cover the T_2* decay. As the contributing fat and water signal are oscillating at different frequencies mapping algorithms must either account for or compensate the varying signal intensity from fat and water. Acquiring T_2*-weighted images at times when fat and water are equally contributing to the MR signal (in-phase) is the simplest approach to achieve this goal. At 7.0 T this is the case for echo times being a multiple of about 0.96 ms due to the chemical shift between the main fat and water peaks of approximately 3.5 ppm (1,043 Hz). Acquisition of echoes with an inter-echo spacing of ∼1 ms constitutes a challenge due to gradient amplitude and rise time limitations, especially when large acquisition matrix sizes are used. Alternatively, interleaved acquisitions can be performed by distributing the acquisition of neighboring echoes across multiple excitations (**Figure 5A**, middle). This approach permits low inter-echo spacing even for large matrix sizes but results in longer scan times since more than one *TR* is required to acquire a full T_2* decay series. While T_2* mapping at clinical field strengths is limited to single cardiac phase acquisitions, CINE T_2* mapping covering the entire cardiac cycle is feasible at UHF [39]. This advanced capability is facilitated by two benefits of UHF-MR. First, due to transversal relaxation time shortening at ultrahigh magnetic fields, *TE* can be limited to a range of approximately $TE = 0$ ms to $TE = 15$ ms to properly sample the myocardial T_2* decay. This approach is beneficial for reducing the duration of the gradient echo trains compared to lower magnetic field strengths enabling breath held multi echo CINE acquisitions. Second, the reduced in-phase echo spacing permits acquisition of a sufficient number of echoes needed to cover the signal decay and to provide an appropriate number of data points for signal fitting. Interleaving of echo times can be combined with distributing the acquisition across multiple breath-holds to ease gradient constraints and limit breath-hold durations for each acquisition (**Figure 5A**, bottom). All described acquisition strategies are capable of producing T_2* maps of similar fidelity as illustrated in **Figure 5B** for a homogenous MR phantom resembling the relaxation properties of human myocardium. To reduce the effect of macroscopic magnetic field gradients on spin dephasing and T_2*, small voxel sizes are preferable. Of course this preference has to be balanced with SNR requirements for accurate mapping which can be challenging particularly at lower magnetic field strengths. **Figure 5B** compares the effect of slice thickness on T_2*.

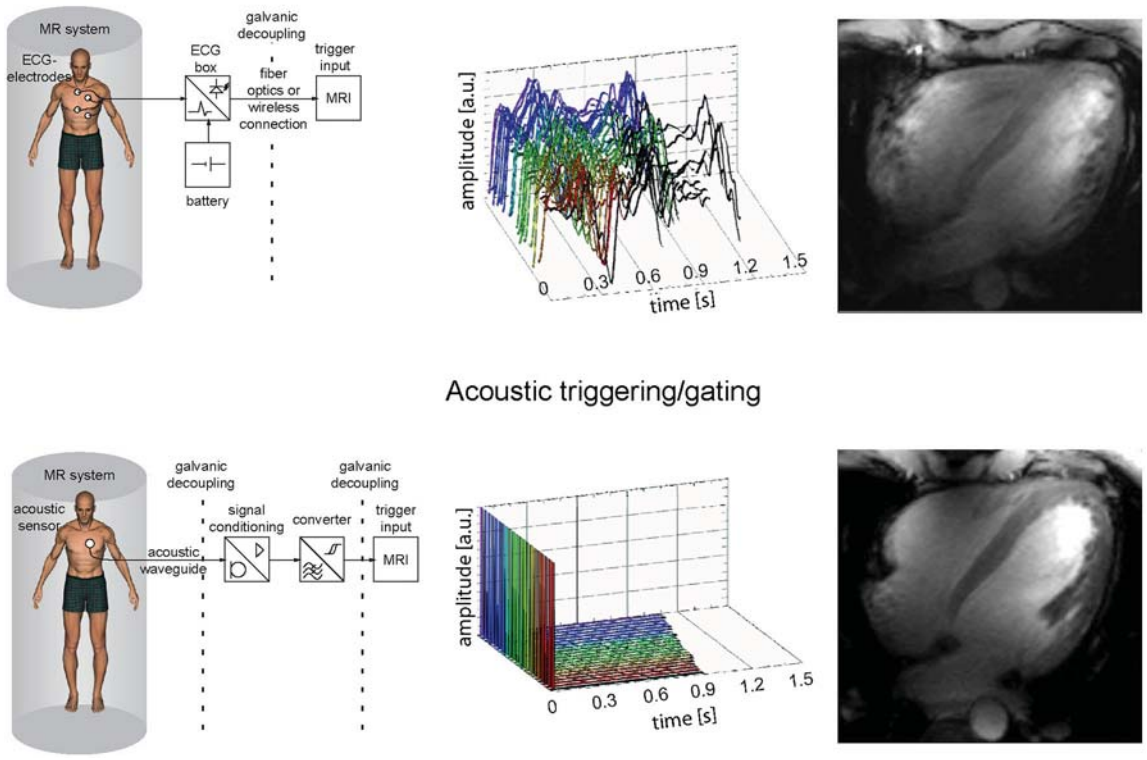

FIGURE 4 | Comparison of ECG and acoustic triggering or gating showing system schemes (left), signal traces acquired in the isocenter of a 7.0 T magnet for 18 cardiac cycles (middle) and corresponding four chamber views acquired at 7.0 T with the respective approaches (right). The ECG gated image shows severe artifacts due to incorrect cardiac synchronization, while the acoustically triggered image reveals decent image quality with good blood myocardium contrast and clear delineation of subtle structures.

While maps acquired with slice thicknesses of 6 mm or above show intra-voxel dephasing and T_2* decrease pronounced at the phantom interfaces, this effect is mitigated for slice thicknesses of 4 mm or less resulting in a more uniform T_2* map. Employing the described multi-breath hold CINE technique at 7.0 T, CINE T_2* mapping with more than 20 cardiac phases is feasible which allows monitoring of myocardial T_2* across the cardiac cycle (**Figure 6**).

In contrast to gradient echo imaging Rapid Acquisition with Relaxation Enhancement (RARE) imaging is rather insensitive to B_0 inhomogeneities, provides images free of distortion due to the use of RF refocused echoes and inherently suppresses blood signal. Cardiac RARE imaging at 7.0 T has been shown to be feasible [76]. These results—in conjunction with the challenges and opportunities of myocardial T_2* mapping at UHF—build the starting point for explorations into RARE based T_2* mapping of the heart at 7.0 T. An evolution time τ inserted after the excitation RF pulse accrues an additional phase to the magnetization that reflects the T_2* effect [77] (**Figure 7A**). As a consequence, the Carr-Purcell-Meiboom-Gill condition cannot be met and destructive interferences between odd and even echo groups configuring the signal in RARE imaging impair the image [78, 79]. Measures to account for this effect include displaced RARE [77, 80], avoiding interferences by discarding one of both echo groups, resulting in an SNR loss of factor two. Split-echo variants hold the benefit that the full available signal is maintained [81] (**Figure 7A**). A series of T_2* weighted images derived from RARE imaging using evolution times τ ranging from 2 to 14 ms is displayed in **Figure 7B** and demonstrates that the geometric integrity of the RARE images is maintained over the range of applied T_2* weighting. The corresponding T_2* map is shown in **Figure 7C**. MEGRE imaging results are shown for comparison and exhibited less myocardium to blood contrast due to the bright-blood characteristic of the technique. Consequently, the delineation of the myocardium in the corresponding T_2* map (**Figure 7C**) is more challenging compared to the RARE based T_2* map. The average effective transversal relaxation time derived from RARE imaging compares well to values previously reported for MEGRE approaches [39]. The concerns of RF power deposition and RF non-uniformity of RARE imaging were offset in this preliminary study. Split-echo RARE hence holds the potential to provide an alternative for T_2* mapping free of geometric distortion and with high blood myocardium contrast.

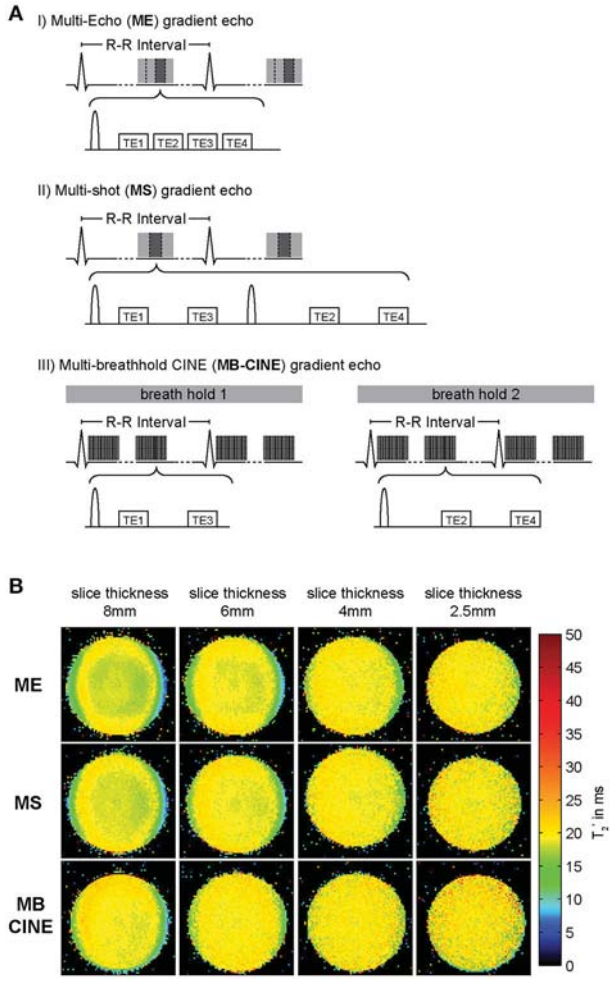

FIGURE 5 | Acquisition schemes used for T_2^* weighted imaging/mapping and corresponding T_2^* maps. **(A) (I)** multi echo gradient echo (MEGRE) acquisition, **(II)** multi shot (MS) interleaved multi gradient echo acquisition, **(III)** multi breath hold CINE (MB-CINE) interleaved multi gradient echo acquisition. **(B)** Comparison of T_2^* maps derived from a homogenous phantom resembling myocardial tissue acquired using the three different approaches and slice thicknesses from 8 to 2.5 mm. All acquisition strategies provide similar T_2^* maps. Through plane dephasing is reduced for lower slice thickness (adapted from Hezel et al. [39].)

Assessment and Control of Main Magnetic Field Homogeneity

The complex MR signal $S(r,t)$ obtained by a gradient echo technique at a location $\boldsymbol{r}$ and time t after signal excitation is given by:

$$S(r,t) = \hat{S}(t) \cdot e^{-i\phi(r,t)}, \hat{S}(t) \propto S_0 \cdot e^{-\frac{t}{T_2^*}} \tag{7}$$

$\hat{S}(t)$ is the magnitude signal, i is the imaginary unit and ϕ is the signal phase. The signal phase ϕ can be written as a function of spatial location and time [82]:

$$\phi(r,t) = \phi_0(r) - \gamma \cdot \Delta B(r) \cdot t \tag{8}$$

with γ being the gyromagnetic constant of the nucleus (for ^{1}H $\gamma = 2.675 \times 10^8$ rad/s/T) and $\Delta B(r)$ representing local magnetic field deviations with regard to the main magnetic field strength. $\phi_0(r)$ represents a constant receiver phase offset, while the time-dependent phase component $\gamma \cdot \Delta B(r) \cdot t$ is dominated by the deviation from the static magnetic field and evolves linearly over time [83]. Assuming there are no other external sources of dephasing such as, e.g., motion or flow, the signal phase ϕ serves as a direct measure of deviations from the main magnetic field B_0.

Equation (1) can be approximated as:

$$\frac{1}{T_2^*} = \frac{1}{T_2} + \frac{1}{T_2'} \cong \frac{1}{T_2} + \gamma |\Delta B| \tag{9}$$

if a linear B_0 gradient within a voxel is assumed [32]. This assumption is justified for typical voxel sizes used in cardiac T_2* mapping at 7.0 T with an in-plane spatial resolution of about 1 mm and a slice thickness of 2–4 mm [39, 84]. $|\Delta B|$ in Equation (9) includes microscopic magnetic field perturbations resulting from microstructural changes, blood oxygenation changes, iron accumulation etc. which are of diagnostic interest as well as macroscopic field changes, e.g., due to magnet imperfections or strong susceptibility transitions at air tissue interfaces. This dependency highlights the need to monitor and possibly compensate B_0 inhomogeneities when performing T_2* assessment to make sure that T_2* decay reflects microscopic susceptibility changes rather than macroscopic field perturbations.

By acquiring images at two echo times (TE), the local magnetic field variations can be calculated at each voxel by making use of Equation (8):

$$\Delta B(r) = \frac{\phi(r, TE_2) - \phi(r, TE_1)}{\gamma \ (TE_2 - TE_1)} \tag{10}$$

where $\Delta B(r)$ is given in Tesla. This procedure is referred to as B_0 mapping. It is also very common to represent local magnetic field variations in Hz by means of off-center frequency maps:

$$\Delta B_{Hz}(r) = \frac{\phi(r, TE_2) - \phi(r, TE_1)}{2\pi \ (TE_2 - TE_1)} \tag{11}$$

B_0 shimming describes the process of adjusting the main magnetic field B_0 to improve macroscopic field homogeneity. Active shimming refers to the adjustment of the main magnetic field by making use of dedicated shim coils thereby creating compensatory magnetic fields up to the 5th order of spherical harmonics [85]. Despite the existence of 5th order shim systems, most scanners provide only shim coils up to 2nd order. Active shimming options include fixed shim current settings or shimming modes based on an individual B_0 map acquired for a specific subject. For cardiac B_0 shimming a cardiac triggered field map acquisition is recommended to avoid motion artifacts. Usually a shim volume of interest is defined covering the target anatomy. Ideally the target volume should cover a small region of interest like the heart, to achieve satisfying field homogeneity

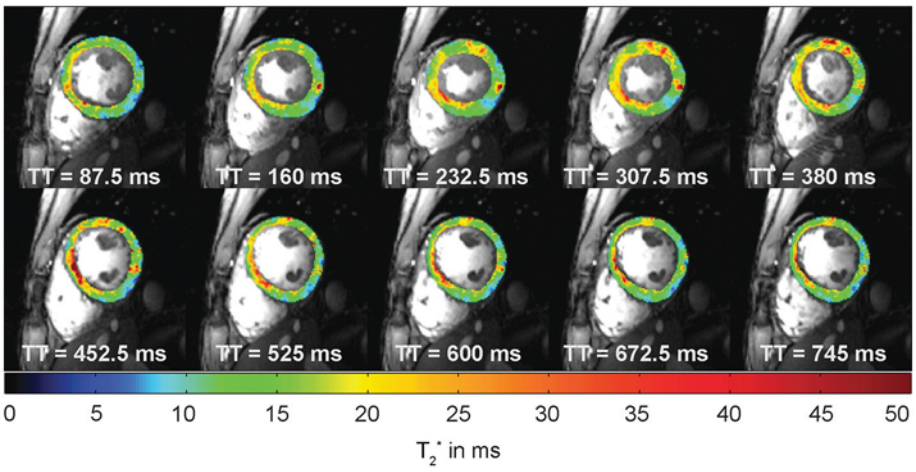

FIGURE 6 | Example of cardiac phase resolved myocardial T_2^* mapping of a short axis view of a healthy volunteer (10 out of 20 phases shown). Spatial resolution = (1.1 × 1.1 × 4.0) mm^3. Temporal resolution = 37 ms. T_2^* variations can be observed across the cardiac cycle. TT indicates the time since the trigger.

even when a limited order of shim coils is available. **Figure 8** compares B_0 homogeneity in the heart of a healthy subject at 7.0 T after applying a volume shim (**Figure 8A**, top), which is focused only on the heart and after applying a global shim (**Figure 8A**, bottom) which includes the entire field of view. Volume selective shimming was found to lead to a significant improvement in macroscopic B_0 homogeneity vs. global B_0 shimming (**Figure 8B**) [39].

Due to increased susceptibility effects, magnetic field inhomogeneities are pronounced at higher magnetic field strengths [36] (compare Equation 6). This is often a concern for T_2* weighted imaging or T_2* mapping at high and ultrahigh magnetic fields. However, by employing dedicated shimming approaches, a mean peak-to-peak off-resonance frequency across the human heart of 80 Hz [39] was reported at 7.0 T. For the left ventricle a B_0 peak-to-peak difference of approximately 65 Hz was observed at 7.0 T after volume selective shimming [39]. These results were obtained with a second order shim system so that the same level of B_0 uniformity reported here should be achievable with the current and next generation of 7.0 T scanners. The frequency shift across the heart obtained at 7.0 T compares well with previous 3.0 T studies which reported a peak-to-peak off-resonance variation of (176 ± 30) Hz over the left ventricle and (121 ± 31) Hz over the right ventricle with the use of localized linear and second-order shimming [86]. The use of an enhanced locally optimized shim algorithm, which is tailored to the geometry of the heart, afforded a reduction of the peak-to-peak frequency variation over the heart from 235 to 86 Hz at 3.0 T [87]. Another study showed a peak-to-peak off-resonance of (71 ± 14) Hz for short axis views acquired at 1.5 T [88] using global shimming. While dedicated shim routines revealed competitive results at 7.0 T vs. lower magnetic fields strength, the feasibility of using these approaches in a clinical setting remains to be investigated.

The achievement of macroscopic B_0 homogeneity across the heart at 7.0 T which is competitive with that obtained at lower magnetic field strengths provides encouragement to pursue susceptibility-based myocardial T_2* mapping at ultrahigh fields. Yet, with the arrival of CINE T_2* mapping techniques enabled by 7.0 T [39], also temporal B_0 fluctuations across the cardiac cycle and their implications on T_2* need to be considered for a meaningful interpretation of dynamic T_2*-weighted acquisitions. Temporal B_0 variation across the cardiac cycle was reported to be negligible at 1.5 T [89], but due to the increase of susceptibility effects at ultrahigh fields further investigations of this potential confounder were required at 7.0 T. It should be noted that T_2*-weighted contrast is determined by magnetic field gradients rather than absolute magnetic field strength, thus it is essential to investigate the change of these gradients over the cardiac cycle. This was done at 7.0 T by assessing macroscopic B_0 gradients across the cardiac cycle in the heart of healthy volunteers together with high temporal and spatial resolution T_2* maps [84, 90]. T_2*-weighted series of short-axis views were acquired using a MEGRE CINE approach (**Figure 9A**, top) for cardiac phase resolved B_0 and T_2* mapping. Temporally-resolved B_0 maps of the heart were calculated (**Figure 9A**, middle). Macroscopic intra-voxel field gradients were determined for each cardiac phase and their fluctuations were analyzed across the cardiac cycle. The septal in-plane gradients were found to be significantly larger compared to through-plane gradients within a voxel [with a mean in-plane field dispersion of (2.5 ± 0.2) Hz/mm against the a mean through-plane field dispersion of (0.4 ± 0.1) Hz/mm] [91].

In order to evaluate how these B_0 gradients affect T_2* measurements, the B_0 gradient-induced change of T_2* represented as ΔT_2* was estimated [84, 91]. **Figure 9B** shows the plot of mean septal T_2*, intra-voxel B_0 gradients and estimated gradient-induced ΔT_2* over the cardiac cycle averaged over a group of healthy subjects. The mean septal T_2* per cardiac phase was found to vary over the cardiac cycle in a range of approximately 23% of the total mean T_2* for all phases. Yet, the temporal range of mean ΔT_2* induced by the calculated intra-voxel macroscopic B_0 gradients represented

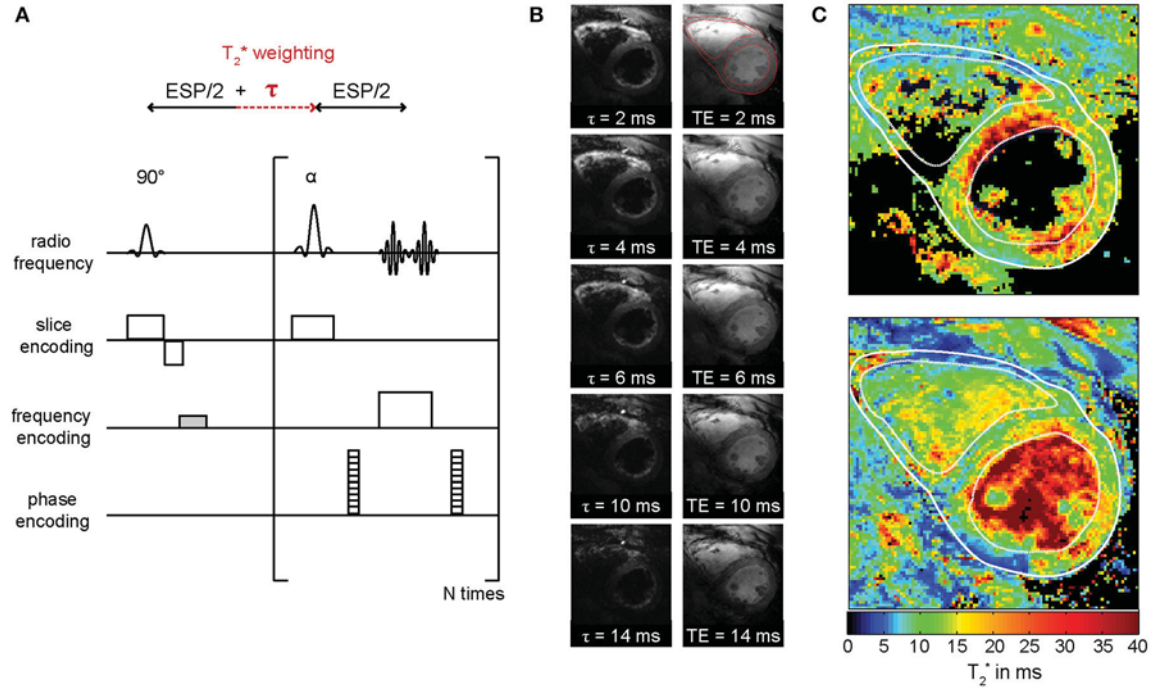

FIGURE 7 | RARE-based myocardial T_2^* mapping at 7.0 T. **(A)** Basic pulse sequence diagram of T_2^* weighted split-echo RARE. T_2^* weighting is introduced into RARE by adding an evolution time τ after the excitation RF pulse. The dephasing gradient in frequency encoding direction is imbalanced (marked in gray) to avoid destructive interferences between odd and even echo groups. **(B)** T_2^*-weighted split-echo RARE images of a short axis view employing evolution times ranging from τ = 2 ms to τ = 14 ms (left). MEGRE images obtained with echo times ranging from 2 to 14 ms (right). For improved visualization, the images do not exhibit identical windowing over the range of increasing susceptibility weighting. The myocardium was delineated and the contour is shown in the images with minimal τ/TE. **(C)** T_2^* maps derived from data in shown in **(B)** are depicted for the RARE (top) and the GRE (bottom) approach. The contours defined in the images with minimal τ/TE were copied to the T_2^* maps for better delineation of the myocardium.

only a 5% change of total mean T_2*. The remaining 18% were suggested to reflect microscopic B_0 gradient changes (potentially caused by physiological events) rather than macroscopic field inhomogeneities [84, 91].

In summary it can be concluded that if careful shimming is applied, macroscopic magnetic field inhomogeneities are not of concern for myocardial T_2* mapping even at a magnetic field strength as high as 7.0 T. Also dynamic B_0 fluctuations across the cardiac cycle can be considered negligible in the ventricular septum. These findings represent an essential prerequisite for meaningful interpretation of myocardial T_2* and its dynamics across the cardiac cycle.

Data Post-processing

The effective transverse relaxation time T_2* can be estimated by fitting an exponential function to a series of gradient echo images with different T_2* weighting, i.e., different echo times (compare Equations 3, 4; **Figure 1**). A common way of calculating such a fit by avoiding non-linear fitting procedures, is to calculate the natural logarithm of the acquired signal intensities and apply a least squares linear fit to the resulting data. This procedure is fast and produces the best solution to represent the linearized data in a least squares sense. Further to this, non-linear fitting approaches which can be applied directly to the measured data are available. The algorithms employ non-linear models in conjunction with optimization algorithms like Levenberg-Marquardt or Simplex [92]. Iterative non-linear fitting algorithms can provide improved fitting accuracy, but can be prone to careful initialization. Fast linear fitting can be used to initialize non-linear fitting algorithms leading to increased robustness and faster convergence. Irrespective of the kind of employed fitting procedure, care should be taken for voxels with intensities being at the noise level and hence potentially deteriorating the fit quality. Low SNR is a common problem particularly for myocardial T_2* mapping where acquisition times are often limited by the tolerable breath hold time. Such voxels should either be excluded from fitting—a procedure referred to as truncation—or included in the fit model as a constant noise term.

Most commercial MR systems support exponential fitting algorithms as part of the systems' software, but using customized fitting routines is often beneficial for research. First, it is often unclear what model or fitting approach is used by commercial software and how good the fit quality was, i.e., how well the fit describes the measured data. Measures like the coefficient of determination R^2 or the standard deviation of the T_2* fit [93] should be used to evaluate the reliability of the results. Taking fitting results for granted without considering fit quality

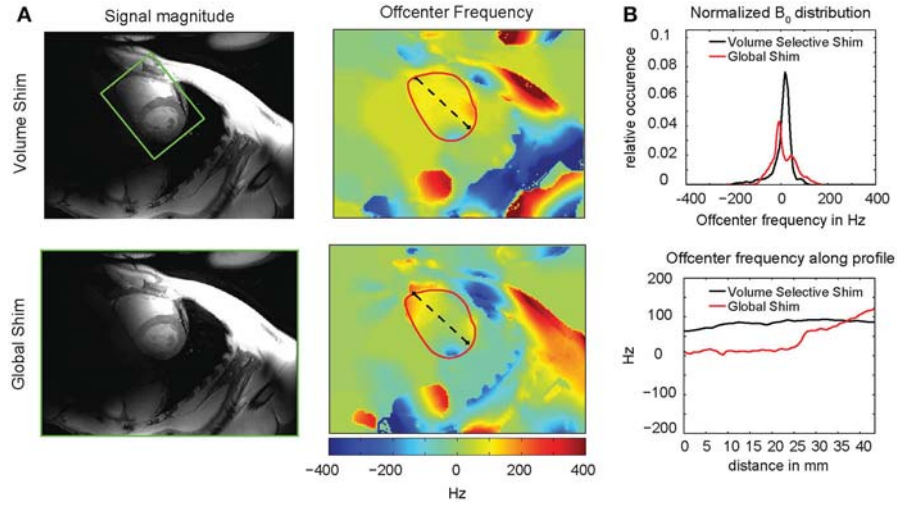

FIGURE 8 | Comparison between volume and global B_0 shimming in the heart of a healthy volunteer at 7.0 T. **(A)** left: placement of the adjustment volume in a magnitude image. **(A)** right: B_0 maps with the region of interest (red) and a profile across the heart through the ventricular septum (dashed black line) overlaid. **(B)** Plot of the histogram detailing the distribution of B_0 in the ROI outlined in the B_0 maps (top) and plots along the profile in the B_0 map (bottom) of volume selective (black) and global (red) shim. A clear improvement of field inhomogeneity can be observed after volume selective shimming indicated by a narrowing of the histogram and a flattened B_0 profile.

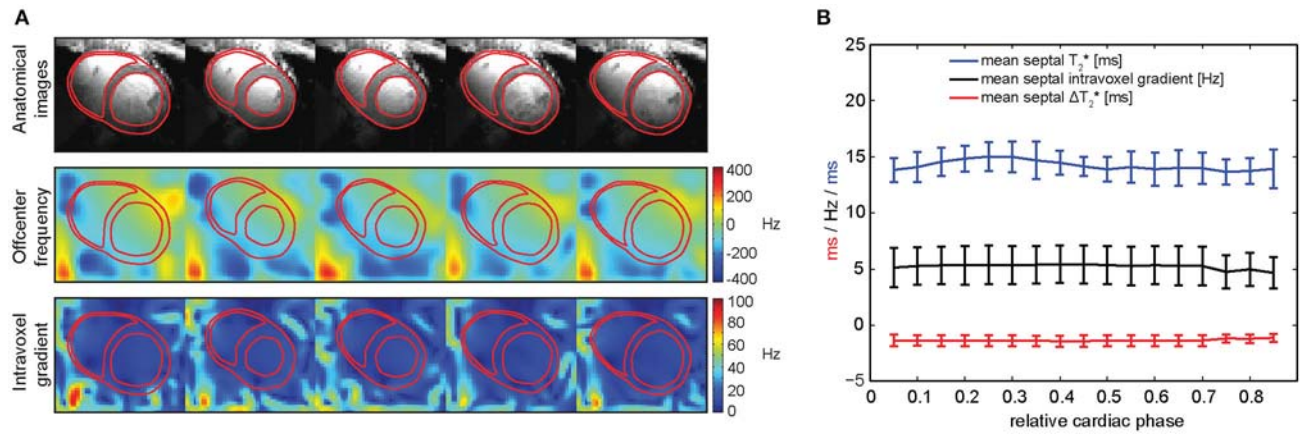

FIGURE 9 | Spatial and temporal variation of macroscopic intra-voxel B_0 gradients in the *in vivo* human heart. **(A)** Magnitude images of a short-axis view (top), in-plane macroscopic B_0 maps (middle) and intra-voxel macroscopic B_0 gradient maps (bottom) over the cardiac cycle. **(B)** Mean septal T_2^* (blue), intra-voxel B_0 gradient (black) and estimated ΔT_2^* caused by this B_0 gradient (red) over the cardiac cycle, averaged among a group of healthy volunteers. Temporal macroscopic magnetic field changes over the cardiac cycle are minor regarding their effects on T_2^* (from Huelnhagen et al. [84] with permission from John Wiley and Sons).

may lead to wrong results and eventually wrong conclusions. Second, tailored fitting procedures offer the freedom to select the most appropriate fit model, optimization approach, truncation threshold, etc. for the particular research question. Depending on the kind of application, it may for example make sense to use a bi-exponential or multi-exponential model instead of a mono-exponential approach.

In contrast to qualitative signal intensity images, relaxation maps like T_2* maps offer the advantage of providing quantitative, comparable results. Yet, effects like B_0 inhomogeneities or signal noise can impair the assessment of T_2* and lead to wrong results. Dedicated B_0 shimming approaches help to mitigate the impact of macroscopic magnetic field inhomogeneities. A reduction in voxel size can further reduce the influence of B_0 gradients on T_2* (**Figure 5B**). Yet, reducing voxel size results in an SNR loss, which can induce poor fit quality offsetting the benefit of the smaller voxel size. While a reduction in SNR might be counteracted by signal averaging and increasing acquisition times in static acquisition situations (e.g., MRI of the brain), it is often not feasible in cardiac applications, where acquisitions need to be synchronized with the cardiac cycle and where it is common to utilize breath held

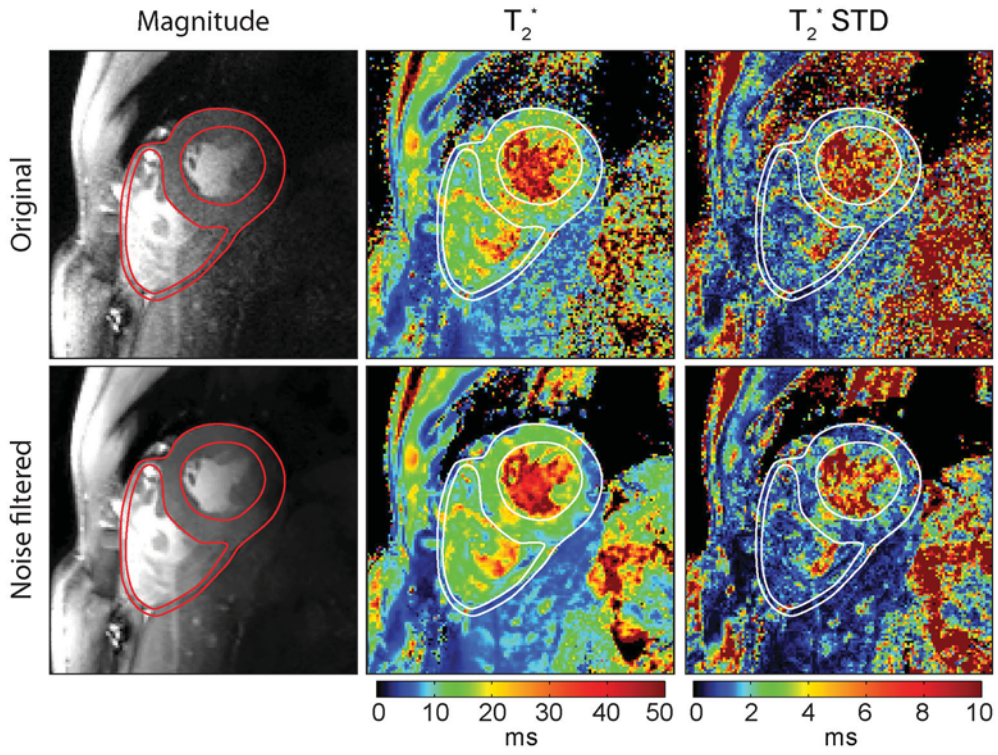

FIGURE 10 | Impact of spatially adaptive non-local means (SANLM) noise filtering on T_2^* maps of a mid-ventricular short axis view of the heart. Left: Original and SANLM filtered signal magnitude images of the first echo (TE = 2.04 ms) of a series of multi-echo gradient echo images. Center: Corresponding T_2^* maps. Right: T_2^* standard deviation maps illustrating the precision of the T_2^* maps. By applying the noise filter, an average decrease in T_2^* fit standard deviation of about 30% in the left ventricular myocardium was achieved.

conditions constraining the viable window of data acquisition to few seconds. This issue is even further pronounced in patients suffering from cardiac diseases and for acquisitions at high spatial or temporal resolution such as CINE T_2* mapping.

Image de-noising presents a viable solution to address this constraint and allows the use of small voxel sizes while still achieving acceptable fit quality. Powerful de-noising approaches like non-local means filtering [94] are readily available and can greatly improve SNR with minimal loss of information. De-noising of the T_2* maps is not recommended, because low fit quality of fitting noisy data can result in large T_2* errors that might even be enlarged or spread out by filtering. Also algorithms that estimate the noise level from the provided data will fail if presented with T_2* maps. Filtering of the magnitude images prior to fitting instead represents a robust way of improving fit quality and has been shown to increase T_2* fitting accuracy and precision [84, 95, 96] without the risk of introducing large errors. **Figure 10** illustrates an example of how T_2* mapping can benefit from noise filtering. Here a 30% reduction of T_2* fit standard deviation was achieved by noise filtering. For applications where SNR is limited such as myocardial T_2* mapping, image de-noising approaches provide a good solution to improve mapping results.

INSIGHTS FROM *IN VIVO* HUMAN MYOCARDIAL T_2* MAPPING AT ULTRAHIGH FIELDS

The technological and methodological developments in ultrahigh field CMR outlined above, permit for the first time the *in vivo* assessment of temporal myocardial T_2* changes across the cardiac cycle. Initial studies have applied these advances to gain first insights from using this technique in healthy volunteers and patients suffering from cardiovascular diseases to investigate their feasibility and potential [39, 84].

CINE Myocardial T_2* Mapping in Healthy Subjects

A first study systematically investigating the temporal changes of myocardial T_2* across the cardiac cycle in healthy subjects at 7.0 T was published in 2016 [84]. The authors analyzed the time course of myocardial T_2* throughout the cardiac cycle along with basic myocardial morphology, i.e., ventricular septal wall thickness and inner left ventricular radius as potential confounders of T_2*. The results demonstrated that myocardial T_2* obtained correlates linearly with the myocardial wall thickness [84], (**Figure 11**). The same study also showed that

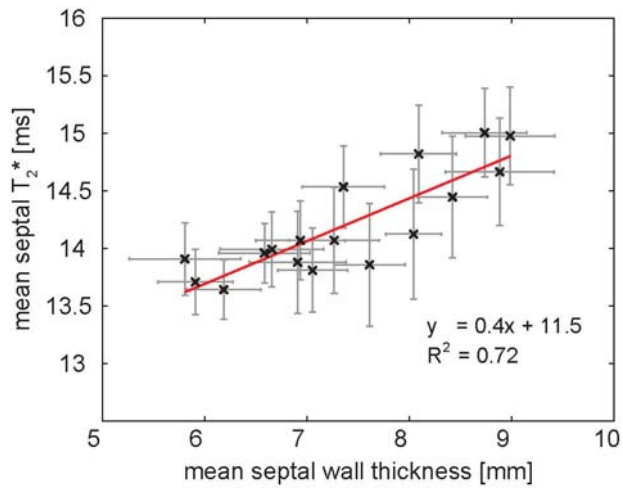

FIGURE 11 | Relationship of mean ventricular septal wall thickness and mean septal T_2^* in a group of healthy volunteers at 7.0 T. One data point corresponds to one cardiac phase. Septal wall thickness and T_2^* are linearly correlated. The result of linear regression is plotted in red. Error bars indicate SEM.

T_2* in the ventricular septum changes periodically across the cardiac cycle [84]. It increases in systole—the part of the cardiac cycle when the ventricles contract—and decreases in diastole—the part of the cardiac cycle when the heart relaxes and refills with blood (**Figure 12A**). The mean systole to diastole T_2* ratio was found to be approximately 1.1. Despite the numerous factors affecting T_2* such as blood volume fraction, hematocrit etc., myocardial T_2* is still often regarded as surrogate for tissue oxygenation. Interpreting T_2* to reflect tissue oxygenation, the observed systolic T_2* increase would imply an increase in left myocardial oxygenation during systole. This is contrary to physiological knowledge. Instead, changes in myocardial blood volume fraction induced by variations in blood pressure and resulting myocardial wall stress are believed to be responsible for the observed cyclic T_2* changes [84]. The contraction of the heart muscle compresses the intramyocardial vasculature such that inflow of arterial blood is interrupted while deoxygenated blood is squeezed out of the myocardium toward the venous coronary sinus [97–100] (**Figure 12B**). The major systolic decrease in blood volume fraction in the myocardium reduces the amount of deoxygenated hemoglobin per tissue volume, thereby increasing—instead of lowering—T_2* during systole. Previous studies of skeletal muscle have also linked T_2* changes to alterations in tissue pH and resulting changes of the tissue water content and distribution after exercise [101, 102]. These studies have examined baseline and post-exercise conditions, which are difficult to compare with the heart which is constantly exercising. Still, T_2 changes driven by tissue water content and distribution changes should be considered as a potential source of T_2* changes also in the heart. The hypothesis, that the observed periodic T_2* changes could be induced by macroscopic B_0 field variations induced by changes in bulk morphology between systole and diastole, was carefully investigated but not confirmed. Both, *in silico* magneto static simulations and *in vivo* temporally resolved B_0 mapping, showed negligible impact of cardiac morphology on the macroscopic B_0 field in the ventricular septum and hence T_2* [84].

Myocardial T_2* Mapping in Patients with Cardiovascular Diseases

Besides the application of myocardial T_2* mapping at ultrahigh magnetic fields in healthy volunteers, first investigations were carried out to explore the potential of the technique to distinguish between healthy and pathologic myocardium. These early UHF-CMR studies focused on T_2* mapping in patients with hypertrophic cardiomyopathy (HCM). HCM is the most common inherited cardiac disease affecting about 0.2–0.5% of the general population [103, 104]. The disease is characterized by an increase in myocardial wall thickness related to myocyte hypertrophy, microstructural changes like myocardial disarray, fibrosis and microvascular dysfunction. HCM patients often remain asymptomatic, but the disease can have a severe outcome in a subgroup of patients where it may cause heart failure and sudden unexpected cardiac death (SCD) in any age group. SCD and has been reported to affect about 6% of HCM patients within a mean follow up time of (8 ± 7) years [105]. This renders risk stratification vital for HCM patients. CMR plays an important role in the diagnosis and prognosis of HCM [106]. While a number of SCD risk factors in HCM have been identified such as degree of hypertrophy or presence of fibrosis the task remains challenging [107]. Consequently, basic research efforts and clinical science activities are required to better characterize HCM patient populations and to direct appropriate therapies to those at risk.

Based on the structural and physiologic changes, differences in myocardial T_2* were hypothesized in HCM patients compared to healthy controls. This hypothesis was investigated using high spatiotemporal resolution T_2* mapping at 7.0 T (**Figure 13**). It was found that septal T_2* is significantly increased in HCM with mean septal T_2* being (17.5 ± 1.4) ms in a cohort of HCM patients compared to (13.7 ± 1.1) ms in a group of gender, age and body mass index matched healthy controls. While variations of myocardial T_2* across the cardiac cycle have been attributed to changes in myocardial blood volume fraction rather than changes in tissue oxygenation [84], two main factors are assumed to cause the observed overall T_2* increase in HCM. Improved tissue oxygenation in the diseased myocardium in the case of HCM is unlikely. Instead, T_2 has been reported to be elevated in HCM [108] related to presence of inflammation and edema. A T_2 increase would also result in increased T_2* as seen from Equation (1). Further to this, reduced myocardial perfusion and ischemia are common in HCM [109], effectively reducing the tissue blood volume fraction resulting in a T_2* increase as suggested by Equation (5). These conditions are also associated with a higher risk for a poor outcome in HCM patients [110]. With this in mind it is fair to conclude that myocardial T_2* mapping could be beneficial for a better understanding of cardiac (patho)physiology *in vivo* with the ultimate goal to support risk stratification in HCM.

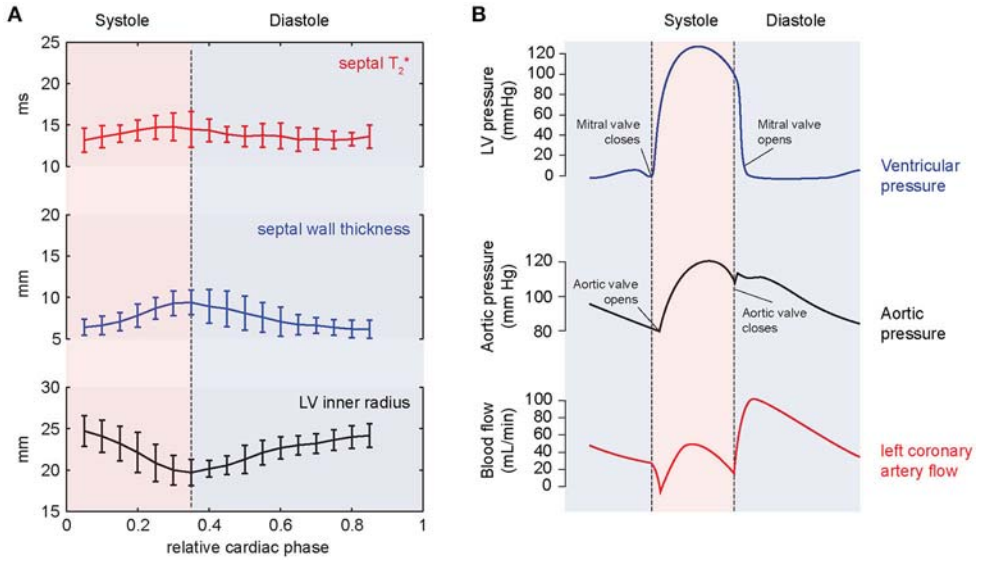

FIGURE 12 | Results of temporally resolved myocardial T_2^* mapping in healthy volunteers at 7.0 T. **(A)** Course of mean septal T_2^*, wall thickness and LV inner radius plotted over the cardiac cycle averaged for a group of healthy volunteers. Error bars indicate SD. Myocardial T_2^* changes periodically across the cardiac cycle increasing in systole and decreasing in diastole. **(B)** The periodic T_2^* changes can be explained by cyclic variations of myocardial blood volume fraction related to differences in blood pressure and myocardial wall stress. The massive pressure increase in the left ventricle in the beginning of systole results in high myocardial wall stress compressing the myocardial vessels leading to a reduced blood supply to the myocardium while blood contained in the tissue is squeezed out. The resulting reduced myocardial blood volume fraction explains the systolic T_2^* increase, which cannot be explained by increased oxygenation.

CONCLUSION AND FUTURE DIRECTIONS

The progress in myocardial T_2* mapping at ultrahigh magnetic fields is promising [111–113]. Yet, there are still a number of questions to be answered and the clinical benefit remains to be carefully investigated. This requires further efforts to tackle unsolved problems and unmet needs standing in the way *en route* to broader clinical studies. For example, the relatively long breath hold times required for the acquisition of high spatiotemporal resolution T_2* maps constitute a challenge particularly in cardiac patients. Free breathing acquisition techniques could offset this constraint permitting broader application and full 3D heart coverage. This would also help to further investigate the effect of through-plane motion. Acquisition approaches like simultaneous multi-slice excitation can be used to reduce scan times while multi-channel transmit systems can be employed to balance excitation field homogeneity and RF power deposition constraints [114, 115].

Based on the multifaceted contributions of physiological parameters on T_2* research will not stop at just mapping myocardial T_2*. Tailored acquisition schemes, data post-processing, analysis and interpretation will allow exploiting the wealth of information encoded into T_2*. For example high spatial resolution T_2* mapping facilitated by ultrahigh magnetic field strengths might be beneficial to gain a better insight into the myocardial microstructure *in vivo* with the ultimate goal to visualize myocardial fibers or to examine their helical angulation, since the susceptibility effects depend on the orientation of blood filled capillaries with regard to the external magnetic field [116]. Myocardial fiber tracking using T_2* mapping holds the promise to be less sensitive to bulk motion than diffusion-weighted MR of the myocardium [117, 118]. The increased susceptibility contrast available at 7.0 T could be exploited to quantitatively study iron accumulation in the heart with high sensitivity and spatial resolution superior to what can be achieved at 1.5 and 3.0 T. This requires the determination of norm values for healthy myocardial T_2* at 7.0 T as a mandatory precursor to broader clinical studies.

At the same time small animal studies employing cardiac disease models can provide a valuable contribution to understanding the underlying biophysical principles and (patho)physiological contrast mechanisms governing T_2*. Unlike human studies they offer the unique possibility to directly compare *in vivo* findings by MRI with *ex vivo* histology, the gold standard for tissue characterization. Recent such studies indicate that T_2* might provide not only an alternative for detection of both replacement and diffuse fibrosis without the need for exogenous contrast agents, but also has potential to distinguish the two by means of relaxation time changes induced by the presence of collagen and other fibrotic elements in the extracellular matrix [17, 18]. This could provide new diagnostic means to a large group of patients excluded from contrast agent injections due to renal insufficiencies. A study employing a mouse myocardial ischemia/reperfusion model has provided first insights into *in vivo* quantification of T_2* changes in the mouse myocardium in relation to tissue damage [16]. Local decrease of T_2* was found in the infarct

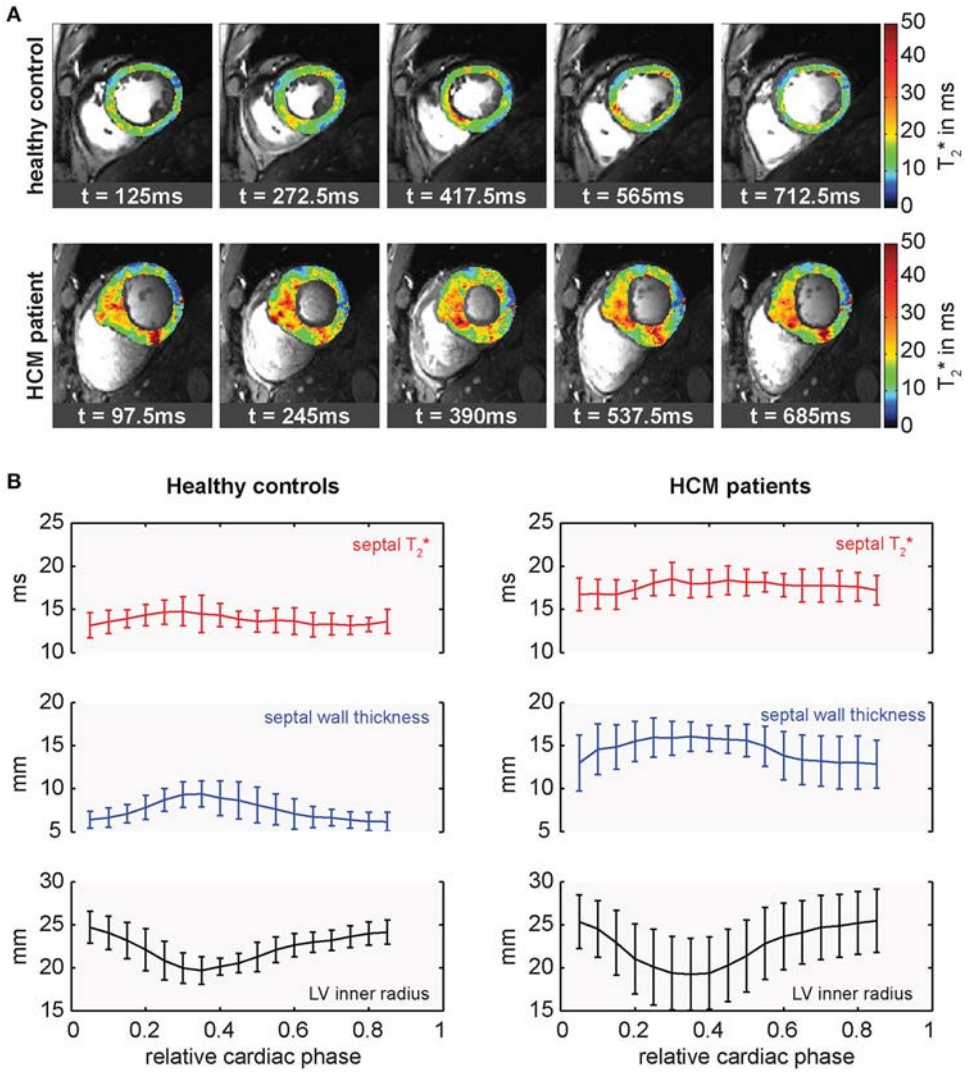

FIGURE 13 | Cardiac phase resolved myocardial T_2^* mapping in healthy volunteers and HCM patients. **(A)** Temporally resolved myocardial T_2^* maps of a short axis view of a healthy control (top) and an HCM patient (bottom), (5 out of 20 phases shown). Spatial resolution (1.1 × 1.1 × 4.0) mm^3. T_2^* variations can be observed across the cardiac cycle. **(B)** Course of mean septal T_2^*, wall thickness and inner LV radius plotted over the cardiac cycle averaged for groups of healthy controls (left) and HCM patients (right). Relative cardiac phase 0 indicates the beginning of systole. T_2^* changes periodically over the cardiac cycle increasing in systole and decreasing in diastole in both, healthy controls and HCM patients, but is significantly elevated in HCM patients.

zone and associated with deposition of collagen. The authors describe that T_2* varies dynamically during infarct development suggesting that it may be used to discriminate between acute and chronic infarctions. Taken together, by concordance the findings between human studies and cardiac disease models of small rodents will provide stronger evidence for fundamental understandings of myocyte biology, and cardiac performance with the goal to provide a more accurate diagnosis and risk stratification. Thanks to the sensitivity gain at 7.0 T the spatial fidelity feasible for T_2* mapping in humans approaches the relative anatomical spatial resolution—in terms of number of voxels with respect to anatomy—demonstrated for cardiac imaging in animal models [119, 120]. This achievement is translatable into opportunities for discovery and translational research.

The ability to probe for changes in myocardial tissue oxygenation using T_2* sensitized imaging/mapping offers the potential to address some of the spatial and temporal resolution constraints of conventional first pass perfusion imaging and holds the promise to obviate the need for exogenous contrast agents. Since microscopic susceptibility increases with field strength, thus making oxygenation sensitivity due to ischemic (patho) physiology more pronounced, T_2* mapping at 7.0 T might be beneficial to address some of the BOLD sensitivity constraints reported for the assessment of regional myocardial oxygenation changes in the presence of coronary artery

stenosis [121] or for the characterization of vasodilator-induced changes of myocardial oxygenation at 1.5 T and at 3.0 T [10].

The pace of discovery is exciting and a powerful motivator to transfer the lessons learned from T_2* mapping research at 7.0 T into the clinical scenario. These efforts are fueled by the quest for advancing the capabilities of quantitative MRI and the wish to overcome the need of exogenous contrast agent injections. The requirements of T_2* mapping at 7.0 T are likely to pave the way for further advances in MR technology and MR systems design. With appropriate multi transmit systems offering more than 16 transmit channels each providing at least 4 kW peak power, an optimistically-inclined scientist might envision the implementation of high density transceiver arrays with 64 and more elements with the ultimate goal to break ground for a many element upper torso or even a body coil array. This vision continues to motivate new research on integrated multi-channel transmission systems [122], on novel RF pulse design, on RF coil design together with explorations into ideal current patterns yielding optimal signal-to-noise-ratio for UHF-CMR [123]. Perhaps another development is the move toward myocardial T_2* mapping using reduced field of views zoomed into the target anatomy enabled by spatially selective excitation techniques which put the capabilities of parallel transmission technology to good use. With more than 45,000 examinations already performed at 7.0 T, the reasons for employing UHF-MR in translational research and for moving UHF-MR into clinical applications are more compelling than ever. This provides strong motivation to put further weight behind pushing the solution of the many remaining problems. As an important step toward this goal a system manufacturer has recently filed for FDA clearing for the clinical use of a 7.0 T system. With this development we can expect more pioneering research institutions, university hospitals and large clinics to become early adopters of CMR at 7.0 T and start harvesting knowledge and know-how that will benefit clinical applications.

ETHICS STATEMENT

In vivo studies of which data is presented in this work were carried out in accordance with the guidelines of the local ethical committee (registration number DE/CA73/5550/09, Landesamt für Arbeitsschutz, Gesundheitsschutz und technische Sicherheit, Berlin, Germany) with written informed consent from all subjects in compliance with the local institutional review board guidelines. All subjects gave written informed consent in accordance with the Declaration of Helsinki. The protocols were approved by the local ethical committee.

AUTHOR CONTRIBUTIONS

TH and TN wrote the manuscript with help from KP, MK, and TS.

FUNDING

This work was supported (in part, TH and TN) by the DZHK (German Centre for Cardiovascular Research, partner site Berlin, BER 601) and by the BMBF (Federal Ministry of Education and Research, Berlin, Germany, FKZ 81Z6100161). TN received support by the BMBF (Federal Ministry of Education and Research, Berlin, Germany, FKZ 01QE1501B) and the EUROSTARS program (E! 9340 hearRT-4-EU).

ACKNOWLEDGMENTS

The authors wish to acknowledge the team at the Berlin Ultrahigh Field Facility (B.U.F.F.) at the Max-Delbrueck Center for Molecular Medicine in the Helmholtz Association, Berlin, Germany; Jeanette Schulz-Menger from the working group for Cardiac Magnetic Resonance, Charite', Berlin, Germany; Peter Kellman (National Institutes of Health, NHLBI, Laboratory of Cardiac Energetics, Bethesda, USA); who kindly contributed examples of their pioneering work or other valuable assistance.

REFERENCES

1. von Knobelsdorff-Brenkenhoff F, Schulz-Menger J. Role of cardiovascular magnetic resonance in the guidelines of the European Society of Cardiology. *J Cardiovasc Magn Reson.* (2016) **18**:6. doi: 10.1186/s12968-016-0225-6
2. Captur G, Manisty C, Moon JC. Cardiac MRI evaluation of myocardial disease. *Heart* (2016) **102**:1429–35. doi: 10.1136/heartjnl-2015-309077
3. Ogawa S, Menon RS, Tank DW, Kim SG, Merkle H, Ellermann JM, et al. Functional brain mapping by blood oxygenation level-dependent contrast magnetic resonance imaging. A comparison of signal characteristics with a biophysical model. *Biophys J.* (1993) **64**:803–12. doi: 10.1016/S0006-3495(93)81441-3
4. Wacker CM, Hartlep AW, Pfleger S, Schad LR, Ertl G, Bauer WR. Susceptibility-sensitive magnetic resonance imaging detects human myocardium supplied by a stenotic coronary artery without a contrast agent. *J Am Coll Cardiol.* (2003) **41**:834–40. doi: 10.1016/S0735-1097(02)02931-5
5. Friedrich M, Niendorf T, Schulz-Menger J. Blood oxygen level-dependent magnetic resonance imaging in patients with stress-induced angina. *ACC Curr J Rev.* (2004) **13**:30. doi: 10.1016/j.accreview.2004.03.013
6. Jahnke C, Gebker R, Manka R, Schnackenburg B, Fleck E, Paetsch I. Navigator-gated 3D blood oxygen level–dependent CMR at 3.0-T for detection of stress-induced myocardial ischemic reactions. *JACC Cardiovasc Imaging* (2010) **3**:375–84. doi: 10.1016/j.jcmg.2009.12.008
7. Karamitsos TD, Leccisotti L, Arnold JR, Recio-Mayoral A, Bhamra-Ariza P, Howells RK, et al. Relationship between regional myocardial oxygenation and perfusion in patients with coronary artery disease insights from cardiovascular magnetic resonance and positron emission tomography. *Circ Cardiovasc Imaging* (2010) **3**:32–40. doi: 10.1161/CIRCIMAGING.109.860148
8. Tsaftaris SA, Tang R, Zhou X, Li D, Dharmakumar R. Ischemic extent as a biomarker for characterizing severity of coronary artery stenosis with blood oxygen-sensitive MRI. *J Magn Reson Imaging* (2012) **35**:1338–48. doi: 10.1002/jmri.23577
9. Wacker CM, Bock M, Hartlep AW, Beck G, van Kaick G, Ertl G, et al. Changes in myocardial oxygenation and perfusion under pharmacological

stress with dipyridamole: assessment using T*2 and T1 measurements. *Magn Reson Med.* (1999) **41**:686–95.
10. Vohringer M, Flewitt JA, Green JD, Dharmakumar R, Wang J, Jr., Tyberg JV, et al. Oxygenation-sensitive CMR for assessing vasodilator-induced changes of myocardial oxygenation. *J Cardiovasc Magn Reson.* (2010) **12**:20. doi: 10.1186/1532-429X-12-20
11. Utz W, Jordan J, Niendorf T, Stoffels M, Luft FC, Dietz R, et al. Blood oxygen level-dependent MRI of tissue oxygenation: relation to endothelium-dependent and endothelium-independent blood flow changes. *Arterioscler Thromb Vasc Biol.* (2005) **25**:1408–13. doi: 10.1161/01.ATV.0000170131.13683.d7
12. Guensch DP, Fischer K, Flewitt JA, Friedrich MG. Impact of intermittent apnea on myocardial tissue oxygenation–a study using oxygenation-sensitive cardiovascular magnetic resonance. *PLoS ONE* (2013) **8**:e53282. doi: 10.1371/journal.pone.0053282
13. Guensch DP, Fischer K, Flewitt JA, Friedrich MG. Myocardial oxygenation is maintained during hypoxia when combined with apnea–a cardiovascular MR study. *Physiol. Rep.* (2013) **1**:e00098. doi: 10.1002/phy2.98
14. Guensch DP, Fischer K, Flewitt JA, Yu J, Lukic R, Friedrich JA, et al. Breathing manoeuvre-dependent changes in myocardial oxygenation in healthy humans. *Eur Heart J Cardiovasc Imaging* (2014) **15**:409–14. doi: 10.1093/ehjci/jet171
15. Fischer K, Guensch DP, Shie N, Lebel J, Friedrich MG. Breathing maneuvers as a vasoactive stimulus for detecting inducible myocardial ischemia - an experimental cardiovascular magnetic resonance study. *PLoS ONE* (2016) **11**:e0164524. doi: 10.1371/journal.pone.0164524
16. Aguor EN, Arslan F, van de Kolk CW, Nederhoff MG, Doevendans PA, van Echteld CJ, et al. Quantitative T2* assessment of acute and chronic myocardial ischemia/reperfusion injury in mice. *Magn Reson Mater Phys Biol Med.* (2012) **25**:369–79. doi: 10.1007/s10334-012-0304-0
17. de Jong S, Zwanenburg JJ, Visser F, van der Nagel R, van Rijen HV, Vos MA, et al. Direct detection of myocardial fibrosis by MRI. *J Mol Cell Cardiol.* (2011) **51**:974–9. doi: 10.1016/j.yjmcc.2011.08.024
18. van Nierop BJ, Bax NA, Nelissen JL, Arslan F, Motaal AG, de Graaf L, et al. Assessment of myocardial fibrosis in mice using a T2*-weighted 3D radial magnetic resonance imaging sequence. *PLoS ONE* (2015) **10**:e0129899. doi: 10.1371/journal.pone.0129899
19. He T. Cardiovascular magnetic resonance T2* for tissue iron assessment in the heart. *Quant Imaging Med Surg.* (2014) **4**:407–12. doi: 10.3978/j.issn.2223-4292.2014.10.05
20. Anderson L, Holden S, Davis B, Prescott E, Charrier C, Bunce N, et al. Cardiovascular T 2-star(T 2*) magnetic resonance for the early diagnosis of myocardial iron overload. *Eur Heart J.* (2001) **22**:2171–9. doi: 10.1053/euhj.2001.2822
21. Mavrogeni S. Evaluation of myocardial iron overload using magnetic resonance imaging. *Blood Transfusion* (2009) **7**:183–7. doi: 10.2450/2008.0063-08
22. Carpenter J-P, He T, Kirk P, Roughton M, Anderson LJ, de Noronha SV, et al. On T2* magnetic resonance and cardiac iron. *Circulation* (2011) **123**:1519–28. doi: 10.1161/CIRCULATIONAHA.110.007641
23. Friedrich MG, Karamitsos TD. Oxygenation-sensitive cardiovascular magnetic resonance. *J Cardiovasc Magn Reson.* (2013) **15**:43. doi: 10.1186/1532-429X-15-43
24. Haacke EM, Brown RW, Thompson MR, Venkatesan R, editors. Magnetization, relaxation and the bloch equation. In: *Magnetic Resonance Imaging - Physical Principles and Sequence Design*. 1st ed. New York, NY: John Wiley & Sons (1999). p. 51–64.
25. Zhao JM, Clingman CS, Närväinen MJ, Kauppinen RA, van Zijl P. Oxygenation and hematocrit dependence of transverse relaxation rates of blood at 3T. *Magn. Reson. Med.* (2007) **58**:592–7. doi: 10.1002/mrm.21342
26. Ogawa S, Lee TM, Kay AR, Tank DW. Brain magnetic resonance imaging with contrast dependent on blood oxygenation. *Proc Natl Acad Sci USA.* (1990) **87**:9868–72. doi: 10.1073/pnas.87.24.9868
27. Brown RW, Cheng Y-CN, Haacke EM, Thompson MR, Venkatesan R. *Magnetic Resonance Imaging*: *Physical Principles and Sequence Design*. New York, NY: John Wiley & Sons (2014).
28. Bernstein MA, King KF, Zhou XJ. *Handbook of MRI Pulse Sequences*. New York, NY: Elsevier (2004).
29. Ogawa S, Tank DW, Menon R, Ellermann JM, Kim SG, Merkle H, et al. Intrinsic signal changes accompanying sensory stimulation: functional brain mapping with magnetic resonance imaging. *Proc Natl Acad Sci USA.* (1992) **89**:5951–5. doi: 10.1073/pnas.89.13.5951
30. Bauer WR, Nadler W, Bock M, Schad LR, Wacker C, Hartlep A, et al. Theory of the BOLD effect in the capillary region: an analytical approach for the determination of T2 in the capillary network of myocardium. *Magn Reson Med.* (1999) **41**:51–62.
31. Guensch DP, Nadeshalingam G, Fischer K, Stalder AF, Friedrich MG. The impact of hematocrit on oxygenation-sensitive cardiovascular magnetic resonance. *J Cardiovasc Magn Reson.* (2016) **18**:42. doi: 10.1186/s12968-016-0262-1
32. Yablonskiy DA, Haacke EM. Theory of NMR signal behavior in magnetically inhomogeneous tissues: the static dephasing regime. *Magn Reson Med.* (1994) **32**:749–63. doi: 10.1002/mrm.1910320610
33. Christen T, Lemasson B, Pannetier N, Farion R, Segebarth C, Rémy C, et al. Evaluation of a quantitative blood oxygenation level-dependent (qBOLD) approach to map local blood oxygen saturation. *NMR Biomed.* (2011) **24**:393–403. doi: 10.1002/nbm.1603
34. Spees WM, Yablonskiy DA, Oswood MC, Ackerman JJ. Water proton MR properties of human blood at 1.5 tesla: magnetic susceptibility, T1, T2, T2*, and non-lorentzian signal behavior. *Magn Reson Med.* (2001) **45**:533–42. doi: 10.1002/mrm.1072
35. Niendorf T, Pohlmann A, Arakelyan K, Flemming B, Cantow K, Hentschel J, et al. How bold is blood oxygenation level-dependent (BOLD) magnetic resonance imaging of the kidney? Opportunities, challenges and future directions. *Acta Physiol.* (2015) **213**:19–38. doi: 10.1111/apha.12393
36. Meloni A, Hezel F, Positano V, Keilberg P, Pepe A, Lombardi M, et al. Detailing magnetic field strength dependence and segmental artifact distribution of myocardial effective transverse relaxation rate at 1.5, 3.0, and 7.0 T. *Magn Reson Med.* (2014) **71**:2224–30. doi: 10.1002/mrm.24856
37. Ocali O, Atalar E. Ultimate intrinsic signal-to-noise ratio in MRI. *Magn Reson Med.* (1998) **39**:462–73. doi: 10.1002/mrm.1910390317
38. Ugurbil K, Adriany G, Andersen P, Chen W, Garwood M, Gruetter R, et al. Ultrahigh field magnetic resonance imaging and spectroscopy. *Magn Reson Imaging* (2003) **21**:1263–81. doi: 10.1016/j.mri.2003.08.027
39. Hezel F, Thalhammer C, Waiczies S, Schulz-Menger J, Niendorf T. High spatial resolution and temporally resolved T_2^* mapping of normal human myocardium at 7.0 tesla: an ultrahigh field magnetic resonance feasibility study. *PLoS ONE* (2012) **7**:e52324. doi: 10.1371/journal.pone.0052324
40. Mueller A, Kouwenhoven M, Naehle CP, Gieseke J, Strach K, Willinek WA, et al. Dual-source radiofrequency transmission with patient-adaptive local radiofrequency shimming for 3.0-T cardiac mr imaging: initial experience. *Radiology* (2012) **263**:77–85. doi: 10.1148/radiol.11110347
41. Vaughan JT, Snyder CJ, DelaBarre LJ, Bolan PJ, Tian J, Bolinger L, et al. Whole-body imaging at 7T: preliminary results. *Magn Reson Med.* (2009) **61**:244–8. doi: 10.1002/mrm.21751
42. Snyder CJ, DelaBarre L, Metzger GJ, van de Moortele PF, Akgun C, Ugurbil K, et al. Initial results of cardiac imaging at 7 Tesla. *Magn Reson Med.* (2009) **61**:517–24. doi: 10.1002/mrm.21895
43. Maderwald S, Orzada S, Schaefer LC, Bitz AK, Brote I, Kraff O, et al., editors. 7T Human *in vivo* cardiac imaging with an 8-channel transmit/receive array. In: *Proceedings of the International Society for Magnetic Resonance Medicine.* Honolulu, HI (2009).
44. van den Bergen B, Klomp DW, Raaijmakers AJ, de Castro CA, Boer VO, Kroeze H, et al. Uniform prostate imaging and spectroscopy at 7 T: comparison between a microstrip array and an endorectal coil. *NMR Biomed.* (2011) **24**:358–65. doi: 10.1002/nbm.1599
45. Ipek O, Raaijmakers AJ, Klomp DW, Lagendijk JJ, Luijten PR, van den Berg CA. Characterization of transceive surface element designs for 7 tesla magnetic resonance imaging of the prostate: radiative antenna and microstrip. *Phys Med Biol.* (2012) **57**:343–55. doi: 10.1088/0031-9155/57/2/343

46. Winter L, Özerdem C, Hoffmann W, Santoro D, Müller A, Waiczies H, et al. Design and evaluation of a hybrid radiofrequency applicator for magnetic resonance imaging and RF induced hyperthermia: electromagnetic field simulations up to 14.0 tesla and proof-of-concept at 7.0 tesla. *PLoS ONE* (2013) **8**:e61661. doi: 10.1371/journal.pone.0061661
47. Oezerdem C, Winter L, Graessl A, Paul K, Els A, Weinberger O, et al. 16-channel bow tie antenna transceiver array for cardiac MR at 7.0 tesla. *Magn Reson Med.* (2016) **75**:2553–65. doi: 10.1002/mrm.25840
48. Raaijmakers AJ, Ipek O, Klomp DW, Possanzini C, Harvey PR, Lagendijk JJ, et al. Design of a radiative surface coil array element at 7 T: the single-side adapted dipole antenna. *Magn Reson Med.* (2011) **66**:1488–97. doi: 10.1002/mrm.22886
49. Ipek O, Raaijmakers AJ, Lagendijk JJ, Luijten PR, van den Berg CA. Intersubject local SAR variation for 7T prostate MR imaging with an eight-channel single-side adapted dipole antenna array. *Magn Reson Med.* (2014) **71**:1559–67. doi: 10.1002/mrm.24794
50. Erturk MA, Raaijmakers AJ, Adriany G, Ugurbil K, Metzger GJ. A 16-channel combined loop-dipole transceiver array for 7 Tesla body MRI. *Magn Reson Med.* (2017) **77**:884–94. doi: 10.1002/mrm.26153
51. Raaijmakers AJE, Italiaander M, Voogt IJ, Luijten PR, Hoogduin JM, Klomp DWJ, et al. The fractionated dipole antenna: a new antenna for body imaging at 7 Tesla. *Magn Reson Med.* (2016) **75**:1366–74. doi: 10.1002/mrm.25596
52. Aussenhofer SA, Webb AG. An eight-channel transmit/receive array of TE_{01} mode high permittivity ceramic resonators for human imaging at 7T. *J Magn Reson.* (2014) **243**:122–9. doi: 10.1016/j.jmr.2014.04.001
53. Alon L, Deniz CM, Brown R, Sodickson DK, Collins CM, editors. A slot antenna concept for high fidelity body imaging at ultra high field. In: *Proceedings of the International Society for Magnetic Resonance Medicine.* Singapore (2016).
54. Versluis MJ, Tsekos N, Smith NB, Webb AG. Simple RF design for human functional and morphological cardiac imaging at 7tesla. *J Magn Reson.* (2009) **200**:161–6. doi: 10.1016/j.jmr.2009.06.014
55. Dieringer MA, Renz W, Lindel T, Seifert F, Frauenrath T, von Knobelsdorff-Brenkenhoff F, et al. Design and application of a four-channel transmit/receive surface coil for functional cardiac imaging at 7T. *J Magn Reson Imaging* (2011) **33**:736–41. doi: 10.1002/jmri.22451
56. Thalhammer C, Renz W, Winter L, Hezel F, Rieger J, Pfeiffer H, et al. Two-Dimensional sixteen channel transmit/receive coil array for cardiac MRI at 7.0 T: design, evaluation, and application. *J Magn Reson Imaging* (2012) **36**:847–57. doi: 10.1002/jmri.23724
57. Winter L, Kellman P, Renz W, Gräßl A, Hezel F, Thalhammer C, et al. Comparison of three multichannel transmit/receive radiofrequency coil configurations for anatomic and functional cardiac MRI at 7.0T: implications for clinical imaging. *Eur Radiol.* (2012) **22**:2211–20. doi: 10.1007/s00330-012-2487-1
58. Graessl A, Winter L, Thalhammer C, Renz W, Kellman P, Martin C, et al. Design, evaluation and application of an eight channel transmit/receive coil array for cardiac MRI at 7.0 T. *Eur J. Radiol.* (2013) **82**:752–9. doi: 10.1016/j.ejrad.2011.08.002
59. Graessl A, Renz W, Hezel F, Dieringer MA, Winter L, Oezerdem C, et al. Modular 32-channel transceiver coil array for cardiac MRI at 7.0T. *Magn Reson Med.* (2014) **72**:276–90. doi: 10.1002/mrm.24903
60. Adriany G, Ritter J, Vaughan JT, Ugurbil K, Moortele PF, editors. Experimental verification of enhanced B1 shim performance with a Z-encoding RF coil array at 7 Tesla. In: *Proceedings of the International Society for Magnetic Resonance Medicine.* Stockholm (2010).
61. Frauenrath T, Hezel F, Renz W, de Geyer TdO, Dieringer M, Knobelsdorff-Brenkenhoff FV, et al. Acoustic cardiac triggering: a practical solution for synchronization and gating of cardiovascular magnetic resonance at 7 Tesla. *J Cardiovasc Magn Reson.* (2010) **12**:67. doi: 10.1186/1532-429X-12-67
62. Togawa T, Okai O, Oshima M. Observation of blood flow E.M.F. in externally applied strong magnetic field by surface electrodes. *Med Biol Eng.* (1967) **5**:169–70. doi: 10.1007/BF02474505
63. Stuber M, Botnar RM, Fischer SE, Lamerichs R, Smink J, Harvey P, et al. Preliminary report on *in vivo* coronary MRA at 3 Tesla in humans. *Magn Reson Med.* (2002) **48**:425–9. doi: 10.1002/mrm.10240
64. Lanzer P, Barta C, Botvinick EH, Wiesendanger HU, Modin G, Higgins CB. ECG-synchronized cardiac MR imaging: method and evaluation. *Radiology* (1985) **155**:681–6. doi: 10.1148/radiology.155.3.4001369
65. Fischer SE, Wickline SA, Lorenz CH. Novel real-time R-wave detection algorithm based on the vectorcardiogram for accurate gated magnetic resonance acquisitions. *Magn Reson Med.* (1999) **42**:361–70.
66. Chia JM, Fischer SE, Wickline SA, Lorenz CH. Performance of QRS detection for cardiac magnetic resonance imaging with a novel vectorcardiographic triggering method. *J Magn Reson Imaging* (2000) **12**:678–88. doi: 10.1002/1522-2586(200011)12:5<678::aid-jmri4>3.0.co;2-5
67. Becker M, Frauenrath T, Hezel F, Krombach GA, Kremer U, Koppers B, et al. Comparison of left ventricular function assessment using phonocardiogram- and electrocardiogram-triggered 2D SSFP CINE MR imaging at 1.5 T and 3.0 T. *Eur Radiol.* (2010) **20**:1344–55. doi: 10.1007/s00330-009-1676-z
68. Frauenrath T, Hezel F, Heinrichs U, Kozerke S, Utting JF, Kob M, et al. Feasibility of cardiac gating free of interference with electro-magnetic fields at 1.5 Tesla, 3.0 Tesla and 7.0 Tesla using an MR-stethoscope. *Invest Radiol.* (2009) **44**:539–47. doi: 10.1097/RLI.0b013e3181b4c15e
69. Brandts A, Westenberg JJ, Versluis MJ, Kroft LJ, Smith NB, Webb AG, et al. Quantitative assessment of left ventricular function in humans at 7 T. *Magn Reson Med.* (2010) **64**:1471–7. doi: 10.1002/mrm.22529
70. Frauenrath T, Niendorf T, Malte K. Acoustic method for synchronization of magnetic resonance imaging (MRI). *Acta Acust. United Acust.* (2008) **94**:148–55. doi: 10.3813/AAA.918017
71. Krug JW, Rose G, Clifford GD, Oster J. ECG-based gating in ultra high field cardiovascular magnetic resonance using an independent component analysis approach. *J Cardiovasc Magn Reson.* (2013) **15**:104. doi: 10.1186/1532-429X-15-104
72. Gregory TS, Schmidt EJ, Zhang SH, Ho Tse ZT. 3DQRS: a method to obtain reliable QRS complex detection within high field MRI using 12-lead electrocardiogram traces. *Magn Reson Med.* (2014) **71**:1374–80. doi: 10.1002/mrm.25078
73. Kosch O, Thiel F, Di Clemente FS, Hein M, Seifert F, editors. Monitoring of human cardio-pulmonary activity by multi-channel UWB-radar. *Antennas and Propagation in Wireless Communications (APWC), 2011 IEEE-APS Topical Conference on.* Torino: IEEE (2011).
74. Gross S, Vionnet L, Kasper L, Dietrich BE, Pruessmann KP. Physiology recording with magnetic field probes for fMRI denoising. *Neuroimage* (in press). doi: 10.1016/j.neuroimage.2017.01.022. [Epub ahead of print].
75. Maclaren J, Aksoy M, Bammer R. Contact-free physiological monitoring using a markerless optical system. *Magn Reson Med.* (2015) **74**:571–7. doi: 10.1002/mrm.25781
76. Fuchs K, Hezel F, Winter L, Oezerdem C, Graessl A, Dieringer M, et al., editors. Feasibility of cardiac fast spin echo imaging at 7.0 T using a two-dimensional 16 channel array of bowtie transceivers. In: *Proceedings of the International Society for Magnetic Resonance Medicine.* Salt Lake City (2013).
77. Norris DG, Boernert P, Reese T, Leibfritz D. On the application of ultra-fast rare experiments. *Magn Reson Med.* (1992) **27**:142–64. doi: 10.1002/mrm.1910270114
78. Carr HY, Purcell EM. Effects of diffusion on free precession in nuclear magnetic resonance experiments. *Phys Rev.* (1954) **94**:630–8. doi: 10.1103/PhysRev.94.630
79. Meiboom S, Gill D. Modified spin-echo method for measuring nuclear relaxation times. *Rev Sci Instrum.* (1958) **29**:688–91. doi: 10.1063/1.1716296
80. Heinrichs U, Utting JF, Frauenrath T, Hezel F, Krombach GA, Hodenius MA, et al. Myocardial T2* mapping free of distortion using susceptibility-weighted fast spin-echo imaging: a feasibility study at 1.5 T and 3.0 T. *Magn Reson Med.* (2009) **62**:822–8. doi: 10.1002/mrm.22054
81. Schick F. SPLICE: sub-second diffusion-sensitive MR imaging using a modified fast spin-echo acquisition mode. *Magn Reson Med.* (1997) **38**:638–44. doi: 10.1002/mrm.1910380418
82. Haacke E, Brown R, Thompson M, Venkatesan R, Bernstein M, King K, et al. *Magnetic Resonance Imaging - Physical Principles and Sequence Design*. New York, NY: John Wiley and Sons (1999).

83. Robinson S, Schodl H, Trattnig S. A method for unwrapping highly wrapped multi-echo phase images at very high field: UMPIRE. *Magn Reson Med.* (2013) **72**:80–92. doi: 10.1002/mrm.24897
84. Huelnhagen T, Hezel F, Serradas Duarte T, Pohlmann A, Oezerdem C, Flemming B, et al. Myocardial effective transverse relaxation time T2* correlates with left ventricular wall thickness: a 7.0 T MRI study. *Magn Reson Med.* (2016) **77**:2381–9. doi: 10.1002/mrm.26312
85. Jaffer FA, Wen H, Balaban RS, Wolff SD. A method to improve the BO homogeneity of the heart *in vivo*. *Magn Reson Med.* (1996) **36**:375–83. doi: 10.1002/mrm.1910360308
86. Schar M, Kozerke S, Fischer SE, Boesiger P. Cardiac SSFP imaging at 3 Tesla. *Magn Reson Med.* (2004) **51**:799–806. doi: 10.1002/mrm.20024
87. Schar M, Vonken EJ, Stuber M. Simultaneous B(0)- and B(1)+-map acquisition for fast localized shim, frequency, and RF power determination in the heart at 3 T. *Magn Reson Med.* (2010) **63**:419–26. doi: 10.1002/mrm.22234
88. Reeder SB, Faranesh AZ, Boxermann JL, McVeigh ER. *In vivo* measurement of T_2^* and field inhomogeneity maps in the human heart at 1.5 T. *Magn Reson Med.* (1998) **39**:988–98. doi: 10.1002/mrm.1910390617
89. Shah S, Kellman P, Greiser A, Weale PJ, Zuehlsdorff S, Jerecic R, editors. Rapid fieldmap estimation for cardiac shimming. In: *Proceedings of the International Society for Magnetic Resonance Medicine 17*. Honolulu, HI (2009).
90. Serradas Duarte T, Huelnhagen T, Niendorf T, editors. Assessment of myocardial B0 over the cardiac cycle at 7.0T: implications for susceptibility-based cardiac MR techniques. In: *Proceedings of the International Society for Magnetic Resonance Medicine 24*. Singapore (2016).
91. Serradas Duarte T. *Detailing Myocardial B0 across the Cardiac Cycle at UHF: B0 Assessment and Implications for Susceptibility-based CMR Techniques*. Lisbon: Universidade Nova de Lisboa (2016).
92. Kelley CT. *Iterative Methods for Optimization*. Philadelphia: Siam (1999).
93. Sandino CM, Kellman P, Arai AE, Hansen MS, Xue H. Myocardial T2* mapping: influence of noise on accuracy and precision. *J Cardiovasc Magn Reson.* (2015) **17**:7. doi: 10.1186/s12968-015-0115-3
94. Manjon JV, Coupe P, Marti-Bonmati L, Collins DL, Robles M. Adaptive non-local means denoising of MR images with spatially varying noise levels. *J Magn Reson Imaging* (2010) **31**:192–203. doi: 10.1002/jmri.22003
95. Feng Y, He T, Feng M, Carpenter JP, Greiser A, Xin X, et al. Improved pixel-by-pixel MRI R2* relaxometry by nonlocal means. *Magn Reson Med.* (2014) **72**:260–8. doi: 10.1002/mrm.24914
96. Huelnhagen T, Pohlmann A, Niendorf T, editors. Improving T2* mapping accuracy by spatially adaptive non-local means noise filtering. In: *Proceedings of the International Society for Magnetic Resonance Medicine 23*. Toronto, ON (2015).
97. Guyton AC, Hall JE, editors. Muscle blood flow and cardiac output during exercise; the coronary circulation and ischemic heart disease. In: *Guyton and Hall Textbook of Medical Physiology*. 10th ed. Philadelphia: Saunders (2000). p. 223–34.
98. Schmidt RF, Lang F, Heckmann M. Herzmechanik. *Physiologie des Menschen: Mit Pathophysiologie*. 31st ed. Heidelberg: Springer (2010). p. 539–64.
99. Deussen A. Herzstoffwechsel und Kroronardurchblutung. In: Schmidt RF, Lang F, Heckmann M, editors. *Physiologie des Menschen: Mit Pathophysiologie*. 31st ed. Heidelberg: Springer (2010). p. 565–71.
100. Judd RM, Levy BI. Effects of barium-induced cardiac contraction on large- and small-vessel intramyocardial blood volume. *Circ Res.* (1991) **68**:217–25. doi: 10.1161/01.RES.68.1.217
101. Fleckenstein JL, Canby RC, Parkey RW, Peshock RM. Acute effects of exercise on MR imaging of skeletal muscle in normal volunteers. *AJR Am J Roentgenol.* (1988) **151**:231–7. doi: 10.2214/ajr.151.2.231
102. Schmid AI, Schewzow K, Fiedler GB, Goluch S, Laistler E, Wolzt M, et al. Exercising calf muscle T2* changes correlate with pH, PCr recovery and maximum oxidative phosphorylation. *NMR Biomed.* (2014) **27**:553–60. doi: 10.1002/nbm.3092
103. Mozaffarian D, Benjamin EJ, Go AS, Arnett DK, Blaha MJ, Cushman M, et al. Heart disease and stroke statistics—2016 update a report from the american heart association. *Circulation* (2015) **133**:e38–360. doi: 10.1161/CIR.0000000000000350
104. Kramer CM, Appelbaum E, Desai MY, Desvigne-Nickens P, DiMarco JP, Friedrich MG, et al. Hypertrophic Cardiomyopathy Registry: the rationale and design of an international, observational study of hypertrophic cardiomyopathy. *Am Heart J.* (2015) **170**:223–30. doi: 10.1016/j.ahj.2015.05.013
105. Maron BJ, Olivotto I, Spirito P, Casey SA, Bellone P, Gohman TE, et al. Epidemiology of hypertrophic cardiomyopathy–related death revisited in a large non-referral-based patient population. *Circulation* (2000) **102**:858–64. doi: 10.1161/01.CIR.102.8.858
106. Noureldin RA, Liu S, Nacif MS, Judge DP, Halushka MK, Abraham TP, et al. The diagnosis of hypertrophic cardiomyopathy by cardiovascular magnetic resonance. *J Cardiovasc Magn Reson.* (2012) **14**:17. doi: 10.1186/1532-429X-14-17
107. Steriotis AK, Sharma S. Risk stratification in hypertrophic cardiomyopathy. *Eur Cardiol Rev.* (2015) **10**:31–6. doi: 10.15420/ecr.2015.10.01.31
108. Abdel-Aty H, Cocker M, Strohm O, Filipchuk N, Friedrich MG. Abnormalities in T2-weighted cardiovascular magnetic resonance images of hypertrophic cardiomyopathy: regional distribution and relation to late gadolinium enhancement and severity of hypertrophy. *J Magn Reson Imaging* (2008) **28**:242–5. doi: 10.1002/jmri.21381
109. Johansson B, Mörner S, Waldenström A, Stål P. Myocardial capillary supply is limited in hypertrophic cardiomyopathy: a morphological analysis. *Int J Cardiol.* (2008) **126**:252–7. doi: 10.1016/j.ijcard.2007.04.003
110. Cecchi F, Olivotto I, Gistri R, Lorenzoni R, Chiriatti G, Camici PG. Coronary microvascular dysfunction and prognosis in hypertrophic cardiomyopathy. *New Engl J. Med.* (2003) **349**:1027–35. doi: 10.1056/NEJMoa025050
111. Niendorf T, Graessl A, Thalhammer C, Dieringer MA, Kraus O, Santoro D, et al. Progress and promises of human cardiac magnetic resonance at ultrahigh fields: a physics perspective. *J Magn Reson.* (2013) **229**:208–22. doi: 10.1016/j.jmr.2012.11.015
112. Niendorf T, Sodickson DK, Krombach GA, Schulz-Menger J. Toward cardiovascular MRI at 7 T: clinical needs, technical solutions and research promises. *Eur Radiol.* (2010) **20**:2806–16. doi: 10.1007/s00330-010-1902-8
113. Niendorf T, Paul K, Oezerdem C, Graessl A, Klix S, Huelnhagen T, et al. W(h)ither human cardiac and body magnetic resonance at ultrahigh fields? Technical advances, practical considerations, applications, and clinical opportunities. *NMR Biomed.* (2016) **29**:1173–97. doi: 10.1002/nbm.3268
114. Schmitter S, Wu X, Uğurbil K, de Moortele V. Design of parallel transmission radiofrequency pulses robust against respiration in cardiac MRI at 7 Tesla. *Magn Reson Med.* (2015) **74**:1291–305. doi: 10.1002/mrm.25512
115. Schmitter S, Moeller S, Wu X, Auerbach EJ, Metzger GJ, Van de Moortele PF, et al. Simultaneous multislice imaging in dynamic cardiac MRI at 7T using parallel transmission. *Magn Reson Med.* (2016) **77**:1010–20. doi: 10.1002/mrm.26180.
116. Reichenbach JR, Haacke EM. High-resolution BOLD venographic imaging: a window into brain function. *NMR Biomed.* (2001) **14**:453–67. doi: 10.1002/nbm.722
117. Reese TG, Weisskoff RM, Smith RN, Rosen BR, Dinsmore RE, Wedeen VJ. Imaging myocardial fiber architecture *in vivo* with magnetic resonance. *Magn Reson Med.* (1995) **34**:786–91. doi: 10.1002/mrm.1910340603
118. Wu MT, Tseng WY, Su MY, Liu CP, Chiou KR, Wedeen VJ, et al. Diffusion tensor magnetic resonance imaging mapping the fiber architecture remodeling in human myocardium after infarction: correlation with viability and wall motion. *Circulation* (2006) **114**:1036–45. doi: 10.1161/CIRCULATIONAHA.105.545863
119. Wagenhaus B, Pohlmann A, Dieringer MA, Els A, Waiczies H, Waiczies S, et al. Functional and morphological cardiac magnetic resonance imaging of mice using a cryogenic quadrature radiofrequency coil. *PLoS ONE* (2012) **7**:e42383. doi: 10.1371/journal.pone.0042383

120. Niendorf T, Pohlmann A, Reimann HM, Waiczies H, Peper E, Huelnhagen T, et al. Advancing cardiovascular, neurovascular, and renal magnetic resonance imaging in small rodents using cryogenic radiofrequency coil technology. *Front Pharmacol.* (2015) **6**:255. doi: 10.3389/fphar.2015.00255
121. Dharmakumar R, Arumana JM, Tang R, Harris K, Zhang Z, Li D. Assessment of regional myocardial oxygenation changes in the presence of coronary artery stenosis with balanced SSFP imaging at 3.0 T: theory and experimental evaluation in canines. *J Magn Reson Imaging* (2008) **27**:1037–45. doi: 10.1002/jmri.21345
122. Poulo L, Alon L, Deniz C, Haefner R, Sodickson D, Stoeckel B, et al. A 32-Channel parallel exciter/amplifier transmit system for 7T imaging. In: ISMRM, editor. *Proceedings of the International Society for Magnetic Resonance Medicine 19*. Montréal (2011). p. 1867.
123. Lattanzi R, Sodickson DK. Ideal current patterns yielding optimal signal-to-noise ratio and specific absorption rate in magnetic resonance imaging: computational methods and physical insights. *Magn Reson Med.* (2012) **68**:286–304. doi: 10.1002/mrm.23198

Conflict of Interest Statement: TN is founder and CEO of MRI.TOOLS GmbH, Berlin, Germany.

The reviewer AIS and handling Editor declared their shared affiliation, and the handling Editor states that the process nevertheless met the standards of a fair and objective review.

The other authors declare that the research was conducted in the absence of any commercial or financial relationships that could be construed as a potential conflict of interest.

Myocardial Effective Transverse Relaxation Time T_2^* Correlates With Left Ventricular Wall Thickness: A 7.0 T MRI Study

Till Huelnhagen, Fabian Hezel, Teresa Serradas Duarte, Andreas Pohlmann, Celal Oezerdem, Bert Flemming, Erdmann Seeliger, Marcel Prothmann, Jeanette Schulz-Menger, and Thoralf Niendorf

Magnetic Resonance in Medicine 77:2381–2389 (2017)

https://doi.org/10.1002/mrm.26312

Lebenslauf

Mein Lebenslauf wird aus datenschutzrechtlichen Gründen in der elektronischen Version meiner Arbeit nicht veröffentlicht.

Mein Lebenslauf wird aus datenschutzrechtlichen Gründen in der elektronischen Version meiner Arbeit nicht veröffentlicht.

Publikationsliste

Artikel in wissenschaftlichen Fachzeitschriften (Peer-Review)

1. **Huelnhagen T**, Ku MC, Reimann HM, Serradas Duarte T, Pohlmann A, Flemming B, Seeliger E, Eichhorn C, A Ferrari V, Prothmann M, Schulz-Menger J, Niendorf T. Myocardial Effective Transverse Relaxation Time T2* is Elevated in Hypertrophic Cardiomyopathy: A 7.0 T Magnetic Resonance Imaging Study. *Sci Rep*. 2018 Mar 5;8(1):3974. doi: 10.1038/s41598-018-22439-x.

2. Reimann HM, Todiras M, Hodge R, **Huelnhagen T**, Millward JM, Turner R, Seeliger E, Bader M, Pohlmann A, Niendorf T. Somatosensory BOLD fMRI reveals close link between salient blood pressure changes and the murine neuromatrix. *Neuroimage*. 2018. pii: S1053-8119(18)30090-9. doi: 10.1016/j.neuroimage.2018.02.002. [Epub ahead of print]

3. Wenz D, Kuehne A, Huelnhagen T, Nagel AM, Waiczies H, Weinberger O, Oezerdem C, Stachs O, Langner S, Seeliger E, Flemming B, Hodge R, Niendorf T. Millimeter spatial resolution in vivo sodium MRI of the human eye at 7 T using a dedicated radiofrequency transceiver array. *Magn Reson Med*. 2018 Jan 12. doi: 10.1002/mrm.27053. [Epub ahead of print]

4. Paul K, **Huelnhagen T**, Oberacker E, Wenz D, Kuehne A, Waiczies H, Schmitter S, Stachs O, Niendorf T. Multiband Diffusion-Weighted MRI of the Eye and Orbit Free of Geometric Distortions Using a RARE-EPI Hybrid. *NMR Biomed*. 2018. doi: 10.1002/nbm.3872. [Epub ahead of print]

5. Pohlmann A, Cantow K, **Huelnhagen T**, Grosenick D, dos Santos Periquito J, Boehmert L, Gladytz T, Waiczies S, Flemming B, Seeliger E, Niendorf T. Experimental MRI Monitoring of Renal Blood Volume Fraction Variations en Route to Renal Magnetic Resonance Oximetry. *Tomography*. 2017;3:4, doi: 10.18383/j.tom.2017.00012.

6. **Huelnhagen T**, Flemming B, Seeliger E, Schulz-Menger J, Niendorf T. Myocardial T2* mapping at ultrahigh magnetic fields: in vivo myocardial tissue characterization and assessment of cardiac physiology with magnetic resonance imaging. *Current Directions in Biomedical Engineering*. 2017;3:433-436.

7. Waiczies S, Millward JM, Starke L, Delgado PR, **Huelnhagen T**, Prinz C, Marek D, Wecker D, Wissmann R, Koch SP, Boehm-Sturm P, Waiczies H, Niendorf T, Pohlmann A. Enhanced Fluorine-19 MRI Sensitivity using a Cryogenic Radiofrequency Probe: Technical Developments and Ex Vivo Demonstration in a Mouse Model of Neuroinflammation. *Sci Rep*. 2017;7(1):9808.

8. **Huelnhagen T**, Paul K, Ku M-C, Serradas Duarte T, Niendorf T. Myocardial T2* Mapping with Ultrahigh Field Magnetic Resonance: Physics and Frontier Applications. Frontiers in Physics. 2017;5, doi: 10.3389/fphy.2017.00022.

9. Niendorf T, Schulz Menger J, Paul K, **Huelnhagen T**, Ferrari VA, Hodge R. High Field Cardiac Magnetic Resonance Imaging: A Case for Ultrahigh Field Cardiac Magnetic Resonance. Circ Cardiovasc Imaging. 2017; Jun; 10(6). DOI: 10.1161/CIRCIMAGING.116.005460

10. Dusek P, Skoloudik D, Maskova J, **Huelnhagen T**, Bruha R, Zahorakova D, Niendorf T, Ruzicka E, Schneider SA, Wuerfel J. Brain iron accumulation in Wilson's disease: A longitudinal imaging case study during anticopper treatment using 7.0T MRI and transcranial sonography. J Magn Reson Imaging. 2017; [Epub ahead of print], doi: 10.1002/jmri.25702.

11. Oberacker E, Paul K, **Huelnhagen T**, Oezerdem C, Winter L, Pohlmann A, Boehmert L, Stachs O, Heufelder J, Weber A, Rehak M, Seibel I, Niendorf T. Magnetic resonance safety and compatibility of tantalum markers used in proton beam therapy for intraocular tumors: A 7.0 Tesla study. Magn Reson Med. 2016; [Epub ahead of print], doi: 10.1002/mrm.26534.

12. **Huelnhagen T**, Hezel F, Serradas Duarte T, Pohlmann A, Oezerdem C, Flemming B, Seeliger E, Prothmann M, Schulz-Menger J, Niendorf T. Myocardial Effective Transverse Relaxation Time T2* Correlates With Left Ventricular Wall Thickness: A 7.0 T MRI Study. Magn Reson Med 2017; 77(6):2381-2389, doi:101002/mrm26312.

13. Dusek P, Bahn E, Litwin T, Jabłonka-Salach K, Łuciuk A, **Huelnhagen T**, Madai VI, Dieringer MA, Bulska E, Knauth M, Niendorf T, Sobesky J, Schneider SA, Czlonkowska A, Brück W, Wegner C, Wuerfel J. Brain iron accumulation in Wilson disease: a post-mortem 7 Tesla MRI-histopathological study. Neuropathol Appl Neurobiol. 2016, Epub ahead of print, doi: 10.1111/nan.12341.

14. Prothmann M, von Knobelsdorff-Brenkenhoff F, Töpper A, Dieringer MA, Shahid E, Graessl A, Rieger J, Lysiak D, Thalhammer C, **Huelnhagen T**, Kellman P, Niendorf T, Schulz Menger J. High Spatial Resolution Cardiovascular Magnetic Resonance at 7.0 Tesla in Patients with Hypertrophic Cardiomyopathy–First Experiences: Lesson Learned from 7.0 Tesla. PLoS One. 2016;11:e0148066, doi: 10.1371/journal.pone.0148066.

15. Reimann HM, Marek J, Hentschel J, **Huelnhagen T**, Todiras M, Kox S, Waiczies S, Hodge R, Bader M, Pohlmann A, Niendorf T; Normothermic Mouse Functional MRI of Acute Focal Thermostimulation for Probing Nociception. Scientific Reports 2016; 6:17230, doi: 10.1038/srep17230.

16. Niendorf T, Pohlmann A, Reimann HM, Waiczies H, Peper E, **Huelnhagen T**, Seeliger E, Schreiber A, Kettritz R, Strobel K., Ku MC, Waiczies S; Advancing Cardiovascular, Neurovascular and Renal Magnetic Resonance Imaging in Small Rodents Using Cryogenic Radiofrequency Coil Technology. Frontiers in Pharmacology 2015; 6:255, doi: 10.3389/fphar.2015.00255.

17. Paul K, Graessl A, Rieger J, Lysiak D, **Huelnhagen T**, Winter L, Lindnder T, Hadlich S, Zimpfer A, Pohlmann A, Heidemann R, Krüger PC, Langner S, Stachs O, Niendorf T; Diffusion-Sensitized Ophthalmic MRI Free of Geometric Distortion at 3.0 T and 7.0 T: A Feasibility Study in Healthy Subjects and Patients with Intraocular Masses; Investigative Radiology 2015; 50(5):309-21, doi: 10.1097/RLI.0000000000000129.

18. Klix S, Els A, Paul K, Graessl A, Oezerdem C, Weinberger O, Winter L, Thalhammer C, **Huelnhagen T**, Rieger J, Mehling H, Schulz-Menger J, Niendorf T. On the subjective acceptance during cardiovascular magnetic resonance imaging at 7.0 Tesla. PloS one 2015;10(1):e0117095, doi: 10.1371/journal.pone.0117095.

19. Niendorf T, Paul K, Oezerdem C, Graessl A, Klix S, **Huelnhagen T**, Hezel F, Rieger J, Waiczies H, Frahm J, Nagel AM, Oberacker E, Winter L. W(h)ither human cardiac and body magnetic resonance at ultrahigh fields? Technical advances, practical considerations, applications, and clinical opportunities. NMR in biomedicine 2015. 29(9):1173-97 doi: 10.1002/nbm.3268.

20. Schwier M, Chitiboi T, **Hülnhagen T**, Hahn H, Automated spine and vertebrae detection in CT images using object-based image analysis, Int j numer method biomed eng, vol. 29, pp. 938-63, 2013, doi: 10.1002/cnm.2582.

21. **Huelnhagen T**, Dengler I, Tamke A, Dang T, Breuel G; Maneuver recognition using probabilistic finite-state machines and fuzzy logic, Intelligent Vehicles Symposium (IV), 2010 IEEE (pp. 65-70). IEEE, doi: 10.1109/IVS.2010.5548066.

Buchkapitel

1. Niendorf T, Winter L, **Huelnhagen T**, Paul K, Human Cardiac Magnetic Resonance at Ultrahigh Fields: Innovations, Early Applications and Opportunities for Discoveries. In: Cardiovascular Magnetic Resonance (ed. Dudley Pennel and Warren Manning), Churchill Livingstone, 3rd Edition: ISBN: 0443075190 (2018)).

2. **Huelnhagen T**, Serradas-Duarte T, Hezel F, Paul K, Niendorf T, Quantification of Myocardial Effective Transverse Relaxation Time with Magnetic Resonance at 7.0 Tesla for a Better Understanding of Myocardial (Patho)physiology : In: Quantification of Biophysical Parameters by Medical Imaging (ed. Ingolf Sack and Tobias Schaeffter), Springer, (2018)

3. Ku MC, **Huelnhagen T**, Niendorf T, and Pohlmann A. Cardiac MRI in small animals. Methods Mol Biol. 2018; 1718:269-284. doi: 10.1007/978-1-4939-7531-0_16

Vorträge und Poster (wissenschaftliche Kongresse)

2013:

1. **Huelnhagen T**, Hezel F, Niendorf T, “Toward Probing Myocardial Microstructure Using Susceptibility Sensitized MRI of the Human Heart at 7.0 T: Assessment and Implications of Static Magnetic Field Variations”, in 2nd International Workshop on MRI Phase Contrast & Quantitative Susceptibility Mapping (QSM), Cornell University, 2013, Ithaca, NY, USA

2. **Huelnhagen T**, Hezel F, Niendorf T, “Toward Probing Myocardial Microstructure Using Susceptibility Sensitized MRI of the Human Heart at 7.0 T: Assessment and Implications of Static Magnetic Field Variations”, in 4th Annual Scientific Symposium on Ultrahigh Field Magnetic Resonance, 2013, Berlin, Germany

2014:

3. **Huelnhagen T**, Pohlmann A, Hezel F, Peper E, Ku M-C, Niendorf T, "Detailing Myocardial Microstructure in the Ex Vivo Rat Heart Using High Isotropic Spatial Resolution Susceptibility Weighted MRI and Quantitative Susceptibility Mapping", Proc Intl Soc Mag Reson Med 22; 2014; Milan, Italy. p 2437

4. **Huelnhagen T**, Hezel F, Niendorf T, "En Route to Probing Human Myocardial Microstructure in vivo Using Susceptibility Based MRI at 7.0 T", Proc Intl Soc Mag Reson Med 22; 2014; Milan, Italy. p 1436

5. **Huelnhagen T**, Pohlmann A, Hezel F, Peper E, Ku M-C, Niendorf T, “Detailing Myocardial Microstructure in the Ex Vivo Rat Heart Using High Isotropic Spa-

tial Resolution Susceptibility Weighted MRI and Quantitative Susceptibility Mapping", in 5th Annual Scientific Symposium on Ultrahigh Field Magnetic Resonance, 2014, Berlin, Germany

2015:

6. **Huelnhagen T**, Pohlmann A, Niendorf T, "Improving T2* mapping accuracy by spatially adaptive non local means noise filtering", Proc Intl Soc Magn Reson Med 23, 2015; Toronto, Canada. p 3753

7. Paul K, Graessl A, Rieger J, Lysiak D, **Huelnhagen T**, Winter L, Heidemann R, Lindner T, Hadlich S, Zimpfer A, Pohlmann A, Krueger P-C, Langner S, Stachs O, Niendorf T, "Diffusion-sensitized Ophthalmic MRI Free of Geometric Distortion in Patients with Intraocular Masses", Proc Intl Soc Magn Reson Med 23, 2015; Toronto, Canada. p 3153

8. Paul K, Graessl A, Rieger J, Lysiak D, **Huelnhagen T**, Winter L, Heidemann R, Lindner T, Hadlich S, Krueger P-C, Langner S, Stachs O, Niendorf T, "Towards High Spatial Resolution Diffusion-Sensitized MR Imaging of the Eye and Orbit at 3.0 T and 7.0 T: Quantitative Assessment of the Anatomic Fidelity of EPI and RARE Variants", Proc Intl Soc Magn Reson Med 23, 2015; Toronto, Canada. p 2932

9. Peper E, **Huelnhagen T**, Pohlmann A, Ku M-C, Niendorf T, "Comparison of High Resolution T 2 * Mapping and Quantitative Susceptibility Mapping to Investigate Myocardial Microstructure in the Ex Vivo Rodent Heart", Proc Intl Soc Magn Reson Med 23, 2015; Toronto, Canada. p 2609

10. **Huelnhagen T**, Hezel F, Pohlmann A, Graessl A, Rieger J, Lysiak D, Thalhammer C, Kellman P, Prothmann M, Schulz-Menger J, Niendorf T, "High Spatial Resolution Myocardial T 2 * Mapping at 7.0 T Reveals Differences between Healthy Volunteers and Patients with Hypertrophic Cardiomyopathy", Proc Intl Soc Magn Reson Med 23, 2015; Toronto, Canada. p 2599

11. Dusek P, Bahn E, Litwin T, Wegner C, Madai VI, Dieringer M, **Huelnhagen T**, Knauth M, Niendorf T, Sobesky J, Czlonkowska A, Brueck W, Paul F, Schneider SA, Wuerfel J, "Brain iron accumulation in Wilson disease: a pilot 7T MR-histopathology correlation study", Proc Intl Soc Magn Reson Med 23, 2015; Toronto, Canada. p 2197

12. Reimann HM, Marek J, Hentschel J, **Huelnhagen T**, Pohlmann A, Niendorf T, "Near-Physiological Mouse fMRI of Nociception", Proc Intl Soc Magn Reson Med 23, 2015; Toronto, Canada. p 2030

13. Klix S, Els A, Paul K, Graessl A, Oezerdem C, Weinberger O, Winter L, Thalhammer C, **Huelnhagen T**, Rieger J, Mehling H, Schulz-Menger J, Niendorf T, "On the Subjective Acceptance during Cardiovascular Magnetic Reso-

nance Imaging at 7.0 Tesla", Proc Intl Soc Magn Reson Med 23, 2015; Toronto, Canada. p 1850

14. **Huelnhagen T**, Paul K, Pohlmann A, Graessl A, Rieger J, Lysiak D, Thalhammer C, Prothmann M, Schulz-Menger J, Niendorf T, "Towards clinical cardiac MR at 7.0 T: Early experience with black blood RARE imaging in patients with hypertrophic cardiomyopathy", Proc Intl Soc Magn Reson Med 23, 2015; Toronto, Canada. p 768

15. Paul K, Graessl A, Rieger J, Lysiak D, **Huelnhagen T**, Winter L, Els A, Endemann B, Lindner T, Hadlich S, Krueger P-C, Stachs O, Langner S, Niendorf T, "In vivo MR Microscopy of the Nervus Opticus at 3.0 T and 7.0 T: Anatomical and Diffusion Weighted Imaging in Healthy Subjects and Patients with Optic Nerve Glioma", Proc Intl Soc Magn Reson Med 23, 2015; Toronto, Canada. p 762

16. Pohlmann A, Arakelyan K, **Huelnhagen T**, Cantow K, Kox S, Balke Y, Flemming B, Seeliger E, Niendorf T, "Ferumoxytol Enhanced T 2 * Mapping for Combined Renal Oxygenation and Blood Volume Assessment at 9.4T", Proc Intl Soc Magn Reson Med 23, 2015; Toronto, Canada. p 459

17. **Huelnhagen T**, Hezel F, Pohlmann A, Graessl A, Rieger J, Lysiak D, Thalhammer C, Kellman P, Prothmann M, Schulz-Menger J, Niendorf T, “High Spatial Resolution Myocardial T2* Mapping at 7.0 T Reveals Differences between Healthy Volunteers and Patients with Hypertrophic Cardiomyopathy”, in 6th Annual Symposium on Ultrahigh Field Magnetic Resonance, 2015, Berlin, Germany

2016

18. Ku M-C, Pohlmann A, Waiczies S, dos Santos Periquito J, **Huelnhagen T**, Niendorf T, "Cerebral blood volume MRI elucidates the impact of ERK1 on high grade glioma growth and invasion", Proc Intl Soc Magn Reson Med 24, 2016; Singapore. p 4342

19. Ralf Mekle, Florian Schubert, Niendorf T, **Huelnhagen T**, Els Ae, Robinson SD, Ittermann B, Madai V, Skowronska M, Dusek P, Wuerfel J, Schneider SA, "Using Proton MR Spectroscopy and Quantitative Susceptibility Mapping (QSM) at 7 Tesla to Decipher Mitochondrial Membrane Protein–Associated Neurodegeneration (MPAN)", Proc Intl Soc Magn Reson Med 24, 2016; Singapore. p 4016

20. **Huelnhagen T**, Serradas Duarte T, Hezel F, Seeliger E, Flemming B, Prothmann M, Schulz-Menger J, Niendorf T, "Myocardial Effective Transverse Relaxation Time at 7.0 T Correlates with Left Ventricular Wall Thickness", Proc Intl Soc Magn Reson Med 24, 2016; Singapore. p 3161

21. Paul K, **Huelnhagen T**, Stachs O, Niendorf T, "Towards Fast Diffusion-Sensitized MR Imaging of the Eye and Orbit with High Anatomic Fidelity: Combining a Segmented RARE variant with Inner Volume Imaging", Proc Intl Soc Magn Reson Med 24, 2016; Singapore. p 3008

22. Milovic C, Pinto JM, Acosta-Cabronero J, Dusek P, Madai VI, **Huelnhagen T**, Niendorf T, Wuerfel J, Tejos C, "Improved magnetic dipole kernel for reconstruction methods in quantitative susceptibility mapping", Proc Intl Soc Magn Reson Med 24, 2016; Singapore. p 2843

23. Serradas Duarte T, **Huelnhagen T**, Niendorf T, "Assessment of Myocardial B0 over the Cardiac Cycle at 7.0T: Implications for Susceptibility-based CMR Techniques", Proc Intl Soc Magn Reson Med 24, 2016; Singapore. p 2541

24. Oberacker E, Paul K, Winter L, Oezerdem C, Els A, Pohlmann A, Boehmert L, Kox S, Ku M-C, **Huelnhagen T**, Stachs O, Heufelder J, Weber A, Niendorf T, "Detailing the MR Safety of Intraocular Tantalum Markers Used for Treatment Planning of Proton Beam Therapy of Uveal Melanoma: A 7.0T Study", Proc Intl Soc Magn Reson Med 24, 2016; Singapore. p 2210

25. Waiczies S, Boehmert L, Jason M. Millward, Kox S, Dos Santos Perquito J, **Huelnhagen T**, Infante-Duarte C, Pohlmann A, Niendorf T, "Blood brain barrier alterations precede ventriculomegaly in experimental autoimmune encephalomyelitis", Proc Intl Soc Magn Reson Med 24, 2016; Singapore. p 1305

26. Pohlmann A, Arakelyan K, Riazy L, **Huelnhagen T**, Kox S, Cantow K, Waiczies S, Flemming B, Seeliger E, Niendorf T, "Towards Quantitative Renal MR Blood Oximetry by Combined Monitoring of T2*, T2 and Blood Volume Fraction", Proc Intl Soc Magn Reson Med 24, 2016; Singapore. p 718

27. Oezerdem C, **Huelnhagen T**, Winter L, Niendorf T, "Abdominal and Body Imaging Using a 16 Channel Dipole RF Array at 7.0 T", Proc Intl Soc Magn Reson Med 24, 2016; Singapore. p 715

28. **Huelnhagen T**, Hezel F, Serradas Duarte T, Pohlmann A, Flemming B, Seeliger E, Prothmann M, Schulz-Menger J, Niendorf T, “Explorations into Cardiac MR at 7.0 T: Insights from High Resolution T2* Mapping of the Normal and Diseased Myocardium”, in 7th Annual Symposium on Ultrahigh Field Magnetic Resonance, 2016, Berlin, Germany

29. **Huelnhagen T**, Pohlmann A, Graessl A, Prothmann M, Schulz-Menger J, Niendorf T, “High Spatial Resolution Myocardial Susceptibility Weighted MRI at 7.0 T Reveals Prolonged T2* for Patients with Hypertrophic Cardiomyopathy compared to Healthy Controls”, in ISMRM Workshop on Ultra High Field MRI: Technological Advances & Clinical Applications, 2016, Heidelberg Germany

30. **Huelnhagen T**, “Cardiovascular MR at 7.0 T: Insights from High Resolution T2* Mapping of the Normal and Diseased Myocardium”, in Cardiovascular and Metabolic Disease Retreat 2016 Joint Summer School, 2016, Bad Saarow, Germany

2017

31. Pham M, Ji Y, Paysen H, Oberacker E, **Huelnhagen T**, Niendorf T, Winter L, "PRF thermometry accuracy at 7.0T for thermal MR applications with and without the presence of fat", Proc Intl Soc Magn Reson Med 25, 2017; Honolulu, HI, USA. p 5439

32. Ku M-C, **Huelnhagen T**, Pohlmann A, Niendorf T, "Cardiac Magnetic Resonance for Characterizing a Spontaneous Hypertrophic Cardiomyopathy Mouse Model", Proc Intl Soc Magn Reson Med 25, 2017; Honolulu, HI, USA. p 4885

33. Periquito J, Paul K, **Huelnhagen T**, Ji Y, Ku M-C, Cantow K, Seeliger E, Flemming B, Grosenick D, Pohlmann A, Niendorf T, "Diffusion-Weighted Split-Echo RARE Imaging Free Of Geometric Distortion for Renal MRI at Ultrahigh Fields", Proc Intl Soc Magn Reson Med 25, 2017; Honolulu, HI, USA. p 3403

34. **Huelnhagen T**, Fillmer A, Els A, Schubert F, Ittermann B, Niendorf T, "Detailing and Enhancing Respiratory Motion Induced Myocardial B0 Field Dispersion at 7.0 T: Implications for Cardiac Imaging and Spectroscopy at Ultrahigh Magnetic Field Strengths", Proc Intl Soc Magn Reson Med 25, 2017; Honolulu, HI, USA. p 2675

35. Oezerdem C, **Huelnhagen T**, Kuehne A, Wenz D, Millward J, Winter L, Niendorf T, "Lighter is better: A Flexible Lightweight Eight Channel Slot Antenna Array for Cardiac MRI at 7.0 Tesla", Proc Intl Soc Magn Reson Med 25, 2017; Honolulu, HI, USA. p 1129

36. Wenz D, Oliver Weinberger,re Kuehne, Waiczies H, Nagel A, Oezerdem C, **Huelnhagen T**, Lysiak D, Winter L, Stachs O, Langner S, Seeliger E, Flemming B, Niendorf T, "Panning for Salt: One Millimeter Resolution In Vivo Sodium MRI of the Human Eye at 7.0 Tesla Using a Six Channel Transceiver Array", Proc Intl Soc Magn Reson Med 25, 2017; Honolulu, HI, USA. p 1127

37. Paul K, Waiczies H, Kuehne A, **Huelnhagen T**, Oberacker E, Stachs O, Niendorf T, "Accelerated Diffusion-Sensitized MR Imaging of the Eye and Orbit at 3.0 T and 7.0 T free of Geometric Distortions Using a Combined RARE-EPI Acquisition Technique", Proc Intl Soc Magn Reson Med 25, 2017; Honolulu, HI, USA. p 1096

38. Reimann HM, Todiras M, **Huelnhagen T**, Bader M, Pohlmann A, Niendorf T, "Detailing the Origin of BOLD fMRI in Mice: Somatosensory Stimulation versus Pharmacologically Induced Blood Pressure Alterations", Proc Intl Soc Magn Reson Med 25, 2017; Honolulu, HI, USA. p 592

39. **Huelnhagen T**, Hezel F, Serradas Duarte T, Ku M-C, Flemming B, Seeliger E, Prothmann M, Schulz-Menger J, Niendorf T, "Myocardial T2* Changes Periodically across the Cardiac Cycle and is Prolonged in Hypertrophic Cardiomyopathy: A 7.0 Tesla MRI Patient Study", Proc Intl Soc Magn Reson Med 25, 2017; Honolulu, HI, USA. p 44

40. **Huelnhagen T**, Hezel F, Serradas Duarte T, Flemming B, Seeliger E, Prothmann M, Schulz-Menger J, Niendorf T, „Myocardial T2* Changes Periodically over the Cardiac Cycle and is Prolonged in Hypertrophic Cardiomyopathy: Lessons Learned from a 7.0 Tesla MRI Patient Study", in Proc. 20th Annual Scientific Sessions Society for Cardiovascular Magnetic Resonance 2017, Washington D.C., MY, USA

41. **Huelnhagen T**, Niendorf T, "Ein- und Aussichten der Magnetresonanztomographie des Herzens bei einer Magnetfeldstärke von 7.0 Tesla: Der ideale Treffpunkt für Physiker, Mediziner und Biologen", in 81. Jahrestagung und DPG-Frühjahrstagung 2017, Münster, Germany

42. **Huelnhagen T**, Fillmer A, Els A, Schubert F, Ittermann B, Niendorf T, "Detailing and Enhancing Respiratory Motion Induced Myocardial B0 Field Dispersion at 7.0 T: Implications for Cardiac Imaging and Spectroscopy at Ultrahigh Magnetic Field Strengths", in 8th Annual Symposium on Ultrahigh Field Magnetic Resonance, 2017, Berlin, Germany

43. **Huelnhagen T**, Hezel F, Serradas Duarte T, Ku M-C, Flemming B, Seeliger E, Prothmann M, Schulz-Menger J, Niendorf T, "Myocardial T2* Changes Periodically across the Cardiac Cycle and is Prolonged in Hypertrophic Cardiomyopathy: A 7.0 Tesla MRI Patient Study", in 8th Annual Symposium on Ultrahigh Field Magnetic Resonance, 2017, Berlin, Germany

44. **Huelnhagen, T**, "Toward Precision Diagnostics Using Ultrahigh Field Magnetic Resonance Imaging", Science Match Future Medicine 2017: Innovation in Health Science, Berlin, 2017

Danksagung

Ich danke meinem Betreuer Herrn Prof. Dr. Thoralf Niendorf für die ausgezeichnete Unterstützung meines Promotionsvorhabens, seine stets kritischen aber konstruktiven und inspirierenden Fragen und seinen weitsichtigen Rat.

Weiter Danke ich dem gesamten Team der Berlin Ultrahigh Field Facility für die technische, inhaltliche Unterstützung meiner Arbeit, die zahllosen Gespräche und gemeinsamen Erinnerungen sowie die tolle Arbeitsatmosphäre am Institut, die ich in den vergangenen Jahren genießen durfte.

Ich danke Frau Prof. Dr. Jeanette Schulz-Menger und den Mitarbeitern der Arbeitsgruppe kardiale MRT am Charité Campus Buch für die fruchtbare Forschungskooperation, die interessanten Diskussionen und die bereitwillige Füllung meiner medizinischen Wissenslücken.

Dr. Erdmann Seeliger und Dr. Bert Flemming danke ich für Ihre stets kritischen aber sehr hilfreichen Fragen und anregenden Diskussionen, die geduldige Erklärung von physiologischen Phänomenen und Sachverhalten und die Versorgung mit entsprechender Literatur.

Weiter danke ich allen nicht namentlich genannten Kooperationspartnern aus Forschung, Klinik und Industrie für die gute Zusammenarbeit und die zahlreichen spannenden Projekte, die angestoßen wurden.

Besonderer Dank gilt meiner Familie und meiner Freundin für die emotionale und stets bedingungslose Unterstützung bei meiner Doktorarbeit.